Computational Analysis of Aerated Stabilization Basins

By

Richard David Toma

B.A.Sc. Mechanical Engineering, University of Alberta, 2001

A THESIS SUBMITTED IN PARTIAL

FULFILLMENT OF THE

REQUIREMENTS FOR THE DEGREE OF

MASTER OF APPLIED SCIENCE

in

THE FACULTY OF GRADUATE STUDIES

(MECHANICAL ENGINEERING)

The University of British Columbia

August, 2005

Abstract

Simulations of aerated waste lagoons were done using computational fluid dynamics (CFD) techniques and the results were compared with experimental data. A computational model simulated the flow through a previously constructed model aerator and basin. A two-phase, axisymmetric simulation was developed specifically for computing the flow through the geometry of the experimental aerator. A velocity profile was computed at the exit of the aerator and applied to an assumed distribution of droplet diameters. A discrete phase, Lagrangian particle tracking model was then used with the assumed particle distribution, while computing the interactions between the droplets and the surrounding air. The results of the Lagrangian simulation provided an appropriate mass and momentum flux distribution induced by the aerator which could then be applied to a single phase lagoon simulation.

A velocity distribution was calculated for the model basin with the same flow rates as in the previous experiments. Using the calculated velocity distribution, it was possible to do tracer studies and compute a residence time distribution for the aerated basin model with an unsteady, species transport model. Reasonable agreement between the simulation and experiments was found.

Having validated a method of reproducing the hydrodynamic effects of the experimental aerator, simulations were also carried out on a geometry representative of a 75 horsepower aerator. A parametric study was performed where the volume and the inlet positions of the lagoon where varied. The effects of varying lagoon volume on the residence time distribution were also investigated.

Table of Contents

List of Figures

List of Symbols

α	-	species volume fraction
ε	-	turbulent kinetic energy dissipation rate
θ	-	time
ρ	-	density
ρ_p	-	particle density
κ	-	Von Karman's constant (0.4)
μ	-	kinematic viscosity
μ_t	-	turbulent kinematic viscosity
σ_k	-	k-epsilon turbulent model constant
σ_ε	-	k-epsilon turbulent model constant
v	-	lagoon volumetric flow-through rate
τ_w	-	wall shear stress
u_p	-	particle velocity
BOD	-	biochemical oxygen demand
c	-	outlet tracer volume fraction
c_o	-	initial tracer concentration
CFD	-	computational fluid dynamics
C_d	-	drag coefficient
D_i	-	diffusion coefficient
F_d	-	drag force
G_k	-	Generation of turbulent kinetic energy due to mean velocity gradients
HRT	-	theoretical hydraulic retention time
Q	-	initial total tracer volume
R_e	-	Reynolds number
RTD	-	residence time distribution
S_{ct}	-	turbulent Schmidt number

Acknowledgements

1   Introduction

1.1 Background

Industrial wastewater is discharged from industries and associated processes utilizing water. Water used for process operations (non-cooling purposes) can become degraded as a result of introduced nutrients, suspended sediments, bacteria, oxygen-demanding matter and toxic chemicals. The aerated stabilization basin (ASB) is the most common secondary wastewater treatment system utilized by the forest products industry. ASBs are partially mixed, aerated reactors that degrade wastes biologically prior to discharge into the environment. These systems are characterized by hydraulic retention times of 3 - 10 days, are 1 - 5 m deep and occupy hectares of surface area. Structurally, these systems are very simple, being essentially shallow, lined, flow-through ponds, usually with mechanical surface aerators included to provide the necessary oxygen and mixing required for waste stabilization [2]. An aerial view of a typical ASB is shown in Figure 1.1. In general the inlets and outlets are placed at opposite ends of the lagoon, in order to maximize both aeration and residence time.
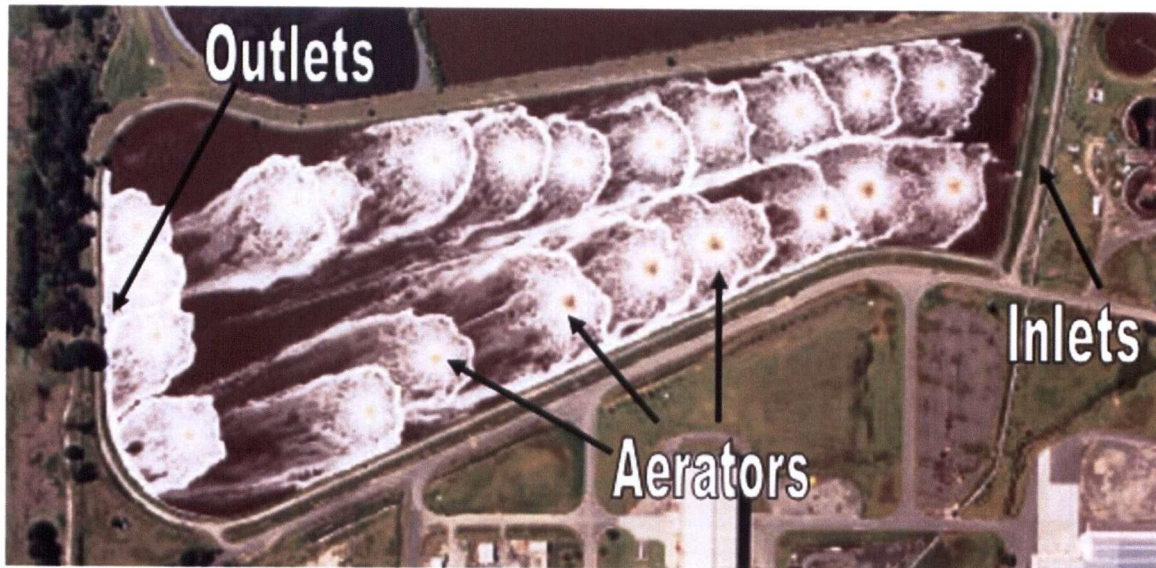
Figure 1.1: Aerated Stabilization Basin

Aerated lagoons contain active, complex populations of aerobic microorganisms which break down organic matter. During treatment aerobic bacteria use a portion of the organic matter to obtain energy to synthesize the remaining organic material into new cells. The remainder of the organic waste is oxidized to low energy compounds such as carbon dioxide, nitrate and sulfate. One common characteristic used to evaluate the quality of industrial wastewater is known as Biochemical Oxygen Demand, or BOD. BOD, usually expressed in milligrams per litre refers to the amount of oxygen used by a mixed population of microorganisms under aerobic conditions to stabilize organic matter in the wastewater [1]. High BOD is caused by large amounts of soluble carbohydrates in the wastewater. Pulp and paper mills and meat and food processing plants all produce high BOD. If wastewater is returned to the environment with excessive BOD, the resulting deoxygenated water will lead to highly anaerobic conditions, fish kills and foul odors. In non aerated lagoons the oxygen required for these processes is provided by algae and wind, however BOD removal rates can be greatly increased trough the use of mechanical aerators.

1.2 Previous Work

1.2.1 Analytical Work

Considerable work has been done over the years on the topic of stabilization basins as it would be most desirable to accurately predict the BOD removal rate for any given pond geometry and any placement and number of aerators. The BOD removal rate can be defined as the difference between the influent and the effluent BOD concentration divided by the mean lagoon residence time. Much of our current understanding of reactor hydraulics is based on the work of Danckwerts [3] who recognized that the assumptions of either "piston flow" or perfectly mixed reactors were invalid in terms of describing the true hydraulic behavior of flow-through reactors. He developed the concept of the residence time distribution, or RTD and correlated various RTDs to corresponding reactor flows. Figure 1.2 shows various dimensionless RTDs, or C-diagrams for different types of reactor flows using the following dimensionless groupings:

$$\frac{\upsilon\theta}{V} \tag{1.2.1}$$

where,

υ = lagoon volumetric flow-through rate $\left(\dfrac{m^3}{s}\right)$

V = lagoon volume $\left(m^3\right)$

θ = time (s)

$$\frac{Vc}{Q} \tag{1.2.2}$$

where,

c   = outlet tracer volume fraction

Q = initial total tracer volume $\left(m^3\right)$

These dimensionless groupings are relevant to tracer studies where a dye tracer, or contaminant is

added to a reactor inlet and concentration measurements are taken at the outlet. In "piston flow"

(Figure 1.2a) it is assumed that all elements of fluid which enter the vessel at the same moment move

through it with constant velocity on parallel paths, leaving when the dimensionless time is equal to

unity.
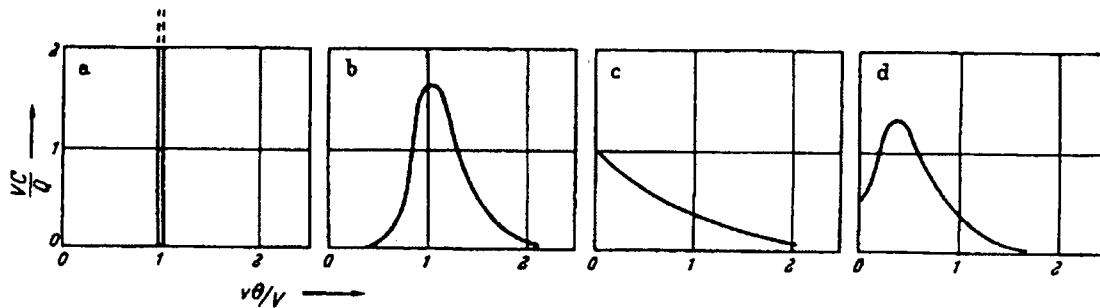
Figure 1.2: C-diagrams proposed by Danckwerts [3]

Figure 1.2b represents piston flow with a more realistic allowance of some longitudinal mixing.

Figure 1.2c shows a typical RTD for vessels where there is a high degree of mixing present, resulting

in an exponentially decaying outlet concentration. Figure 1.2d represents a vessel with a

considerable volume of very slow moving or "dead" water. It has peak similar to the flow through

case, as much of the tracer will bypass the dead water.

Nameche and Vasel [4] compared several mathematical models based on the dispersion model

and the dimensionless Peclet number relating the length, width and depth of the lagoons as well as

the aerator power input. They concluded that mathematical and empirical models are limited in their

ability to account for the presence and position of baffles, aerator positions, specific pond geometry,

wind velocities and directions, and the number and position of inlet/outlet structures. These

parameters are extremely difficult to express in simple mathematical forms and fail to predict such

effects as short-circuiting and dead spaces in lagoons.

1.2.2 Computational Work

The use of modern computational methods presents the possibility of overcoming some of the limitations of previous mathematical models as described by Nameche and Vasel [4]. Using Computational Fluid Dynamics (CFD) any lagoon geometry could possibly be analyzed. Wood [5] found that many of Australia's 220 wastewater treatment ponds were operating at sub-optimal levels of performance due to hydrodynamic problems, including short-circuiting, stratification in the hot Australian climate and solid settling. He found that the failure of existing design techniques to adequately account for these factors threatened the continued use of pond systems. Wood [5] developed the two dimensional grid shown in Figure 1.3.
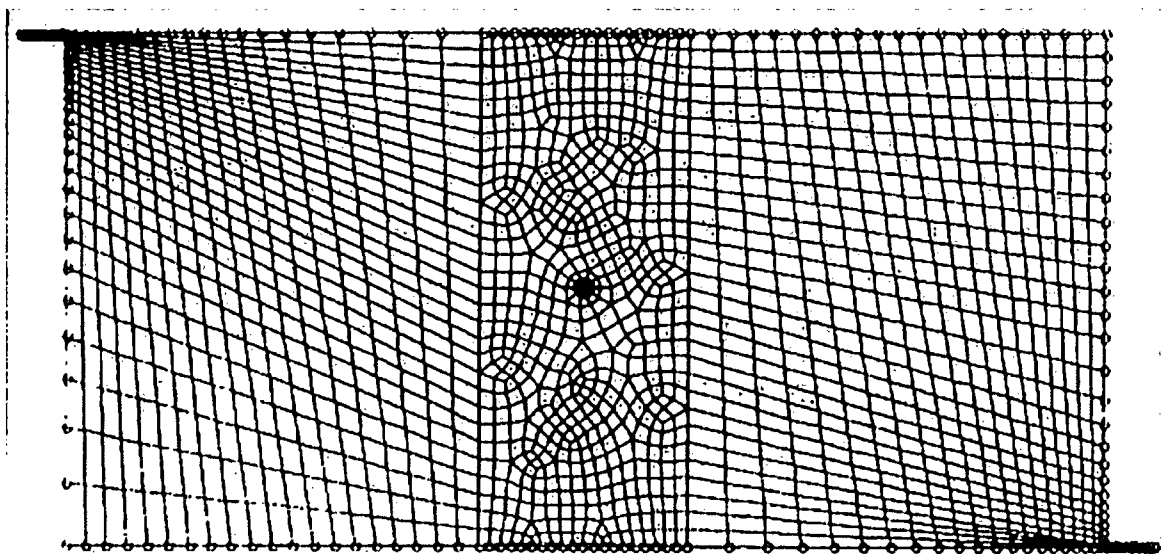
Figure 1.3: Two dimensional lagoon grid of M.G. Wood [5]

Solving for the flow throughout the domain it was found that significant stagnant regions were present. It was suggested that these stagnant zones were sites of sludge settling and odor release in addition to representing wasted pond volume. Wood [5] made some slight modifications to the grid shown in order to evaluate the effect that baffles might have on the flow field in the lagoon. This type of evaluation was not previously possible until the advent of modern CFD codes. An attempt

was made to evaluate the presence of an aerator in the domain. This was modeled as what Wood

simply described as a "regional acceleration". It was found that a large, circular flow with regions of

high velocity was established around the aerator.

Ta and Brignal [6] investigated the hydraulic characteristics of a specific reservoir in use in

Banbury, Oxfordshire, UK. A basic layout of the two hundred thousand cubic meter pond is shown

in Figure 1.4.
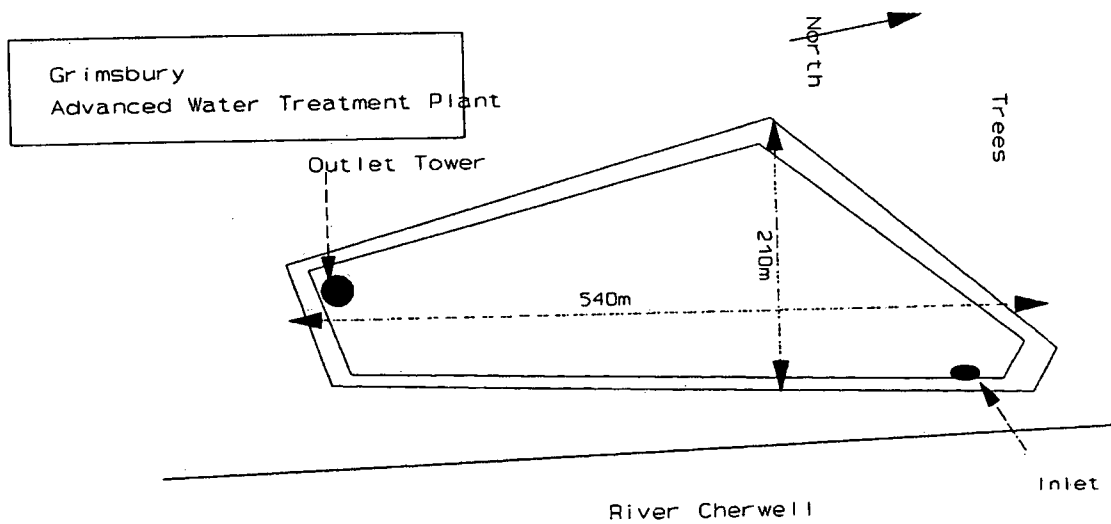
Figure 1.4: Grimsbury Reservoir, Ta [6]

In order to provide a more accurate analysis, Ta and Brignal used a three dimensional grid in this

case. As a 3D grid allows for flow variations below the surface, it was possible to accurately

calculate a residence time distribution. A 3D grid also allows for greater choices in evaluating

different geometric characteristics in the lagoon. A manifold inlet, a submerged baffle and a central

outlet were all tested. Residence time distributions were then computed for all the arrangements and

shown in Figure 1.5. It was concluded that the submerged baffle arrangement produced the best

residence time and mixing with the least short circuiting. No aerators were simulated in this

particular study.
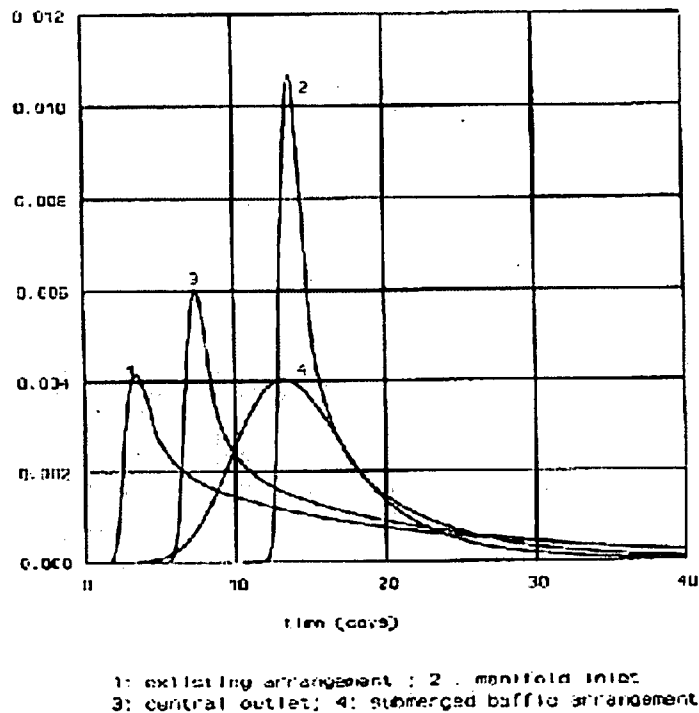
Figure 1.5: Computed RTD Results for Grimsbury reservoir [6]

H.E. Salter et al. [7] performed a very similar three-dimensional CFD analysis in order to study

the hydraulic regime in an un-aerated lagoon. Baffle positions were again analyzed. A calculation of

the temperature profiles in the lagoon was also performed. The results showed that thermal

stratification is quite significant in lagoons. It was also concluded that in lagoons where baffles are

not present, the flow tends to follow a wall from the inlet to the outlet. This causes a significant

decrease in the predicted retention time.

Jenkinson [2] studied the problem of aerated lagoons extensively. He designed, built, and tested a

small model aerator and lagoon. Using the experimental apparatus, he completed some tracer studies

on the lagoon, measuring a set of RTDs with and without the model aerator present. The RTD

results without aeration were also simulated using CFD methods with good agreement between the

two.

1.3 Motivation for Present Studies

Surface aerators are a very common method of increasing the BOD removal rates in lagoon wastewater treatment facilities, including those in the pulp and paper industry. As the name implies, surface aerators float on the surface of the lagoon, tethered in place by cables.

Aerators vary widely in power usage and flow rate. Similarly lagoons vary in all dimensions and in total volume. The previously described computational work has analyzed lagoons of various shapes, with various inlet/outlet and baffle configurations. Unfortunately the published works and current research are lacking significant computational work on the analysis of typical aerators, and the hydrodynamic effects they produce on lagoons.

The complex flows involved in the operation of a surface aerator present a number of difficulties for numerical simulation. A cutaway view of an industrial sized aerator is shown in Figure 1.6. If we begin our analysis inside the aerator, we find an impeller driving the flow. This impeller will produce a turbulent, swirling flow which is difficult to reproduce computationally in detail. Following the impeller, shielded by a draft tube, the flow encounters a curved diffusion head. At this point, part of the flow has a free surface, exposed to the surrounding air. In trying to simulate these flows, the interaction between two distinct phases in the domain must be computed as well. As the free jet leaves the surface aerator, it begins to break up into droplets. Jet break up is a very complex process which is difficult to describe mathematically and therefore difficult to simulate accurately with current CFD codes. The droplets form a non-uniform diameter distribution, and then follow trajectories through the air where they are subjected to drag forces. Once the droplets strike the lagoon surface, mass and momentum are imparted to the lagoon at the initial landing point and through secondary splashes and waves.
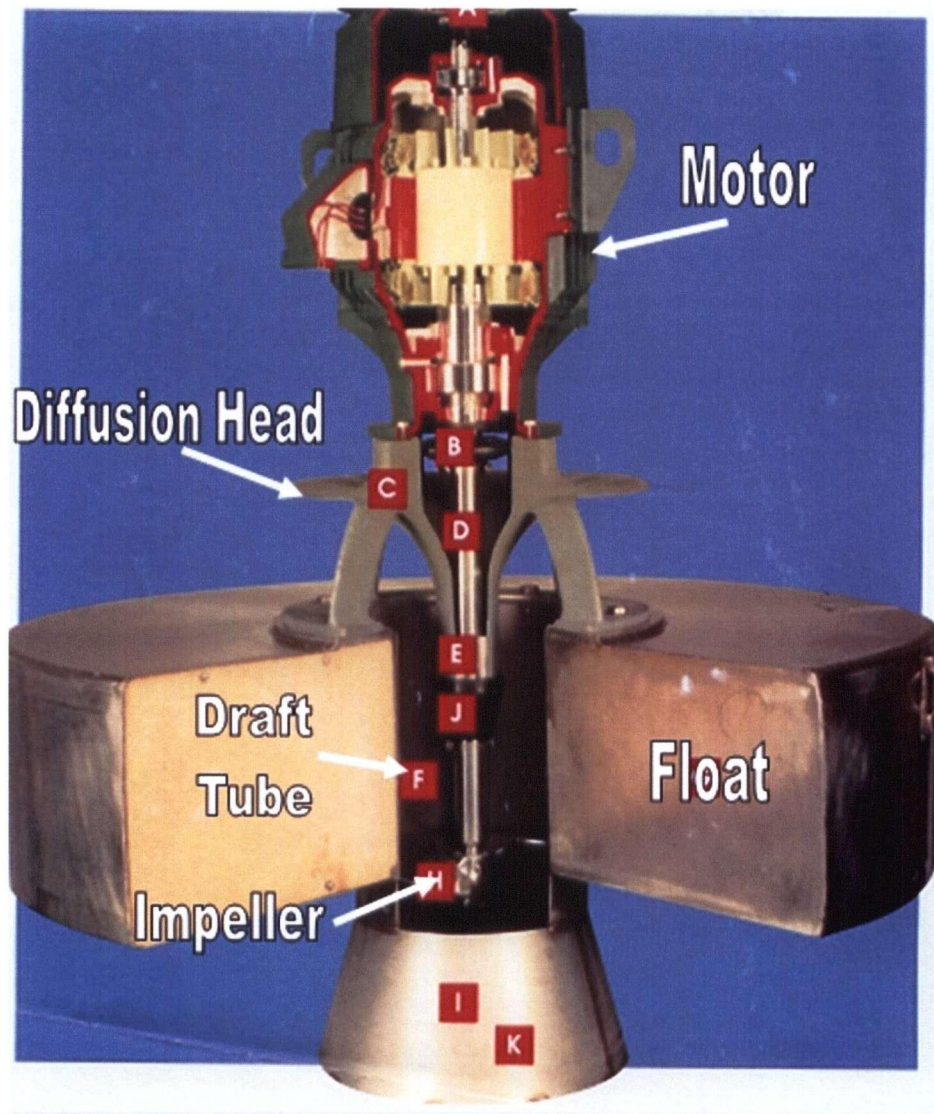
Figure 1.6: Cutaway View of Industrial Aerator

1.4 Objective and Scope

The objective of this present work is to address the need discussed above to develop and validate an efficient numerical tool suitable for modeling aerated lagoons. Numerical simulations could potentially provide detailed information about flow fields and produce RTDs relatively quickly.

K. Pougatch from the Department of Mechanical Engineering has performed several preliminary calculations simulating an aerator and the subsequent aerator/lagoon interaction. Using the FLUENT CFD package, the Volume of Fluid model was implemented by Pougatch to simulate the free surface

effects and compute the flowfield in a full sized aerator. The results from this simulation were used to calculate droplet trajectories from the aerator. With these results a mass and momentum flux were applied to a single phase lagoon simulation. A large industrial lagoon installation was successfully reproduced computationally by Pougatch [11].

In this present study the same numerical techniques used by Pougatch are applied in order to develop and refine an efficient method of aerator/lagoon analysis. The measured results obtained by Jenkinson [2] are used to validate and tune the model developed through the following three step process:

Step 1: A grid is designed to simulate the flow through the experimental aerator using the Volume of Fluid model. The effects of swirl velocities following the impeller are also considered. These calculations are described in Chapter 3.

Step 2: A complete and instantaneous jet breakup is assumed at the edge of the diffusion head. The velocity distribution at that point computed in Step 1 is used to compute the trajectory of a spray of droplets using a discrete phase, Lagrangian particle tracking method. These calculations are also described in Chapter 3. In Chapter 4, Steps 1 and 2 are applied to a 75hp aerator.

Step 3: The results of the particle trajectory calculations are used to apply an appropriate mass and momentum flux to a single phase representation of the basin. These calculations are described in Chapter 5.

The final part of this thesis involves the analysis of aerators in lagoons of differing volumes and different inlet/outlet configurations in order to determine how they affect the RTD. These calculations are described in Chapter 6.

2   Computational Models

As previously described the flows taking place in aerated lagoons are quite complex and cannot be accurately reproduced by a single model. The experiments of Jenkinson [2] will therefore be reproduced computationally in three separate simulations using the commercial CFD code FLUENT. The following computationally models are used as described in the FLUENT documentation [12]

2.1 Internal Aerator Flows

For this study, the Volume of Fluid (VOF) model is used to simulate the flow through the experimental apparatus of Jenkinson. As the flow moves through the apparatus, the interactions with the aerator components and the surrounding air must be computed.

The VOF model solves a single set of momentum equations and tracks the volume fraction for two immiscible fluids within the domain. The tracking of the interface between the phases is accomplished by the solution of a continuity equation for the volume fraction of one of the phases for a 2D, axisymmetric coordinate system:

$$\frac{\partial \alpha_q}{\partial t} + \frac{\partial}{\partial x}\left(\alpha_q v_x\right) + \frac{\partial}{\partial r}\left(\alpha_q v_r\right) + \frac{\alpha_q v_r}{r} = 0 \qquad (2.1.1)$$

where:

α = Volume fraction of given phase

v = velocity (m/s)

The primary phase volume fraction is computed based on the following constraint:

$$\sum_{q=1}^{n} \alpha_q = 1 \qquad (2.1.2)$$

The properties appearing in the transport equations are determined by the presence of the component phases in each control volume. In this two phase system, the phases are represented by the subscripts 1 and 2; the density in each cell is given by:

$$\rho = \alpha_2 \rho_2 + (1 - \alpha_2) \rho_1 \qquad (2.1.3)$$

Similarly, viscosity is computed in each cell with the following equation:

$$\mu = \alpha_2 \mu_2 + (1 - \alpha_2) \mu_1 \qquad (2.1.4)$$

A single momentum equation is solved throughout the domain, and the resulting velocity field is shared among the phases. The momentum equations, shown below, are dependent on the volume fractions of all phases through the properties ρ and μ. For 2D axisymmetric geometries, the axial and radial momentum conservation equations are given by:

$$
\begin{aligned}
\frac{\partial}{\partial t}(\rho v_x) + \frac{1}{r}\frac{\partial}{\partial x}(r\rho v_x v_x) + \frac{1}{r}\frac{\partial}{\partial r}(r\rho v_r v_x) \;=\; & -\frac{\partial p}{\partial x} \\
& + \frac{1}{r}\frac{\partial}{\partial x}\left[r\mu\left(2\frac{\partial v_x}{\partial x} - \frac{2}{3}(\nabla \cdot \vec{v})\right)\right] \\
& + \frac{1}{r}\frac{\partial}{\partial r}\left[r\mu\left(\frac{\partial v_x}{\partial r} + \frac{\partial v_r}{\partial x}\right)\right] \\
& + F_x \qquad (2.1.5)
\end{aligned}
$$

and

$$\frac{\partial}{\partial t}(\rho v_r) + \frac{1}{r}\frac{\partial}{\partial x}(r\rho v_x v_r) + \frac{1}{r}\frac{\partial}{\partial r}(r\rho v_r v_r) = -\frac{\partial p}{\partial r}$$

$$+ \frac{1}{r}\frac{\partial}{\partial x}\left[r\mu\left(\frac{\partial v_r}{\partial x} + \frac{\partial v_x}{\partial r}\right)\right]$$

$$+ \frac{1}{r}\frac{\partial}{\partial r}\left[r\mu\left(2\frac{\partial v_r}{\partial r} - \frac{2}{3}(\nabla \cdot \vec{v})\right)\right]$$

$$- 2\mu\frac{v_r}{r^2} + \frac{2}{3}\frac{\mu}{r}(\nabla \cdot \vec{v}) + \rho\frac{v_z^2}{r}$$

$$+ F_r \tag{2.1.6}$$

where:

$$\nabla \cdot \vec{v} = \frac{\partial v_x}{\partial x} + \frac{\partial v_r}{\partial r} + \frac{v_r}{r} \tag{2.1.7}$$

2.2 Aerator Spray

The process by which the bulk fluid is converted into smaller drops is known as atomization, and in this case begins prior to the edge of the splash-plate and continues as the fluid leaves the plate. In any free jet, or sheet of fluid it has been hypothesized by Kolmogorov [9] that breakup is caused by the kinetic energy of turbulent fluctuations within the jet. Given the surface tension present, this causes a competition on the jet surface between the cohesive and disruptive forces. The bulk fluid spreads out along the plate and expands until equilibrium exists between the inertial forces and the surface tension. Under favourable conditions, these turbulent oscillations are amplified until the sheet disintegrates into drops. This process is known as primary atomization. If the drops formed exceed a critical size, they disintegrate further, into smaller droplets. This process is known as

secondary atomization. Since these processes are not reproducible with the VOF model, it was

decided to assume that complete breakup occurs at the splash-plate edge. A distribution of droplet

diameters can then be assumed, with velocities based on the profiles computed with the VOF model.

It is possible to calculate the trajectory of the droplets by integrating the force balance on the

particle, which is written in a Lagrangian reference frame. This force balance equates the particle

inertia with the forces acting on the particle, and can be written as:

$$\frac{du_p}{dt} = F_D(u - u_p) + \frac{g_x(\rho_p - \rho)}{\rho_p} + F_x \qquad (2.2.1)$$

where,

u = local velocity of the continuous phase,

u_p = particle velocity,

ρ_p = particle density,

F_D is the drag force on the particles which is calculated as follows:

$$F_D = \frac{18\mu}{\rho_p d_p^2} \frac{C_D R_e}{24} \qquad (2.2.2)$$

where,

$$R_e = \frac{\rho d_p |u_p - u|}{\mu} \qquad (2.2.3)$$

As the trajectory of a particle is computed, the momentum gained or lost by the particle stream

that follows that trajectory is incorporated in the subsequent continuous phase calculations. While the

continuous phase always impacts the discrete phase, the effect of the discrete phase trajectories on

the continuous phase is also taken into account. This is accomplished by alternately solving the

discrete and continuous phase equations until the solutions in both phases have stopped changing.

The momentum transfer from the continuous phase to the discrete phase is computed by examining

the change in momentum of a particle as it passes through each control volume. This momentum

change is computed as:

$$F = \sum \left(\frac{18\mu C_D R_e}{\rho_p d_p^2 24} (u_p - u) \right) m_p^* \Delta t \qquad (2.2.4)$$

where,

u = local velocity of the continuous phase,

u_p = particle velocity,

ρ_p = particle density,

μ = viscosity of the fluid,

d_p = diameter of the particle,

m_p = mass flow rate of the particles,

Δt = time step

This momentum exchange appears as a momentum sink in the continuous phase momentum balance.

2.3 Single Phase Lagoon Calculations

2.3.1 Mass and Momentum Conservation

Following the VOF and discrete phase calculations used to determine the aerator splash zone, a

three dimensional, single phase calculation is performed to determine the flowfield in the

experimental lagoon used by Jenkinson. The standard mass and momentum equations shown below

are solved in the lagoon domain.

$$\frac{\partial \rho}{\partial t} + \nabla \cdot \left(\rho \vec{v} \right) = 0 \qquad (2.3.1)$$

$$\frac{\partial}{\partial t}\left(\rho \vec{v}\right) + \nabla \cdot \left(\rho \vec{v} \vec{v}\right) = -\nabla p + \nabla \cdot \left(\overline{\overline{\tau}}\right) + \rho \vec{g} \qquad (2.3.2)$$

The stress tensor $\overline{\overline{\tau}}$ is given by:

$$\overline{\overline{\tau}} = \mu \left[\left(\nabla \vec{v} + \nabla \vec{v}^T \right) - \frac{2}{3} \nabla \cdot \vec{v} I \right] \qquad (2.3.3)$$

2.3.2 Species Transport Model

Once a steady state velocity field is obtained for the model lagoon, it is possible to reproduce the experimental tracer studies by applying a time dependent species transport model to the solution. The mass fraction of each species in the domain, Y_i, is predicted through the solution of the following convection-diffusion equation:

$$\frac{\partial}{\partial t}\left(\rho Y_i\right) + \nabla \cdot \left(\rho \vec{v} Y_i\right) = -\nabla \cdot \vec{J_i} \qquad (2.3.4)$$

The mass diffusion is computed in the following form:

$$\vec{J_i} = -\left(\rho D_{i,m} + \frac{\mu_t}{Sc_t} \right) \nabla Y_i \qquad (2.3.5)$$

Where Sc_t is the turbulent Schmidt number, $\frac{\mu_t}{\rho D_i}$ and $D_{i,m}$ is the diffusion coefficient for species i in the mixture (determined to be $5.0 \times 10^{-4} m^2/s$ [2]).

2.4 Turbulence Modeling

2.4.1 K-Epsilon Turbulence Model

The turbulence model used in many of the simulations in this thesis is the commonly used standard K-Epsilon (k-ε) turbulence model. The standard k-ε model is a semi-empirical model based on model transport equations for the turbulence kinetic energy (k) and its dissipation rate (ε). The turbulent kinetic energy, and its rate of dissipation, are obtained from the following transport equations:

$$\frac{\partial}{\partial t}(\rho k) + \frac{\partial}{\partial x_i}(\rho k u_i) = \frac{\partial}{\partial x_j}\left[\left(\mu + \frac{\mu_t}{\sigma_k}\right)\frac{\partial k}{\partial x_j}\right] + G_k + G_b - \rho\varepsilon - Y_M + S_k \qquad (2.4.1)$$

and,

$$\frac{\partial}{\partial t}(\rho\varepsilon) + \frac{\partial}{\partial x_i}(\rho\varepsilon u_i) = \frac{\partial}{\partial xj}\left[\left(\mu + \frac{\mu_t}{\sigma_\varepsilon}\right)\frac{\partial\varepsilon}{\partial x_j}\right] + C_{1\varepsilon}\frac{\varepsilon}{k}(G_k + C_{3\varepsilon}G_b) - C_{2\varepsilon}\rho\frac{\varepsilon^2}{k} + S_\varepsilon$$

$$(2.4.2)$$

In these equations, G_k represents the generation of turbulence kinetic energy due to the mean velocity gradients.

$$G_k = -\rho u_i u_j \frac{\partial u_j}{\partial x_i} \qquad (2.4.3)$$

G_b is the generation of turbulence kinetic energy due to buoyancy. It is calculated using the following equation:

$$G_b = -g_i \frac{\mu_t}{\rho \, \mathrm{Pr}_t} \frac{\partial \rho}{\partial x_i}$$ (2.4.4)

The values of k and ε are combined in order to compute the turbulent, or eddy viscosity $\left(\mu_t\right)$ using the following equation:

$$\mu_t = \rho C_\mu \frac{k^2}{\varepsilon}$$ (2.4.5)

where C_μ is a constant. The following model constants were applied to the model. These values have been determined from experiments with air and water for a variety of cases. They have been found to work well for wall bounded shear flows.

Parameter	Value
C_u	0.09
$C_{1\varepsilon}$	1.44
$C_{2\varepsilon}$	1.92
σ_k	1.0
σ_ε	1.3

Table 2.1: K-Epsilon Model Constants

2.4.2 Reynolds Stress Turbulence Model

As it was desired to analyze the effect of imposed swirl velocities on the internal aerator flow, another turbulence model had to be chosen. The Reynolds Stress Model (RSM) was chosen as it accounts for the effects of streamline curvature and swirl in a more rigorous manner than the K-Epsilon turbulence model. RSM involves calculation of the individual Reynolds stresses, $\overline{u'_i u'_j}$ using differential transport equations. The transport equations for the transport of the Reynolds stresses may be written as follows:

$$\underbrace{\frac{\partial}{\partial t}(\rho\,\overline{u_i'u_j'})}_{\text{Local Time Derivative}} + \underbrace{\frac{\partial}{\partial x_k}(\rho u_k\overline{u_i'u_j'})}_{C_{ij}\,\equiv\,\text{Convection}} =$$

$$\underbrace{-\frac{\partial}{\partial x_k}\left[\rho\,\overline{u_i'u_j'u_k'} + \overline{p\left(\delta_{kj}u_i' + \delta_{ik}u_j'\right)}\right]}_{D_{T,ij}\,\equiv\,\text{Turbulent Diffusion}} + \underbrace{\frac{\partial}{\partial x_k}\left[\mu\frac{\partial}{\partial x_k}(\overline{u_i'u_j'})\right]}_{D_{L,ij}\,\equiv\,\text{Molecular Diffusion}}$$

$$\underbrace{-\rho\left(\overline{u_i'u_k'}\frac{\partial u_j}{\partial x_k} + \overline{u_j'u_k'}\frac{\partial u_i}{\partial x_k}\right)}_{P_{ij}\,\equiv\,\text{Stress Production}} \underbrace{-\rho\beta(g_i\overline{u_j'\theta} + g_j\overline{u_i'\theta})}_{G_{ij}\,\equiv\,\text{Buoyancy Production}}$$

$$+\underbrace{\overline{p\left(\frac{\partial u_i'}{\partial x_j} + \frac{\partial u_j'}{\partial x_i}\right)}}_{\phi_{ij}\,\equiv\,\text{Pressure Strain}} - \underbrace{2\mu\overline{\frac{\partial u_i'}{\partial x_k}\frac{\partial u_j'}{\partial x_k}}}_{\epsilon_{ij}\,\equiv\,\text{Dissipation}}$$

$$\underbrace{-2\rho\Omega_k\left(\overline{u_j'u_m'}\epsilon_{ikm} + \overline{u_i'u_m'}\epsilon_{jkm}\right)}_{F_{ij}\,\equiv\,\text{Production by System Rotation}} + \underbrace{S_{\text{user}}}_{\text{User-Defined Source Term}}$$

$$(2.4.6)$$

$D_{T,ij}$, G_{ij}, ϕ_{ij}, and ε_{ij} need to be modeled to close the equations.

$D_{T,ij}$ is modeled as follows:

$$D_{T,ij} = \frac{\partial}{\partial x_k}\left(\frac{\mu_t}{\sigma_k}\frac{\partial\overline{u_i'u_j'}}{\partial x_k}\right) \qquad (2.4.7)$$

where $\sigma_k = 0.82$

The turbulent viscosity μ_t is computed similarly to the k-ε model:

$$\mu_t = \rho C_\mu \frac{k^2}{\varepsilon}$$

(2.4.8)

where $C_\mu = 0.09$

ϕ_{ij} uses the following decomposition:

$$\phi_{ij} = \phi_{i,j,1} + \phi_{i,j,2} + \phi_{i,j,w}$$

(2.4.9)

where $\phi_{ij,1}$ is the slow pressure-strain term, ϕ_{ij2} is the rapid pressure-strain term, and $\phi_{ij,w}$ is the wall-reflection term

The slow pressure-strain term, $\phi_{ij,1}$, is modeled as:

$$\phi_{ij,1} = -C_1 \rho \frac{\varepsilon}{k} \left[\overline{u_i' u_j'} - \frac{2}{3} \delta_{ij} k \right]$$

(2.4.10)

where $C_1 = 1.8$.

The rapid pressure-strain term, ϕ_{ij2}, is modeled as:

$$\phi_{ij,2} = -C_2 \left[\left(P_{ij} + F_{ij} + G_{ij} - C_{ij} \right) - \frac{2}{3} \delta_{ij} \left(P + G - C \right) \right]$$

(2.4.11)

where $C_2 = 0.60$, $P = \frac{1}{2} P_{kk}$, $G = \frac{1}{2} G_{kk}$ and $C = \frac{1}{2} C_{kk}$

The wall-reflection term, $\phi_{ij,w}$, is modeled as:

$$\phi_{ij,w} = C_1 \frac{\varepsilon}{k} \left(\overline{u_k' u_m'} n_k n_m \delta_{ij} - \frac{3}{2} \overline{u_i' u_k'} n_j n_k - \frac{3}{2} \overline{u_j' u_k'} n_i n_k \right) \frac{k^{\frac{3}{2}}}{C_l \varepsilon d}$$

$$+ C_2 \left(\phi_{km} 2 n_k n_m \delta_{ij} - \frac{3}{2} \phi_{ik} 2 n_j n_k - \frac{3}{2} \phi_{jk} 2 n_i n_k \right) \frac{k^{\frac{3}{2}}}{C_l \varepsilon d}$$

(2.4.12)

where $C_1 = 0.5$, $C_2 = 0.3$, n_k is the x_k component of the unit normal to the wall, d is the normal distance to the wall, and $C_l = C_\mu^{3/4} / \kappa$, where $C_\mu = 0.09$ and κ is the von Karman constant (= 0.4187).

The production term due to buoyancy is modeled as:

$$G_{ij} = \beta \frac{\mu_t}{\text{Pr}_t} \left(g_i \frac{\partial T}{\partial x_j} + g_j \frac{\partial T}{\partial x_i} \right)$$

(2.4.13)

where Pr_t is the turbulent Prandtl number.

The dissipation tensor, ε_{ij}, is modeled as:

$$\varepsilon_{ij} = \frac{2}{3} \delta_{ij} \rho \varepsilon \quad .$$

(2.4.14)

The scalar dissipation rate, ε, is computed with a model transport equation similar to that used in the standard k-ε model:

$$\frac{\partial}{\partial t}(\rho\varepsilon) + \frac{\partial}{\partial x_i}(\rho\varepsilon u_i) = \frac{\partial}{\partial x_j}\left[\left(\mu + \frac{\mu_t}{\sigma_\varepsilon}\right)\frac{\partial \varepsilon}{\partial x_j}\right] +$$

$$C_{\varepsilon 1}\frac{1}{2}[P_{ii} + C_{\varepsilon 3}G_{ii}]\frac{\varepsilon}{k} - C_{\varepsilon 2}\rho\frac{\varepsilon^2}{k}$$

(2.4.15)

where $\sigma_\varepsilon = 1.0,, C_{\varepsilon 2} = 1.92$.

2.5 Summary

The models described in the preceding sections were chosen to best describe the three main flows taking place in lagoon aeration. For the first step of the analysis the Volume of Fluid Model was used along with the Reynolds Stress turbulence model. The VOF model was required in order to

account for the free surface flows taking place within the aerator, and the Reynolds Stress model was required to account for turbulence in the swirling flows present.

For the second step of the analysis a Lagrangian particle tracking method is used to compute the trajectories of a distribution of spherical droplets. As the interactions of these droplets with the continuous phase are also computed, the standard K-Epsilon turbulence model is applied to account for turbulence in the air surrounding the aerator.

For the third and final part of the analysis, the K-Epsilon turbulence model is again used to account for turbulence as the transport equations are solved in the three dimensional, single phase, basin domain, followed by the unsteady species transport equations to reproduce the tracer studies.

3   Prediction of Flows Produced by a Model Aerator

3.1 Problem Description

In order to reproduce the effect of the model aerator on the surrounding lagoon, it was first necessary to have a reasonably accurate description of the flow through the aerator itself. The model aerator as shown in Figure 3.1 is comprised of similar components to those of full-sized mechanical aerators used in the wastewater industry. The flow was driven by a 3.8 cm diameter impeller through a 0.2m long draft tube. Water is drawn up through the draft tube, and directed at the splash plate, where it moves radially outwards and begins to break up into droplets. The dimensions shown in Figure 3.2 reflect the typical values used for which most of the experimental data was collected; those dimensions were used in the computational study. The impeller was driven by a variable speed motor. Since most of the experimental trials were conducted with a motor speed which produced a flow rate of 3.1 L/s, the boundary conditions were set accordingly in the computational model.
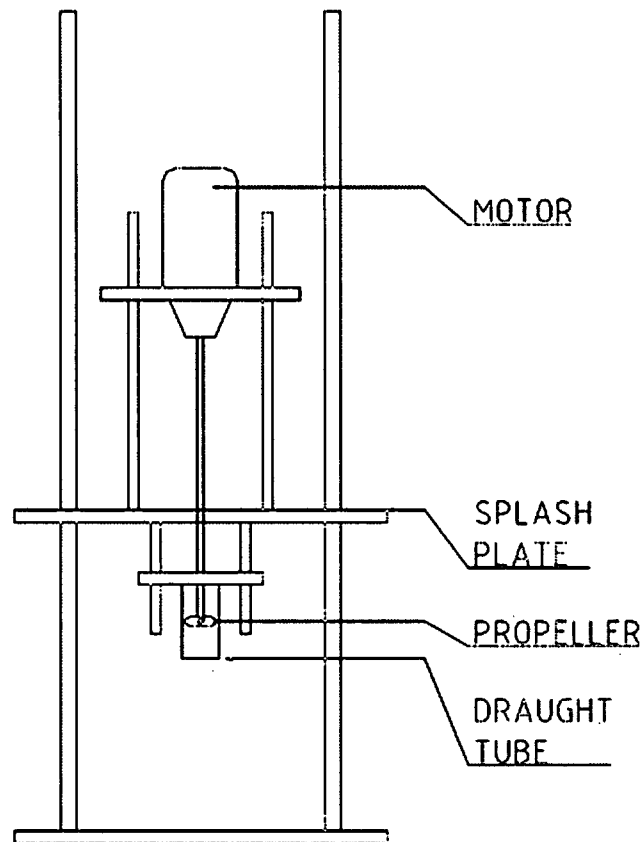
Figure 3.1: Model Aerator Schematic of Jenkinson [2]

3.2 Volume of Fluid Simulations

3.2.1 Computational Grid

A drawing of the grid used in the VOF simulations is shown in Figure 3.2. A rectangular grid was laid out over the domain with a spacing of 2 mm. Although uniform over most of the domain, the grid was coarsened up to 2.6 mm in the area above the splash plate. This was done in order to minimize the number of cells and therefore the computational time. A coarser grid was allowable in the area above the splash plate as the velocity in that area was not of specific interest to this study. This spacing produced grid of 6995 cells. The grid could have been made finer, but in the interest of speeding up the convergence of an initial solution this spacing was chosen.

y=0.19m

X=0.192m

Splash Plate

Axis of Symmetry

X=0.142m

X=0.092m

X=0.072m

y=0.29m

Draft Tube Walls

Water Inlet

X=0m

y=0.02m
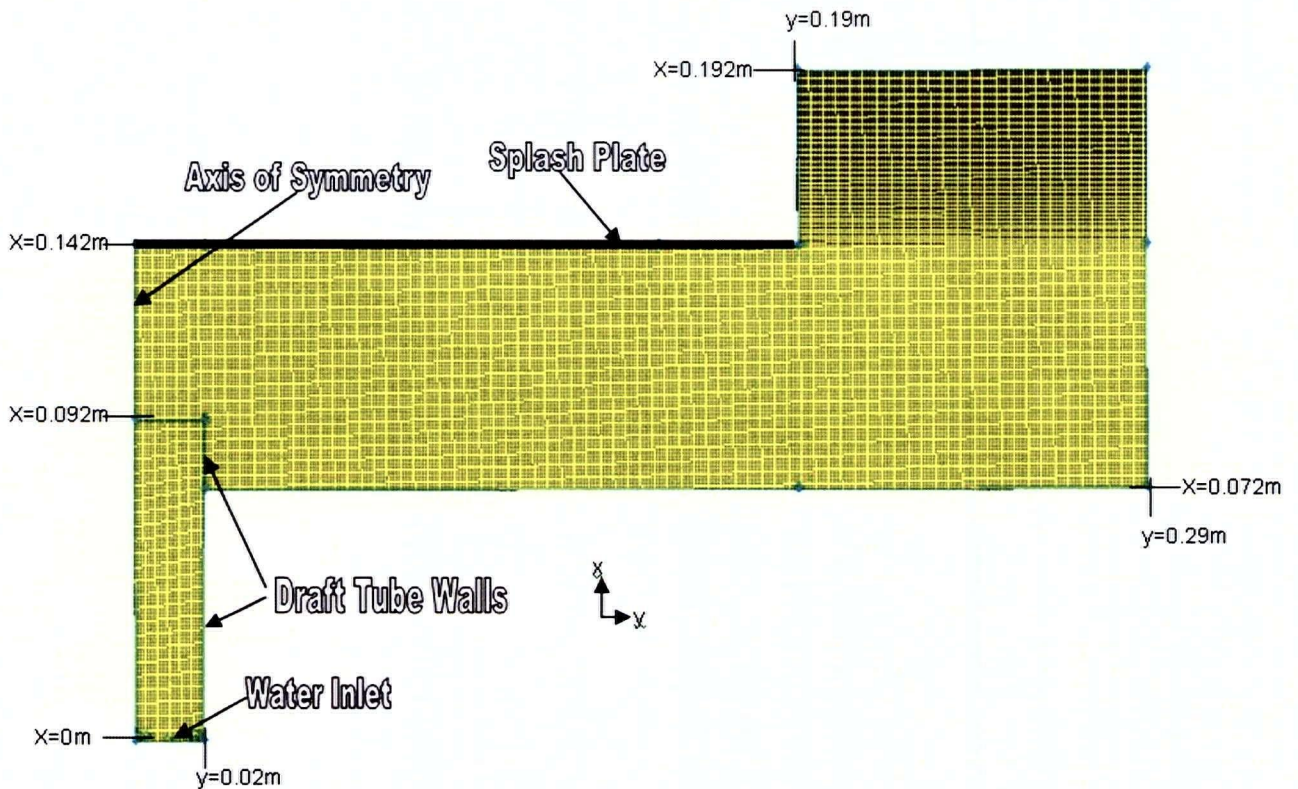
Figure 3.2: Computational Grid

3.2.2 Boundary Conditions

The boundary conditions were set as to best reproduce the experimental model. The following

conditions, are applied, along with the chosen mathematical models in order to solve for u, v, P, α, k

and ε.

Water Inlet

Water Inlet	
Vx	2.47m/s
Vy	0m/s
Ω	0rad/s
Turbulence Intensity	20%

Table 3.1: Inlet Boundary Conditions

The boundary shown as water inlet was set as a prescribed velocity. Immediately following an impeller, highly turbulent, swirling flows are produced. Analyzing the exact flows following the specific geometry of the impeller used in this experiment is beyond the scope of this study. A uniform velocity at the inlet was assumed and applied in order to simplify the simulation. The set boundary conditions are listed in Table 3.1.

Wall Boundaries

Both the splash plate and draft tube boundaries are set as no-slip, zero-flux walls. As the flow is presumed to be fully turbulent, the law-of-the-wall model is used to determine the wall shear stress and turbulent parameters based on the flow profile near the wall. The equations used to compute the wall shear stress are shown below as described in FLUENT documentation [12]:

$$\tau_w = \frac{\rho C_\mu^{0.25} k_p^{0.5} \kappa U_p}{\ln(E \cdot y_p^+)} \qquad (3.1)$$

$$y^+ = \frac{\rho C_\mu^{0.25} k_p^{0.5} y_p}{\mu} \qquad (3.2)$$

where

k_p = turbulent kinetic energy at point P (m^2/s^2),

U_p = mean velocity of the fluid at point P (m/s),

E = empirical constant (9.81),

y_p = distance from point P to wall (m),

κ = von Karman's constant (0.42), and

C_μ = k-ε turbulent model constant (0.09).

Outlet Boundaries

At all outlet boundaries constant atmospheric pressure (P=101 kPa) was imposed.

3.2.3 Solution Procedure

As previously described in Chapter 2 the volume of fluid (VOF) model was used to compute the phase distribution throughout the domain. Turbulence was computed using the Reynolds Stress turbulence model. In order to solve these equations over the chosen grid it was first required to initialize a solution for the volume fraction of each phase in the domain. The area representing the draft tube was initialized to contain water and the remainder of the domain was initialized to contain only air as shown in Figure 3.3.
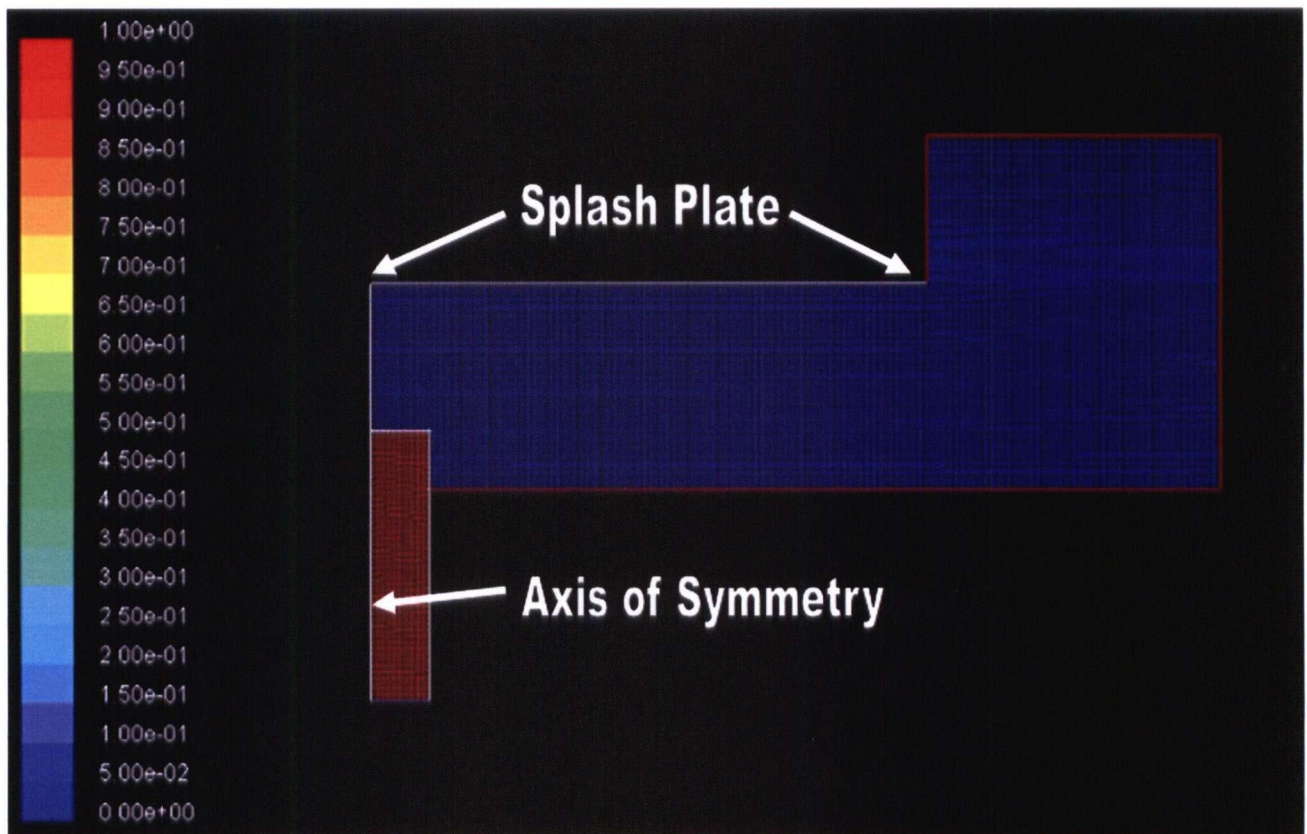
Figure 3.3 Initial Volume Fraction of Water

Using the previously mentioned boundary conditions and the initial phase distribution shown, the initial solution had to be marched forward in time. It was found that, in order to march the solution forward in time from the initial condition, a time step of 10 µs was required. At the end of each

iteration the residual sum for each of the conserved variables is computed and stored. These

residuals are computed as described in Appendix A. The solution is only marched forward in time

once the scaled residuals decrease to a preset value. The FLUENT documentation claims that the

default residual value of 0.001 for continuity, u, v, k and ε are sufficient for most problems, and

therefore this value was used as the convergence criterion. The solution was marched forward until

the water passed the edge of the splash-plate and began to exit the right of the domain. This steady

state was achieved approximately 0.5 seconds from the initial conditions. It did however require 3

days to solve the equations to this point on a 2 GHz Pentium processor. Shown in Figure 3.4 is the

volume fraction distribution.
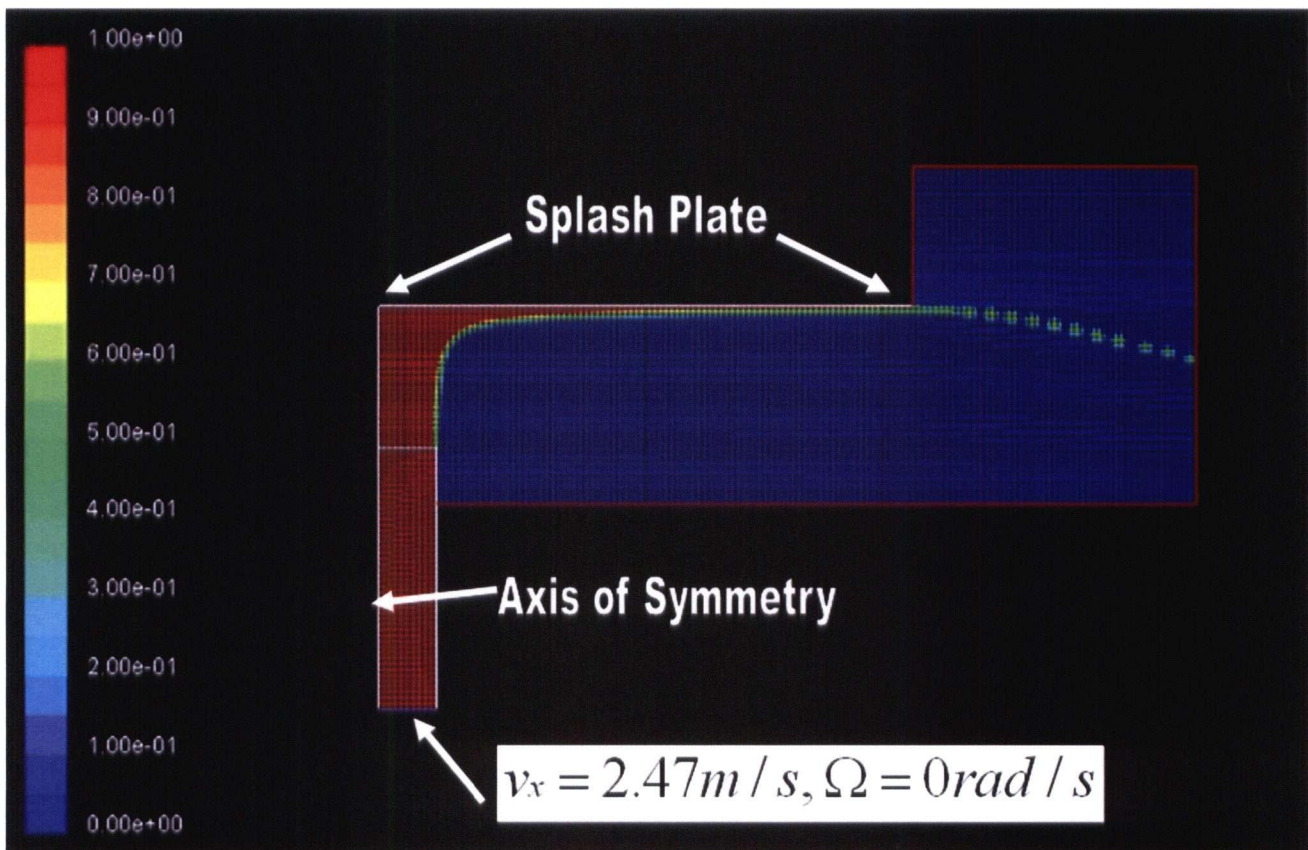
Figure 3.4 Contours of Volume Fraction of Water t=0.5s

The green area represents cells in which both phases exist. Since one assumption of the VOF model is that the two fluids are not interpenetrating, these cells contain the computed boundary between the two fluids. This problem is axisymmetric, which results in the total mass flux passing through an ever decreasing number of cells as the water moves along the plate. For a grid spacing of 2 mm the result is that all of the water passes through no more than two cells. It was therefore decided to refine the grid locally, in the cells which contain water in the initial solution.
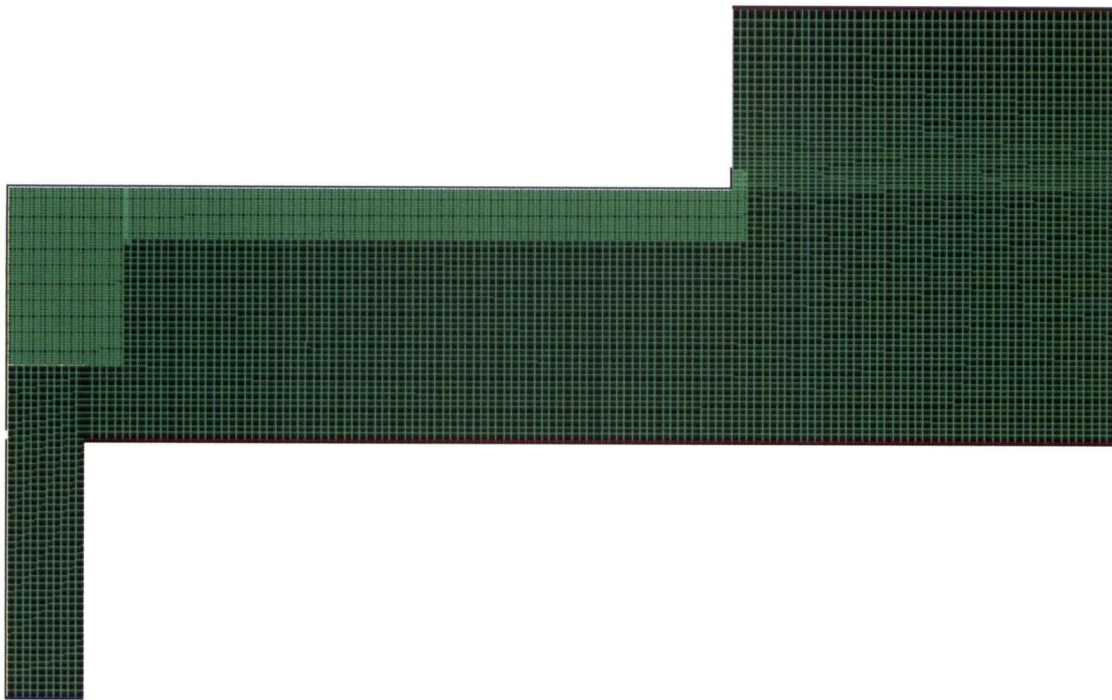
Figure 3.5: Refined Grid

The grid was refined locally by a factor of two, with a new cell spacing of 1 mm as shown in Figure 3.5. The initial solution was applied to the new grid, and allowed to run until the solution reached a steady state. Although the area beneath the splash-plate contains twice as many cells in the second case, the film of water near the edge of the plate is thinned to such an extent that is still only

contained within three cells. It was therefore decided to repeat the process of refining the grid and

converging a solution twice more. As convergence became much slower with each successive grid

refinement, the grid was only refined in the area containing water, beneath the splash plate in each

case. In order to check convergence, the mass flux at the edge of the splash plate was computed after

each refinement. With each successive refinement, the result approached the exact value of 3.1kg/s

as shown in Figure 3.6. The final grid spacing was set at 0.112 mm.
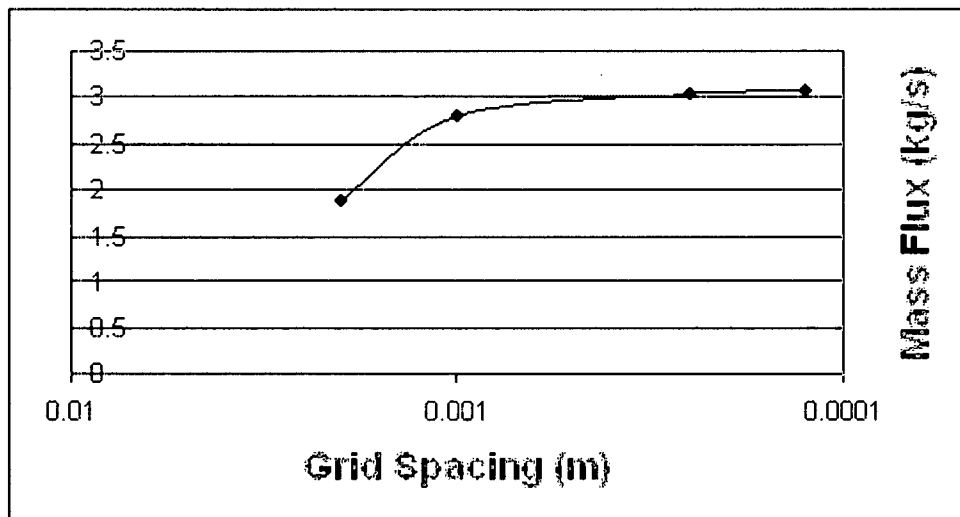
Figure 3.6: VOF Grid Convergence

3.2.4 Phase Distribution Results and Discussion

The final, refined phase distribution is shown in Figure 3.7.
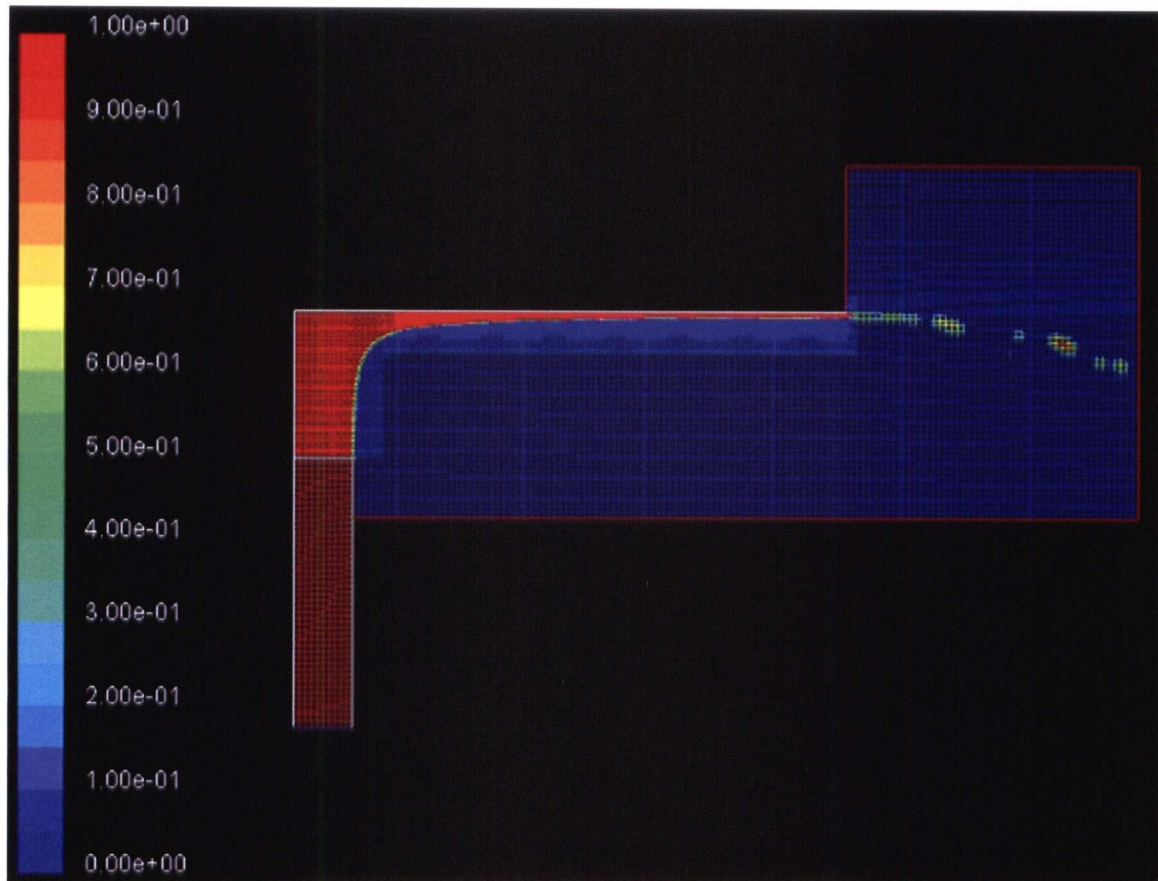
Figure 3.7: Volume Fraction of Water

In this final grid, the thickness of the stream leaving the plash plate occupies 10 cells. This allows

for a reasonable velocity profile of the water stream to be computed at the edge of the splash plate.

The finest grid consisted of 56,668 cells. At this level of refinement convergence behavior began to

slow considerably. Velocity contours of both phases are shown in Figure 3.8.
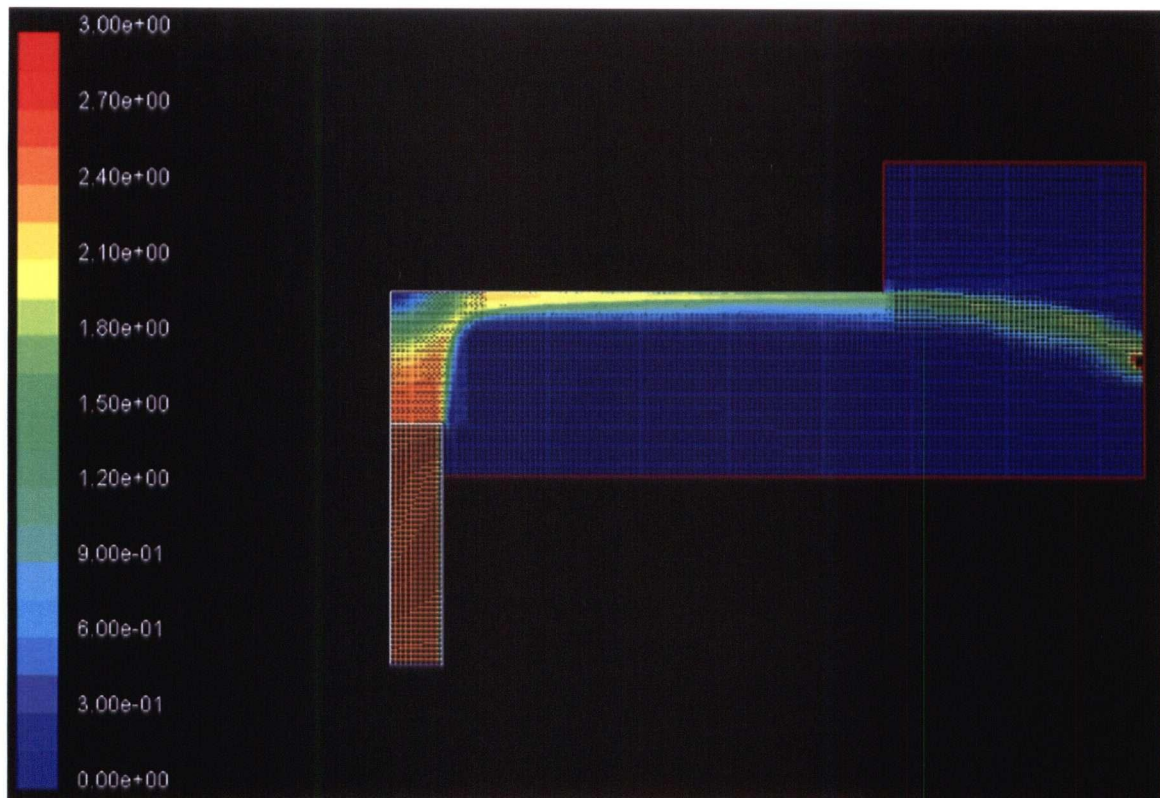
Figure 3.8: Velocity Magnitude Distribution (m/s)

3.2.5 Swirl Velocity Analysis

As the impeller on any aerator imparts momentum to the flow, significant swirl velocities will

invariably exist in the region following the impeller. The presence of swirl velocities may

significantly affect the flow regime in the lagoon. Although the specific swirl velocities will vary

tremendously depending on impeller rpm and geometry, it has been shown that typical swirl

velocities may be in the range of 10 to 30 rad/s for an impeller similar in size to that of an industrial

aerator [8]. As the rpm of the impeller used in the experimental apparatus is unknown, swirl

velocities of 80 and 160 rad/s were applied at the inlet in order to provide some initial solutions and

study swirl velocities throughout this type of geometry. An applied swirl velocity of 160rad/s

imposes a maximum swirl velocity similar in magnitude to the axial velocity in the draft tube. The

angular momentum imparted by the impeller could increase the radial velocities at the edge of the

splash plate/diffusion head, or it is also possible significant swirl velocities will remain throughout

the domain thereby imparting a tangential component to the droplets and therefore a tangential component to the momentum imparted to the lagoon. Figure 3.9 shows the swirl velocity for the experimental aerator domain with a swirl velocity of 160 rad/s as well as the three points used for computing velocity profiles.
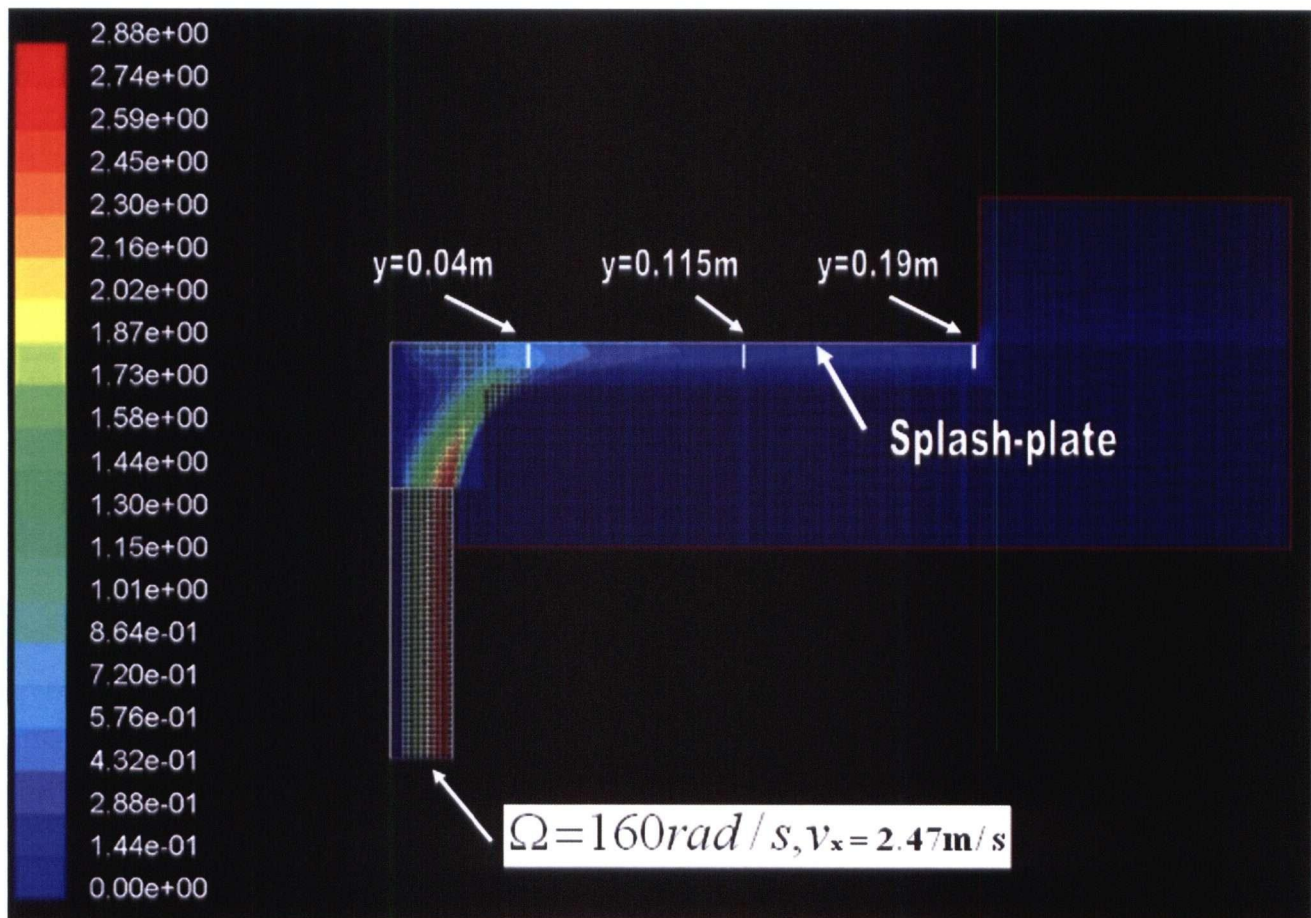
Figure 3.9: Contours of Experimental Aerator Swirl Velocities (m/s)
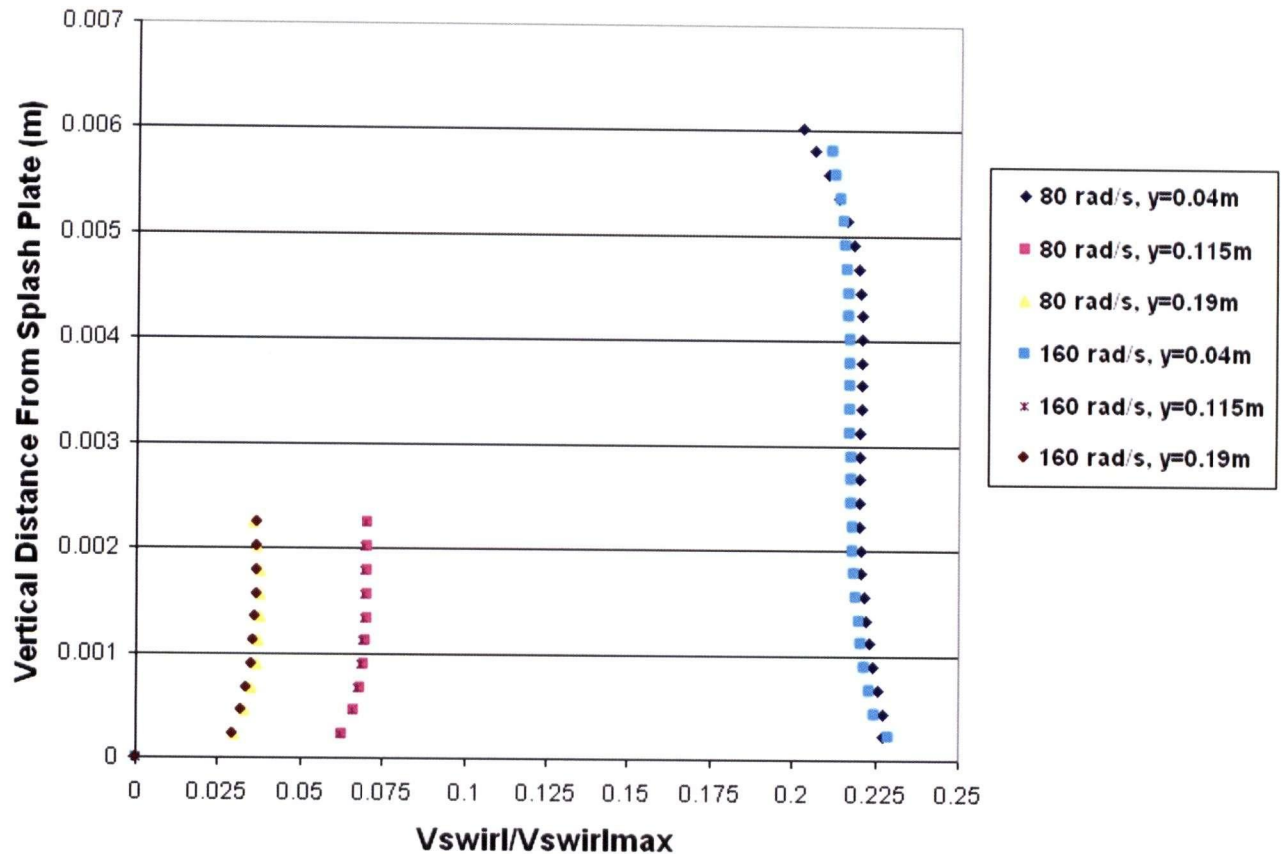
Figure 3.10: Computed Model Aerator Swirl Velocities

Figure 3.10 shows the plots of the swirl velocity profiles at the points shown in Figure 3.9.

Kelvin's Circulation theorem states that the circulation about any contour containing the same fluid

particles is constant for an inviscid, incompressible fluid. For a roughly flat swirl velocity profile

spreading over the splash-plate we should then expect the swirl magnitude to decrease linearly with

increasing radius. If we look at the plots of Vswirl/Vswirlmax in Figure 3.10 we see that they are in

the range of 0.175-0.25 at a radial position of 0.04m. If we increase the radial position by a factor of

approximately 3 or to 0.115m we find values of Vswirl/Vswirlmax in the range of 0.05 to 0.075.

Similarly, when the radial coordinate is increased from 0.115m to 0.19m the values of

Vswirl/Vswirlmax lie in the range of 0.025 to 0.04. Naturally, we cannot expect perfect agreement

with Kelvin's theorem as this is not an inviscid flow, however for this simulation reasonable

agreement with Kelvin's theorem is found. Figures 3.11, 3.12 and 3.13 show the radial velocity

profiles and the points shown in Figure 3.8. The simulations indicate that very little of the excess

energy added to the flow via swirl is transferred to the radial velocity component.
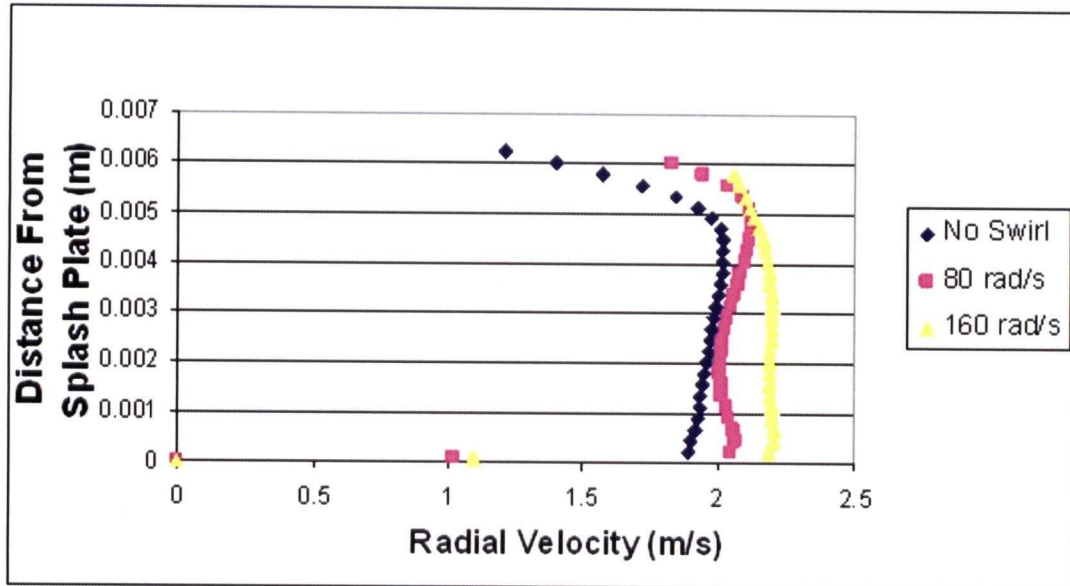
Figure 3.11: Radial Velocity Profiles y=0.04m
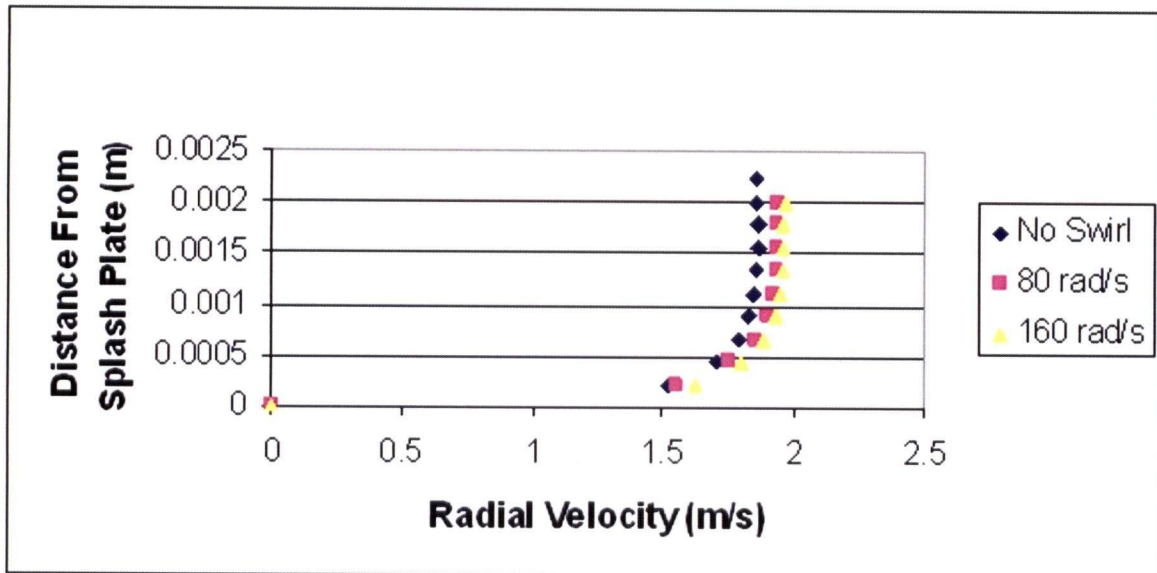
Figure 3.12: Radial Velocity Profiles y=0.115m
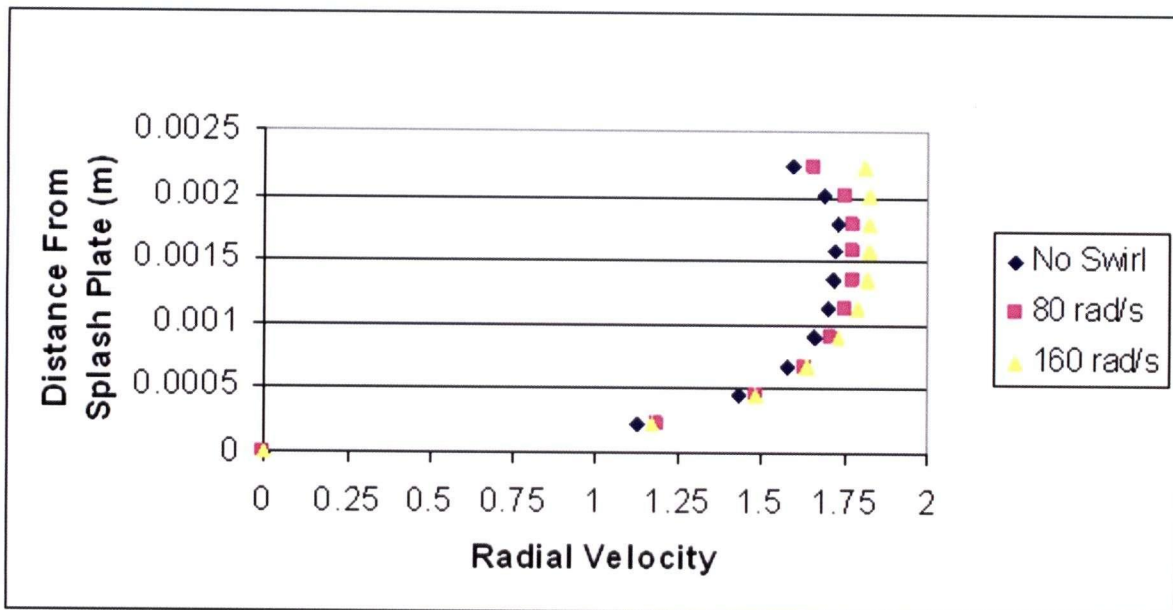
Figure 3.13: Radial Velocity Profiles y=0.19m

It has been shown through the volume of fluid analysis that no more than 2.5% of the maximum

applied swirl velocity magnitude remains at the edge of the splash-plate of the experimental

apparatus. This seems plausible as the splash plate extends radially outwards by 0.19m compared to

the draft tube radius of 0.02m. According to Kelvin's theorem this would account for a drop of 9

tenths of the maximum applied swirl velocity. This geometry is slightly more complex than a simple

plate in that it involves the passage of fluid upwards through the draft tube and a sharp turn as it

strikes the plate. Combined with viscosity effects, this may account for the rest of the losses. The

radial velocity at the edge of the splash-plate increased by no more than 9% when 160rad/s of swirl

was applied at the inlet. As it is evident that the addition of swirl has very little effect on the flow

leaving the experimental aerator when reasonable magnitudes are applied, the presence of swirl is

neglected in subsequent calculations pertaining to the experiments of Jenkinson [2].

3.3 Droplet Trajectory Calculation

The discrete phase method described in Section 2.2 is used to compute the trajectories of particles leaving the aerator. These calculations have been performed with the assumption of a complete breakup of the jet at the edge of the splash-plate.

3.3.1 Droplet Size Distribution

Sprays generated by disintegrating sheets of fluid do not produce droplets of uniform diameter. The droplet diameter affects the drag force on the droplet, and therefore the trajectory of the droplet. Because this calculation assumes spherical droplets, a reasonable diameter distribution must also be assumed. The most widely used diameter distribution to date is that proposed by Rosin and Rammler [9]. It may be expressed in the following form:

$$1 - Q = \exp{-\left(D/X\right)^q} \tag{3.3}$$

Where Q is fraction of the total volume contained in drops of diameter less than D. It is possible to describe the droplet distribution in terms of the two parameters X and q. The parameter q provides a measure of the spread of drop sizes. The higher the value of q, the more uniform the spray. As the true range of droplet diameters is unknown, maximum and minimum droplet diameters were set at 3 and 0.5 millimeters respectively with an average diameter of 1 millimeter. This range was obtained using values of 2.5 and 0.0012 for q and X respectively. The distribution, shown in Figure 3.14, is used as a starting point to produce a splash zone distribution and study the effects of diameter on landing radius.
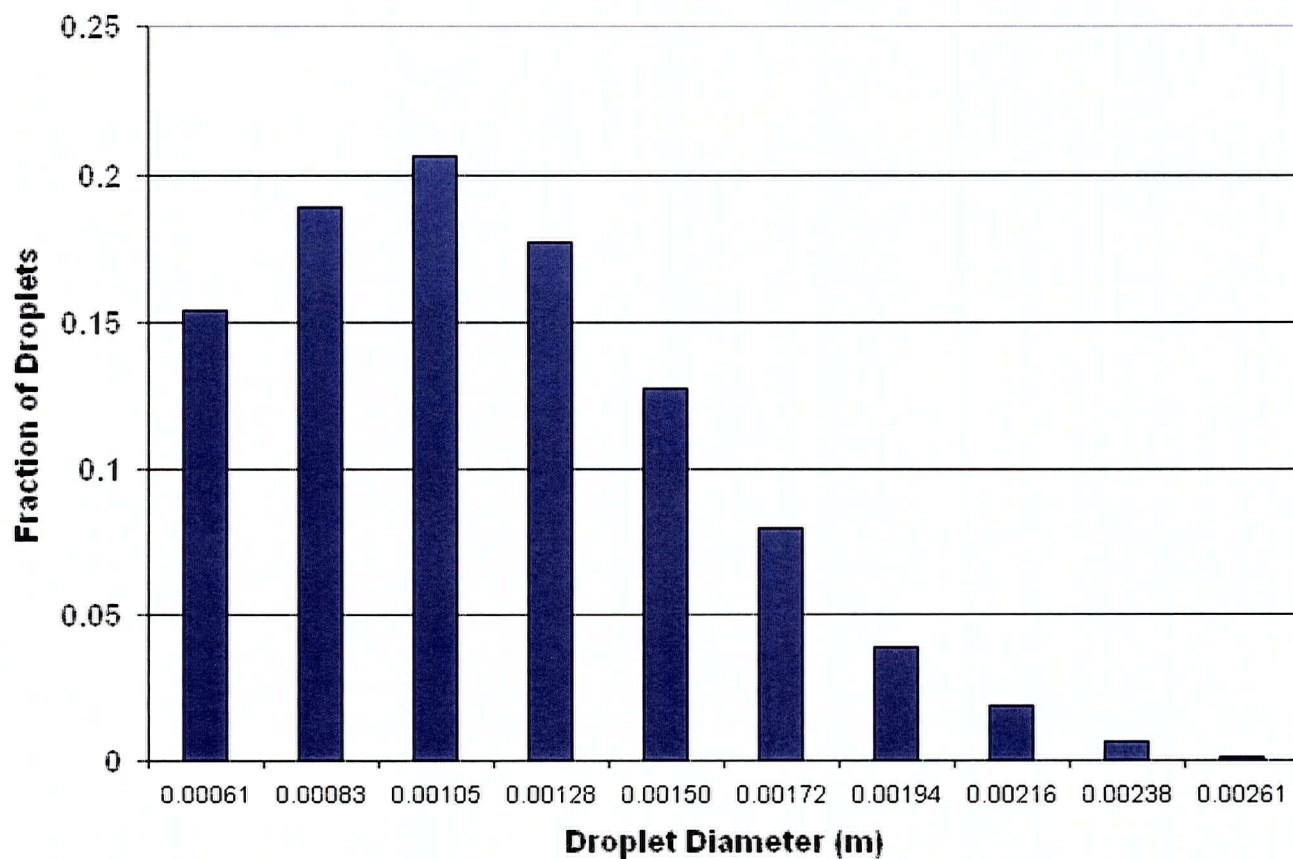
Figure 3.14: Rosin-Rammler Droplet Diameter Histogram

3.3.2 Computational Grid

The computational grid used encapsulates a similar area to that of the 2 phase simulation and is

shown in Figure 3.15.
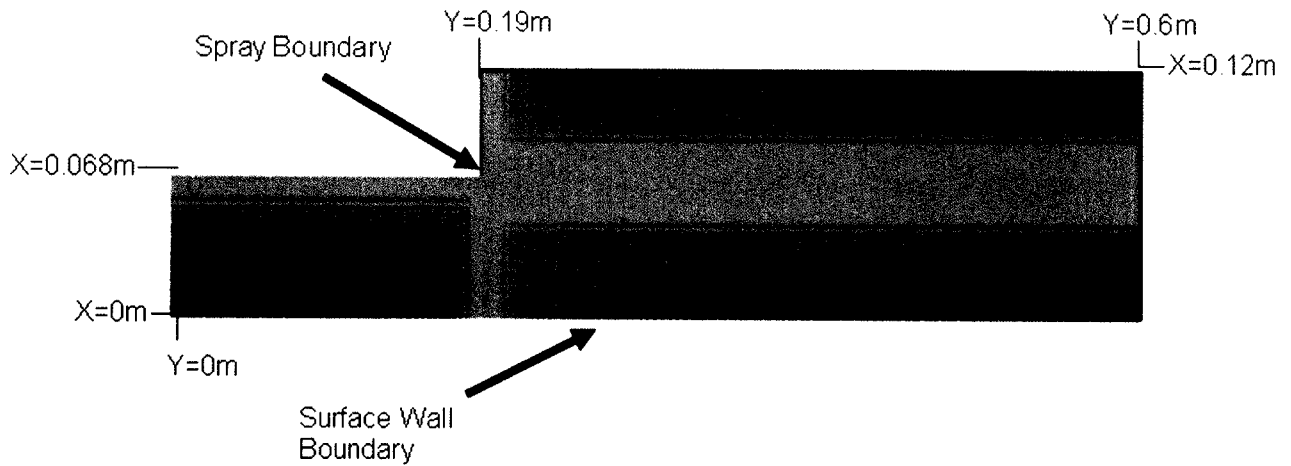
Figure 3.15: Initial Grid

This domain was used to simulate the trajectory of the droplets from the tip of the splash-plate, to the model lagoon surface. As the motion of air surrounding the spray is critical to the drag force on each droplet, the domain includes the volume both beneath and above the splash plate. The initial grid spacing was varied from 44 μm in the region surrounding the spray boundary. In the far corners of the domain, where exact air velocities are of little interest, the grid was coarsened up to 1.5 cm. This grid was used to obtain an initial solution.

3.3.3 Boundary Conditions

Similar boundary conditions were used for this phase of the calculations. At all boundaries with the exception of the lagoon surface constant atmospheric pressure (P=101 kPa) was imposed. The lagoon surface was set as a free slip condition. The Spray boundary shown in Figure 3.14 was divided into 9 separate surfaces which where set as particle sources. The particle sources were each assigned mass fluxes and velocity components based on the velocity profile computed in the Volume of Fluid calculation as shown in Table 3.2.

Source	Height from Surface (m)	Mass Flux (kg/s)	Radial Velocity (m/s)	Axial Velocity (m/s)
1	0.0701	0.006	1.540	0.0360
2	0.0699	0.300	1.558	0.0375
3	0.0697	0.391	1.611	0.0291
4	0.0695	0.396	1.631	0.0255
5	0.0693	0.398	1.639	0.0184
6	0.0691	0.399	1.645	0.0128
7	0.0688	0.401	1.653	0.0048
8	0.0686	0.401	1.653	-0.0138
9	0.0684	0.393	1.645	-0.027

Table 3.2: Particle Sources

3.3.4 Solution Procedure

In order to obtain a solution for this simulation, a solution for the continuous phase must first be initialized. Having set the velocity field to zero in the domain, the solution process involves computing the particle trajectories for the current continuous phase solution. Following this step, the momentum imparted to the continuous phase is calculated from the particle trajectories. A solution for the velocity field in the continuous phase is then obtained, and the process is repeated again. After several cycles the continuous phase residual remains very low after each trajectory calculation, and eventually converges to the set residual value. Once an initial solution was obtained, the grid was refined in the region surrounding the particle trajectories as shown in Figure 3.16. The grid size was reduced to 0.119 mm. This was done in order to increase the accuracy of the continuous phase flow field surrounding the particle streams, as well as to provide better accuracy for the landing points of the particles.
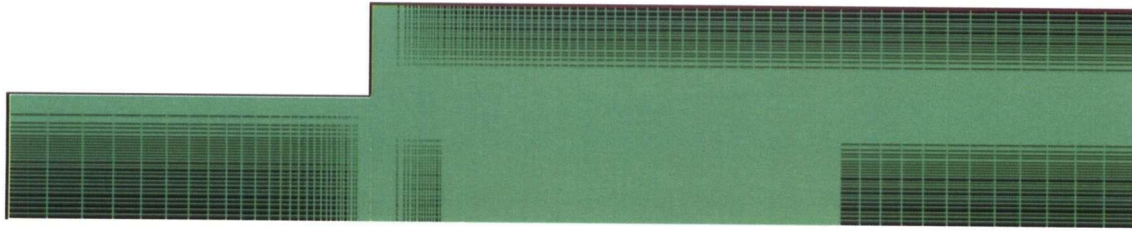
Figure 3.16: Refined Grid

3.3.5 Droplet Trajectory Results and Discussion

The trajectories of the assumed particle distribution from the edge of the splash plate to the surface of the model lagoon are computed and shown in Figure 3.17.
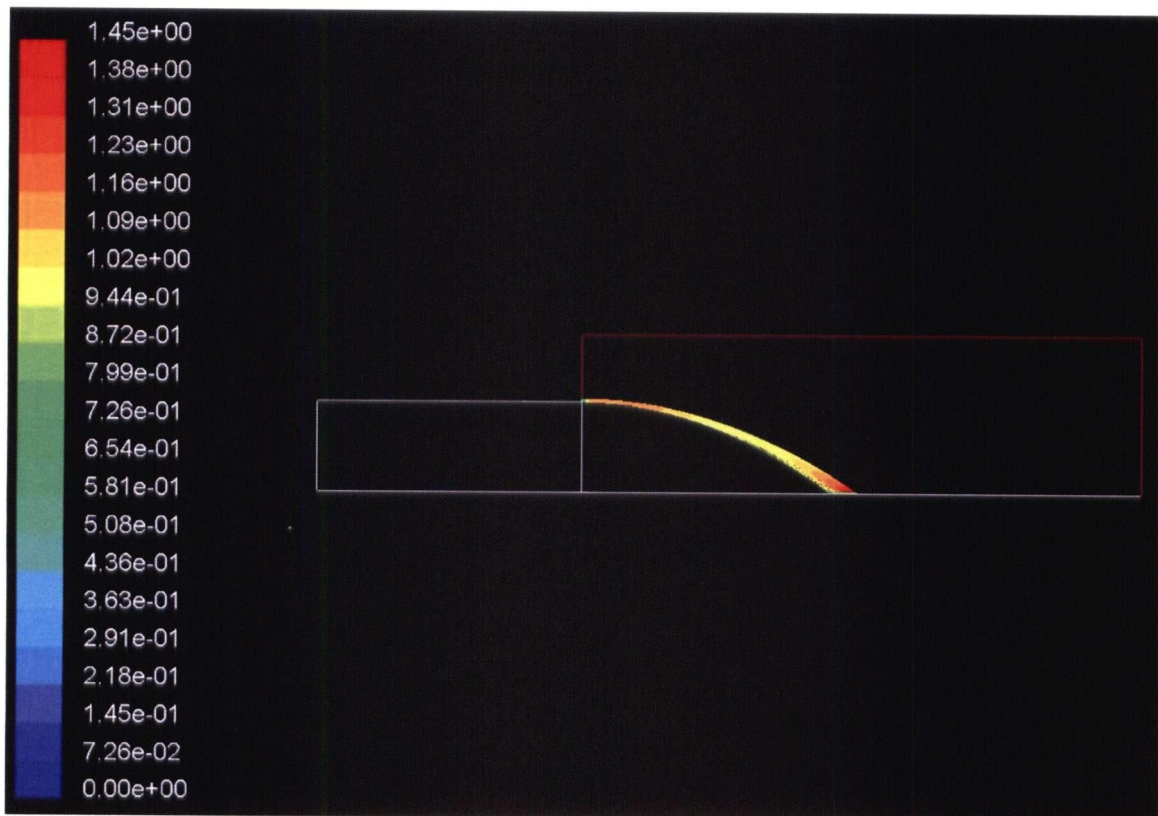
Figure 3.17: Particle Trajectories Colored by Velocity (m/s)

Although some spread is observed, all the droplets land between 0.37 m and 0.39 m from the aerator.

A plot of the splash zone mass flux is shown in Figure 3.18.
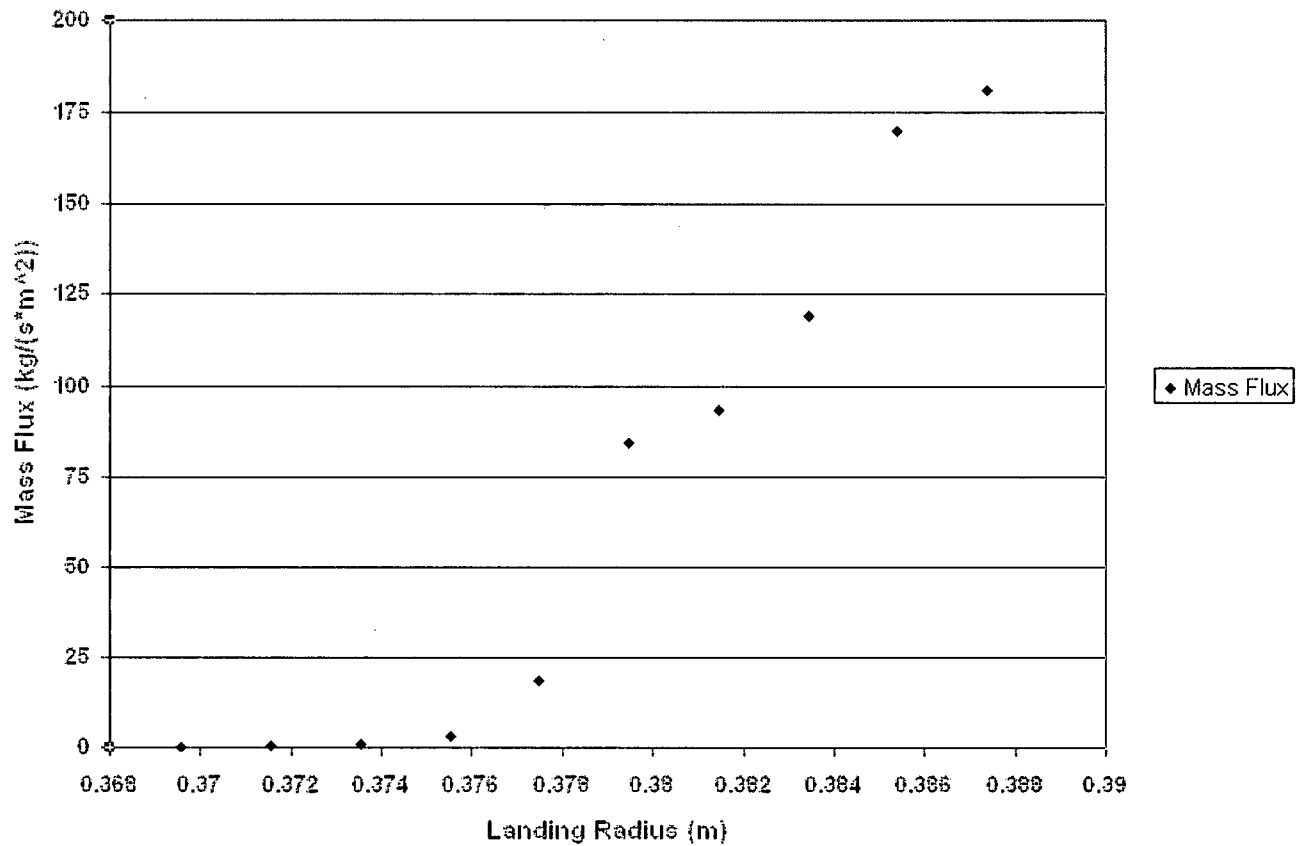
Figure 3.18: Splash Zone Mass Flux

The highest mass flux is at the outer rim of the splash zone. This is due to the fact that the largest

droplets go the farthest. If we observe the velocity vectors of the continuous phase shown in Figure

3.19 we see that in the vicinity of the stream of particles, the air velocity reaches that of the particles.
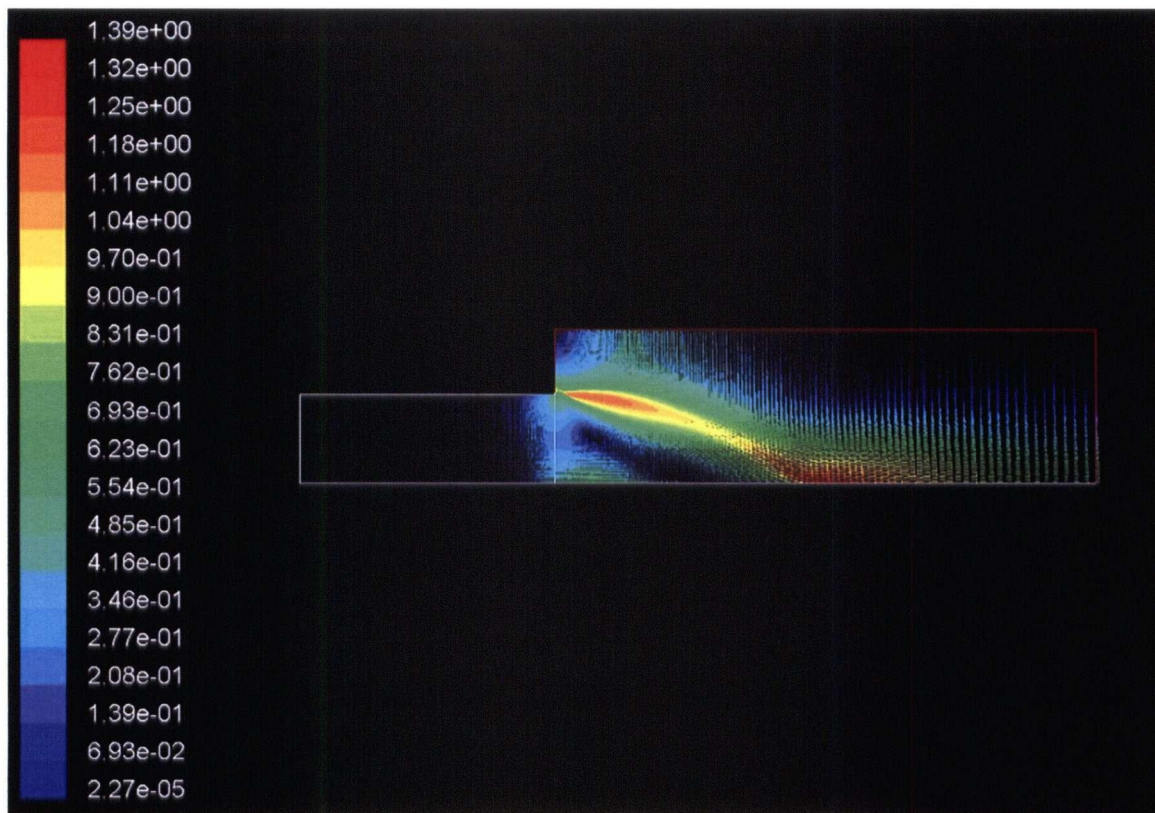
Figure 3.19: Continuous Phase Velocity Vectors Colored by Velocity (m/s)

Since the relative velocity air velocity with respect to the particles then becomes very small, the

drag force on the particles becomes very small. There is therefore very little difference in particle

trajectory based on particle size. A ballistics calculation, neglecting drag effects, results in a landing

radius of 0.38m, which implies that the droplet trajectory is nearly ballistic. Another reason the

droplets land in such a narrow range of radii may be due to the assumption of complete breakup at

the splash plate edge. The stream of water is most likely breaking up into droplets all along the

splash plate. It would be difficult to perform this type of calculation by assuming several particle

sources along the splash plate as the particle source velocities are based on the velocity profile from

the Volume of Fluid calculation. If mass were removed upstream of the plate edge, the downstream

flow would be affected. The final limitation of the discrete phase model used is that the effects of

secondary splash are completely neglected. In reality when a droplet strikes a body of water, part of

it may be absorbed by the surface, imparting mass and momentum to the fluid via waves on the

surface and currents beneath the surface. Some of the droplet may bounce off the surface, imparting some momentum initially, and then imparting more mass and momentum at successive landing points. A third possibility is that when the droplet strikes the lagoon surface, momentum is imparted in such a way that it causes some of the body of water to form new droplets. It is most likely that the splash zone is formed be a chaotic combination of these three phenomena which are beyond the capabilities of both the codes available and the computational power at our disposal. It was noted that the maximum extent of the splash zone was 50 cm in radius when the experiments were performed. Although some of this discrepancy may be due to inaccuracies carried over from the volume of fluid calculation, it is most likely due to the fact that all secondary splash phenomena were neglected. It seems quite reasonable that most of the droplets landed in the 38cm range and that secondary splash phenomena extended the observed splash zone to approximately 50cm. For these reasons there is little to be gained from refining the splash zone further. Any perceived increase in precision would be lost in the basin simulations due to the vast differences in length scales. These results provide a basis for modeling the presence of an aerator in the single phase, model lagoon simulations described in Chapter 5.

3.4 Summary

Using the Volume of Fluid model, the flow field throughout the experimental aerator used by Jenkinson was calculated. A velocity profile at the edge of the splash plate was calculated with the intention of applying the result to a droplet trajectory calculation. The propagation of swirl velocities throughout the domain was also evaluated and it was found that only 2.5% of the maximum applied swirl velocity magnitude remained at the edge of the splash plate. The splash plate edge velocity profile obtained was used to create a series of particle sources, based on the assumption of a complete jet breakup at the edge of the splash plate. Droplet trajectories were calculated to the lagoon surface taking into account the interactions with the surrounding air. Considering the fact

that secondary splash was neglected, the splash zone radius obtained compares favorably with experimental observations. The computed splash zone radius obtained is identical to what would have been obtained from a simple ballistics calculation, as the high air velocities surrounding the particles made for negligible drag effects.

4   Prediction of Flows Produced by a 75hp Aerator

4.1 Problem Description

Having developed a reasonable method of analyzing the flows through an experimental sized

aerator, the next logical step is to simulate the flow through a typical full-sized 75hp aerator. Given

that the geometry and Reynolds numbers differ significantly between the two situations, very

different results can be expected. A cutaway picture of a full sized aerator is shown in Figure 1.6.

Unlike the experimental setup, there is a smooth curved diffusion head as opposed to a flat plate.

Furthermore, the diffusion head does not extend out more than two draft tube radii, whereas in the

experimental case the splash plate has a radius ten times larger than that of the draft tube. These

geometry changes are likely to produce different flow patterns and losses within the aerator.

Although aerators are manufactured in a wide range of sizes varying from one to 150 horsepower,

one given size had to be chosen to perform the calculation. The commonly used, midrange 75 hp

model manufactured by Aqua-Aerobic Systems was chosen.

4.2 Volume of Fluid Simulations

4.2.1 Computational Grid

The grid was designed with the same basic methodology as for the experimental case, the main

difference being the presence of the diffusion head. The grid was set as fairly fine with a spacing of

5 mm underneath the diffusion head, as this is the primary area of interest for this particular

calculation. The grid was coarsened up to 3 cm in the far corners of the grid where only some

circulating air was expected, which was of no interest in this study. The grid is shown in Figure 4.1.

Boundary conditions were set in the same fashion as with the model aerator solution with the

diffusion head and draft tube represented by wall boundaries with shear computed as described in

Section 3.2.2. All other boundaries are fixed as constant atmospheric pressure (P=101325Pa).

Water Inlet	
Vx	6.2m/s
Vy	0m/s
Ω	0rad/s
Turbulence Intensity	20%

Table 4.1: Inlet Boundary Conditions
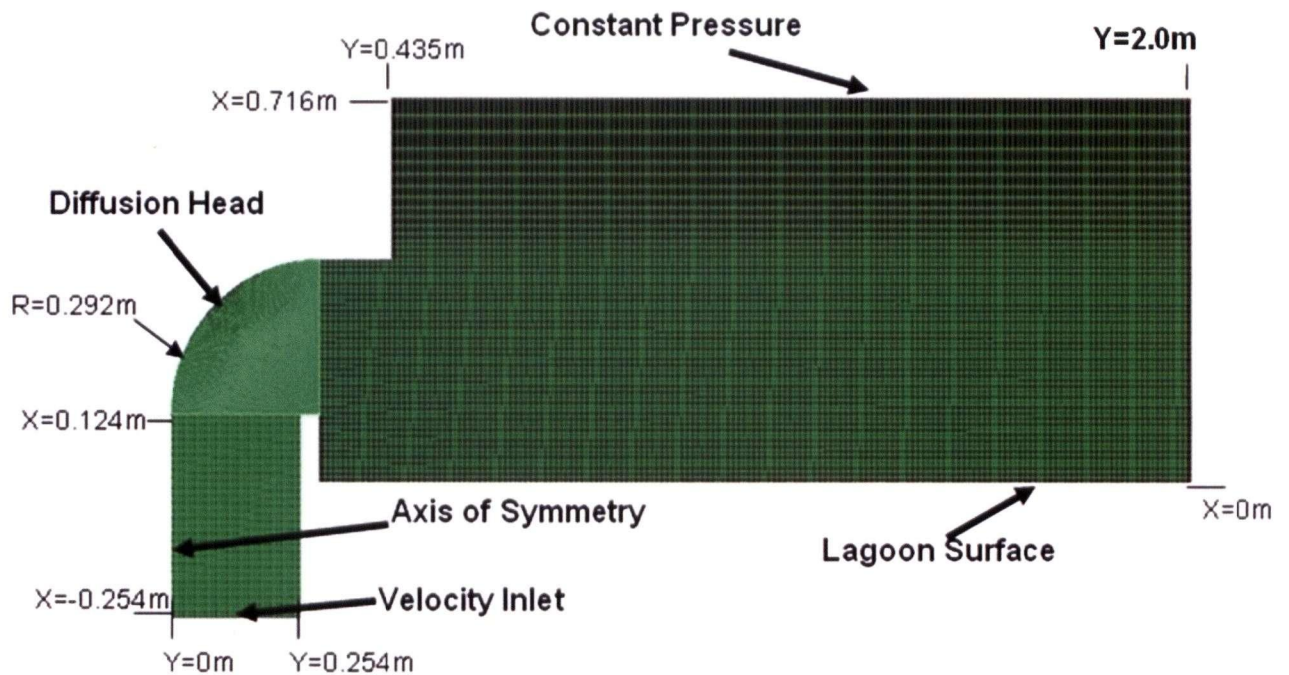
Figure 4.1 Computational Grid

4.2.2 Volume of Fluid Results

The same solution procedure was applied for the 75hp case as for the experimental aerator. An initial phase distribution was set, with the draft tube containing only water and the remainder of the domain containing only air. The solution was then marched forward in time with a time step of 100 μs. It was found that for this case convergence was obtained within a few iterations on virtually every time step, providing a phase distribution within approximately 36 hours. The calculated phase distribution is shown in Figure 4.2.
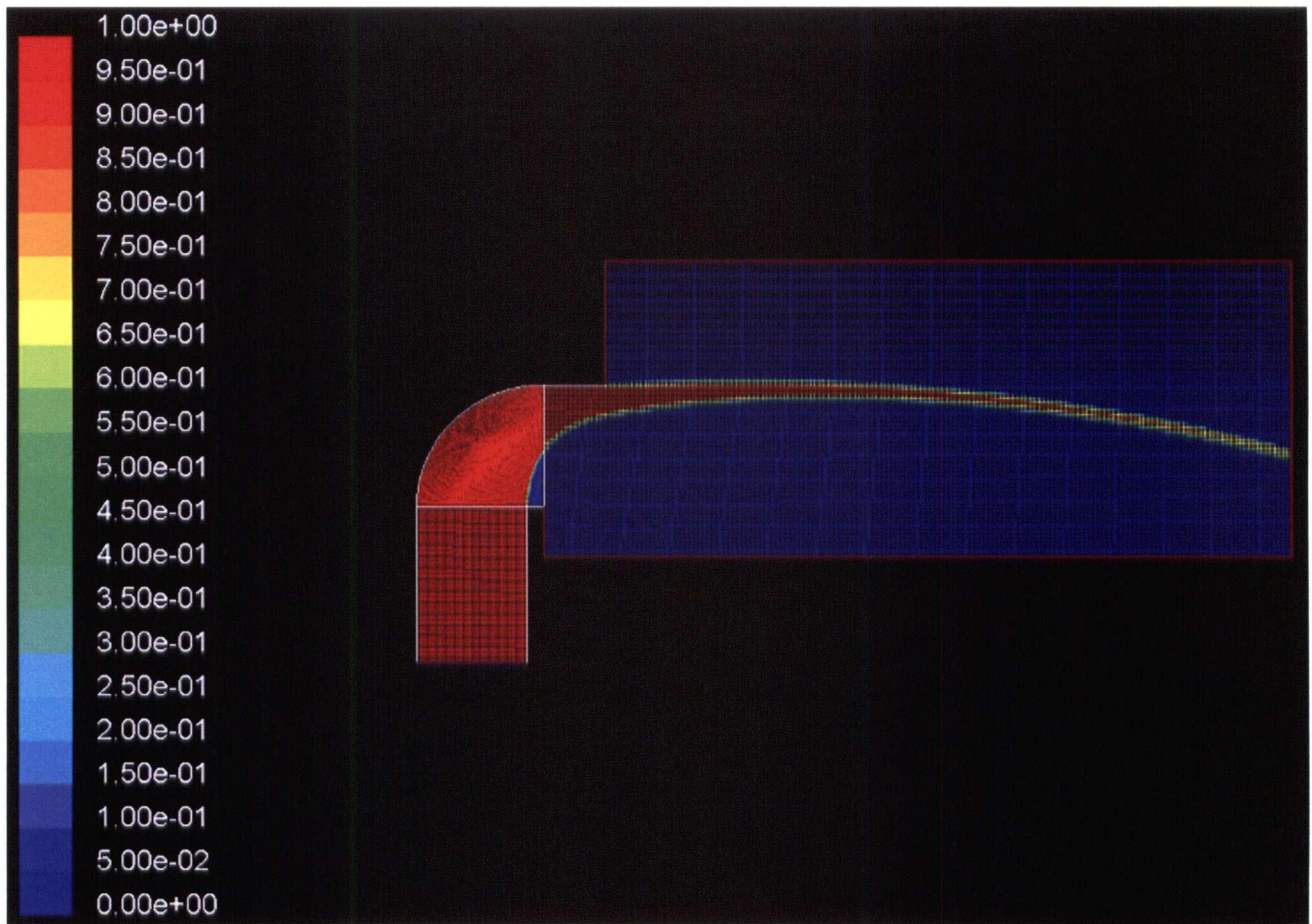
Figure 4.2: 75hp Aerator Water Volume Fraction

The grid was then refined by a factor of two in the cells containing water, and the solution was again

marched forward in time.   The velocity distribution throughout the domain is shown in Figure 4.3.

In this case, the velocity at the edge of the splash plate is only slightly higher than the velocity in the

draft tube. Unlike in the experimental setup, the flow of water can hardly be considered a free jet the

moment it leaves the draft tube. A stagnant region forms along the diffusion head, causing an

increase in pressure in the draft tube and a corresponding velocity increase at the edge of the

diffusion head. The velocity profile at the edge of the diffusion head is plotted in Figure 4.7,

showing a maximum velocity of 6.7m/s.
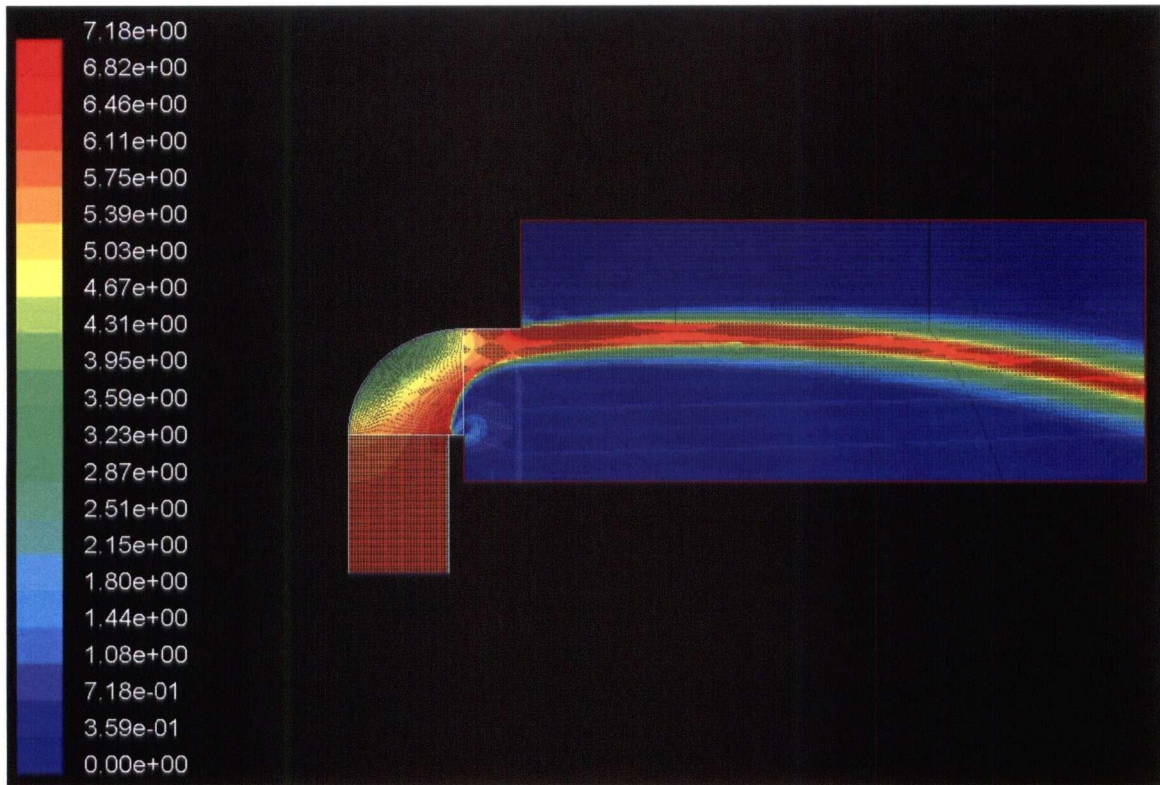
Figure 4.3: 75hp Aerator Velocity Distribution (m/s)
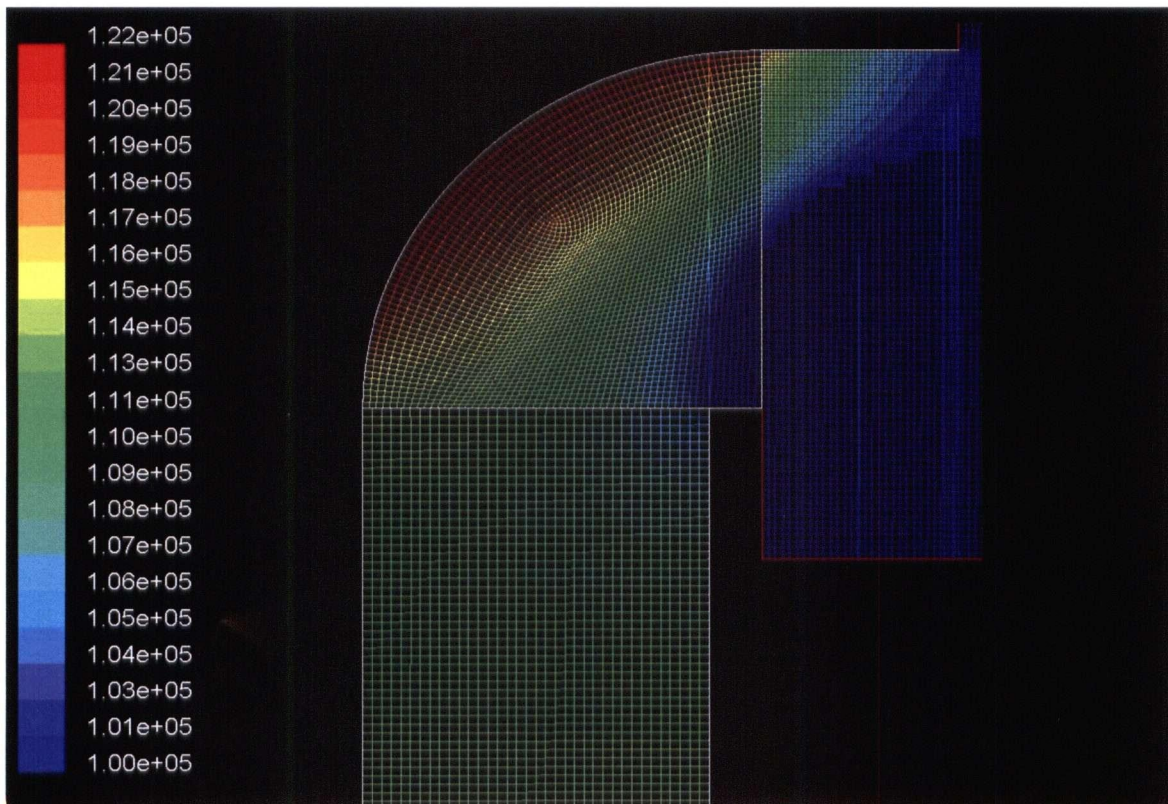
Figure 4.4: 75hp Aerator Pressure Distribution (Pa)

4.2.3 Swirl Velocity Analysis

With an initial phase distribution calculated, it was then possible to apply some swirl velocities at the inlet in order to see how these applied velocities affect the velocity distribution at the edge of the diffusion head. Solutions were computed with swirl velocities of 10, 20, and 30 rad/s at the inlet. The ratios between maximum swirl velocity and average axial velocity in the draft tube are 0.4, 0.8 and 1.2 respectively. These were considered high estimates of the maximum possible swirl velocities which might be present in a 75hp aerator. A step change at the velocity inlet boundary was applied to the initial solution, and the solution was marched forward in time with a time step of 10^-4 seconds, for about 0.5 seconds, giving the solution ample time to reach a steady state.
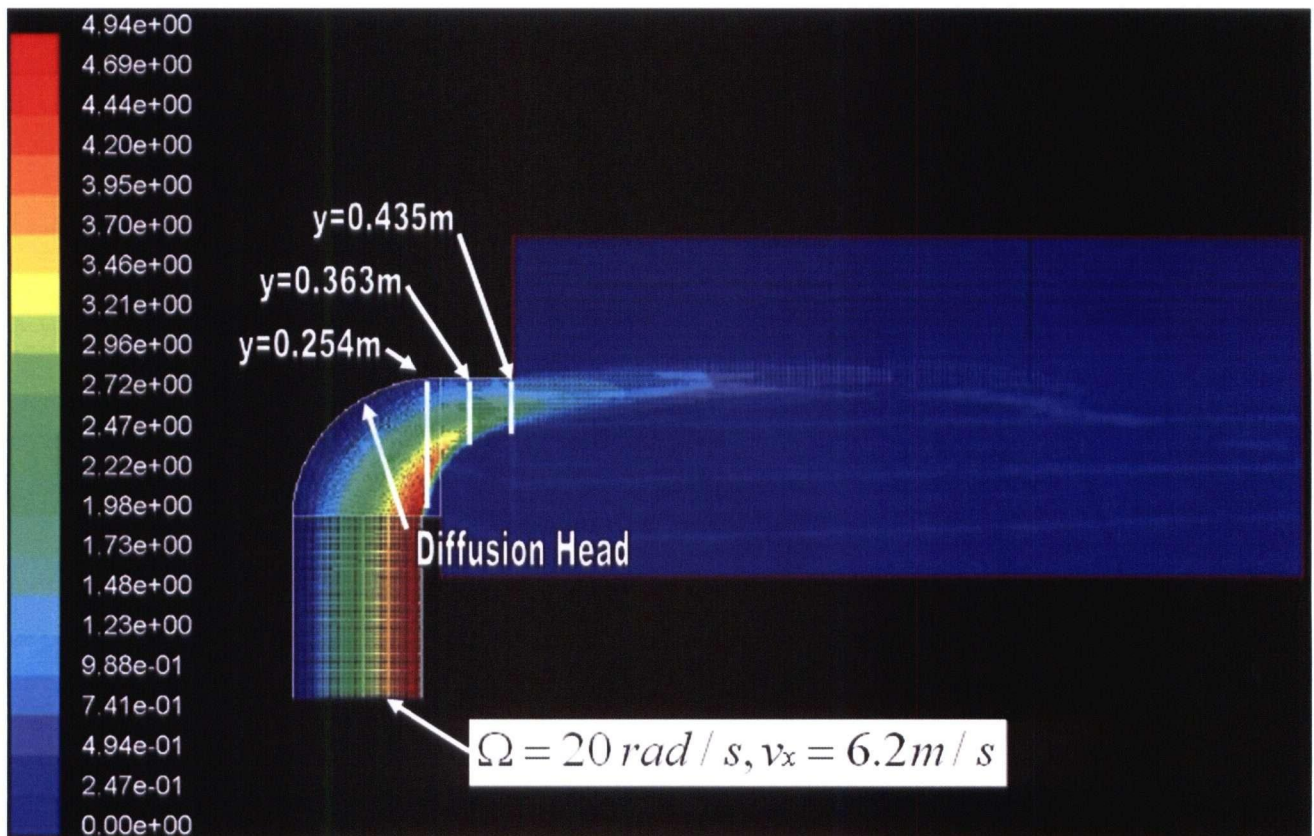
Figure 4.5: 75hp Aerator Computed Swirl Velocity Contours (m/s)

Figure 4.5 shows the computed swirl velocities for the 20 rad/s case as well as the three points used for plotting velocity profiles. Similar distributions were obtained for all applied swirl velocities. Unlike the experimental aerator calculation a significant proportion of the applied swirl

velocity remains at the edge of the diffusion head. Figure 4.6 shows the relative swirl velocity

(Vswirl/Vswirlmax) at different positions along the diffusion head for both the 10 and 20 rad/s cases

(where Y represents the distance from the axis of symmetry).
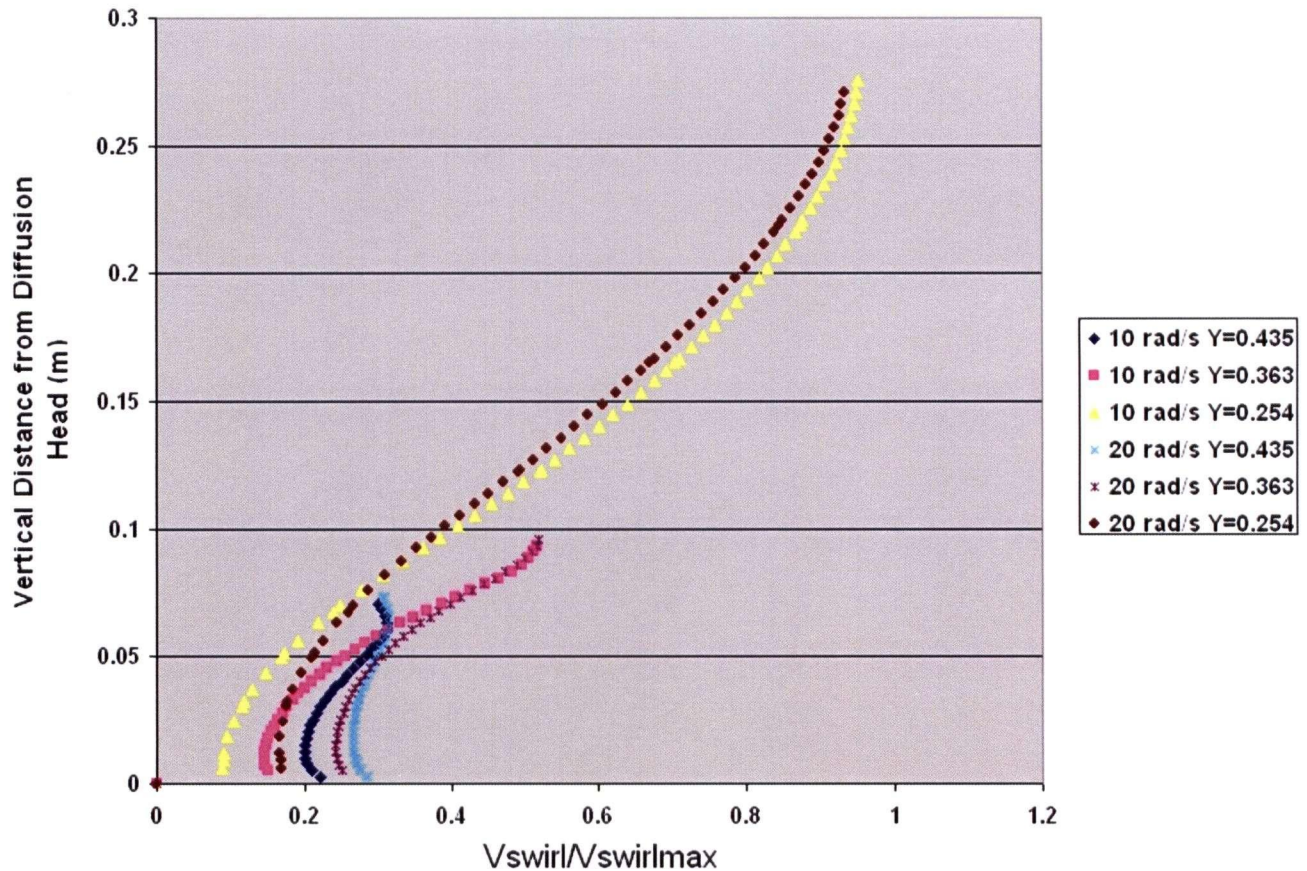
Figure 4.6 Computed 75hp Aerator Swirl Velocities

Depending on the case, between 20 and 30 percent of the initial swirl velocity is conserved at the

aerator exit. This represents a dramatic difference from the experimental aerator case where only

2.5% of the maximum swirl velocity remained at the edge of the splash plate. It is also desired to

understand how these swirl velocities affect the radial velocity profiles, as all these components will

affect the eventual splash zone. The radial velocity profiles at the edge of the diffusion head

(Y=0.435m) are plotted in Figure 4.7. A slight increase in the radial velocity with increasing swirl is

observed.
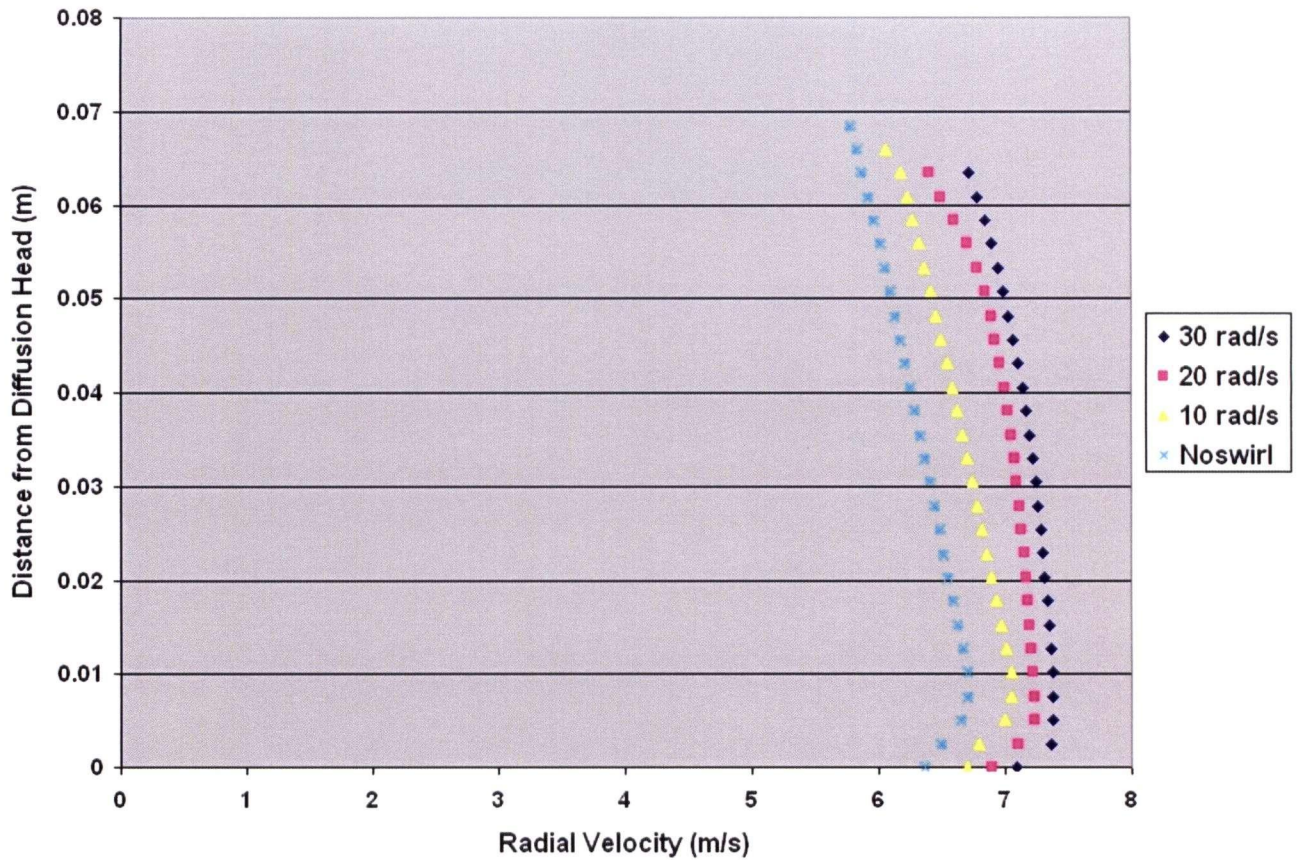
Figure 4.7: 75hp Aerator Computed Radial Velocity Profiles (m/s)

4.3 Droplet Trajectory Analysis

Given a set of solutions from the Volume of Fluid model for the domain encompassed by a 75hp

aerator, it is now possible to apply the same methodology used in Chapter 3 whereby a complete

breakup of the jet is assumed at the edge of the diffusion head. The trajectories of an assumed

particle distribution can then be computed to estimate a probable splash zone. It is also desired to

understand the effect which swirl velocities will have on the predicted splash zone. For these

calculations it is once again assumed that complete jet break up occurs at the edge of the diffusion

head. It is also assumed that the swirl present at the diffusion head edge is conserved in the breakup

process and transferred to the spray.

4.3.1 Computational Grid

The grid was designed in the same fashion as for the experimental case, with the particle sources

placed at the same location as the diffusion head edge, the lagoon surface represented by a free slip

wall, and the remainder of the boundaries set as atmospheric pressure. The grid spacing was set at

0.119 mm in the area to the right of, and below the spray boundary.
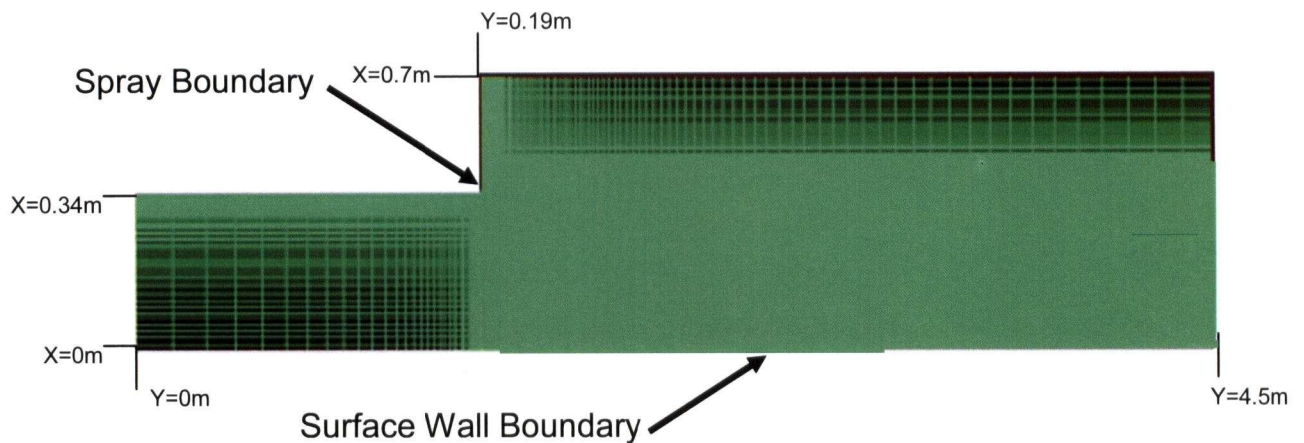
Figure 4.8: 75hp Discrete Phase Computational Grid

Two cases were run for this particular setup. Velocity profiles from both the case without swirl,

and the case with 20 rad/s of swirl were converted into 8 particle sources described in Tables 4.2 and

4.3. The total mass flux was the same for both cases. The Rosin-Rammler particle distribution was

once again assumed for all particle sources with particle diameters ranging from one to 4 millimeters.

Source	Height from Surface (m)	Mass flux (kg/s)	Axial Velocity (m/s)	Radial Velocity (m/s)
1	0.411	184.9	0.21	6.51
2	0.401	186.9	0.46	6.87
3	0.391	186.3	0.69	6.53
4	0.381	179.8	0.92	6.46
5	0.371	185.1	1.13	6.32
6	0.361	182.1	1.33	6.24
7	0.353	89.8	1.46	6.13
8	0.348	65.9	1.49	5.92

Table 4.2: Discrete Phase Particle Sources without Swirl

Source	Height from Surface (m)	Mass flux (kg/s)	Axial Velocity (m/s)	Radial Velocity (m/s)	Swirl Velocity (m/s)
1	0.411	179.58	0.27	7.02	1.39
2	0.401	177.88	0.60	7.13	1.35
3	0.391	177.91	0.90	6.92	1.36
4	0.381	179.86	1.18	6.85	1.41
5	0.371	184.44	1.45	6.76	1.48
6	0.361	191.94	1.73	6.72	1.56
7	0.353	96.73	1.87	6.65	1.59
8	0.348	72.53	1.79	6.58	1.57

Table 4.3: Discrete Phase Particle Sources with 20rad/s Swirl

4.3.2 Droplet Trajectory Results and Discussion

Droplet trajectories were computed, along with the flow of the surrounding air using the same procedure described in section 3.3.4. Figure 4.9 shows the particle tracks for the case where swirl was applied at the aerator inlet.
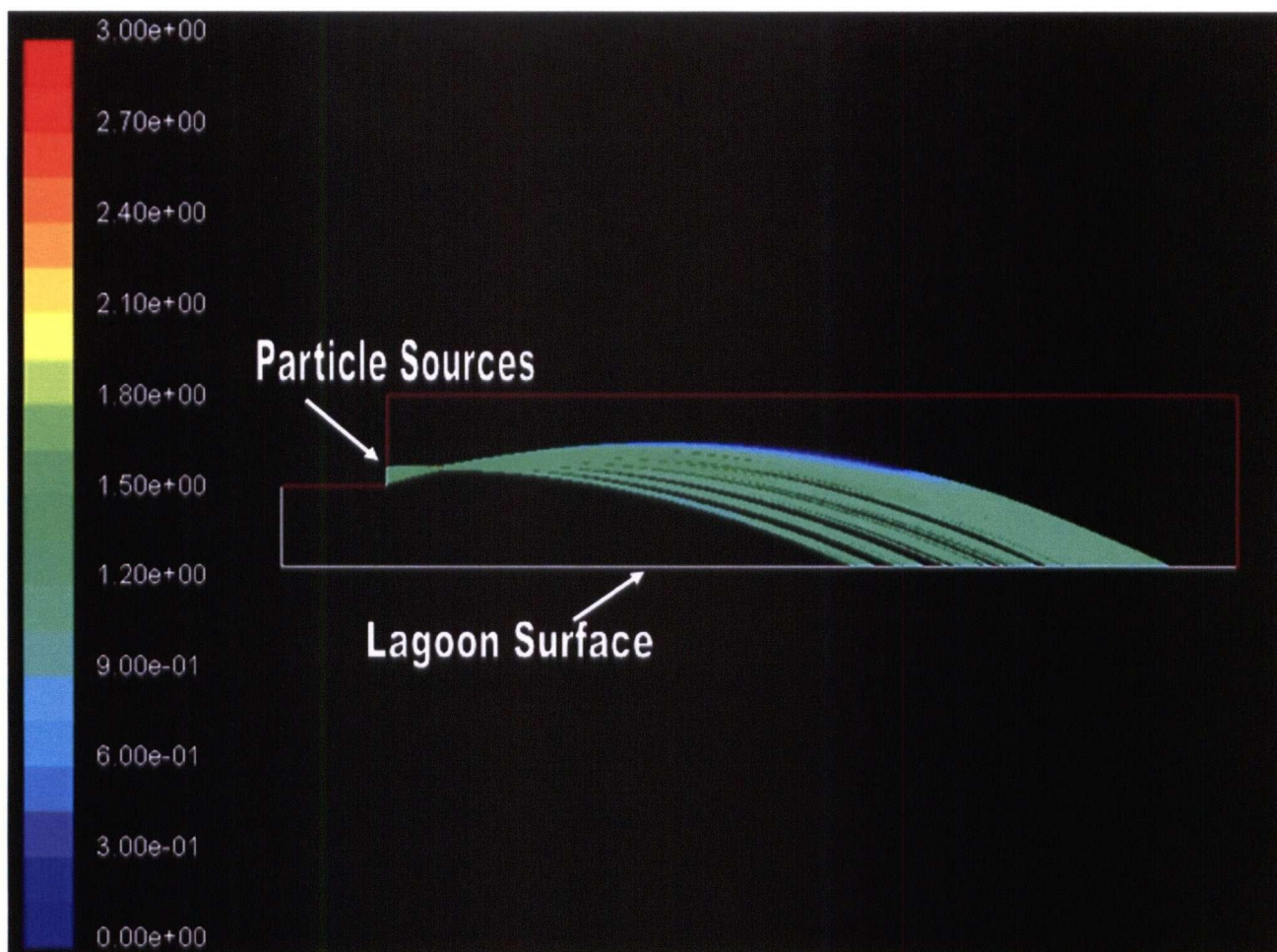
Figure 4.9: 75hp Aerator Computed Droplet Tracks Colored by Swirl Velocity (m/s)

It can be concluded that most of the swirl velocity imparted to the droplets is conserved

throughout their trajectories to the lagoon surface. The droplets do carry a tangential velocity

component to the lagoon; however it is very likely that the magnitude of this component will

decrease to negligible levels with increasing depth and radial distance from the aerator in any large

lagoon. The second main effect which swirl velocities have on aerator/lagoon analysis is a change in

the landing radius of most of the droplets. Figure 4.10 highlights this effect as we see a slight

difference between the beginning and end of the initial splash zones for the cases with and without

swirl. In the 20 rad/s case the splash zone extends 50 cm further from the aerator centerline than in

the case without swirl. The effects of splash zone thickness on lagoon RTDs are examined in

Chapter 5.
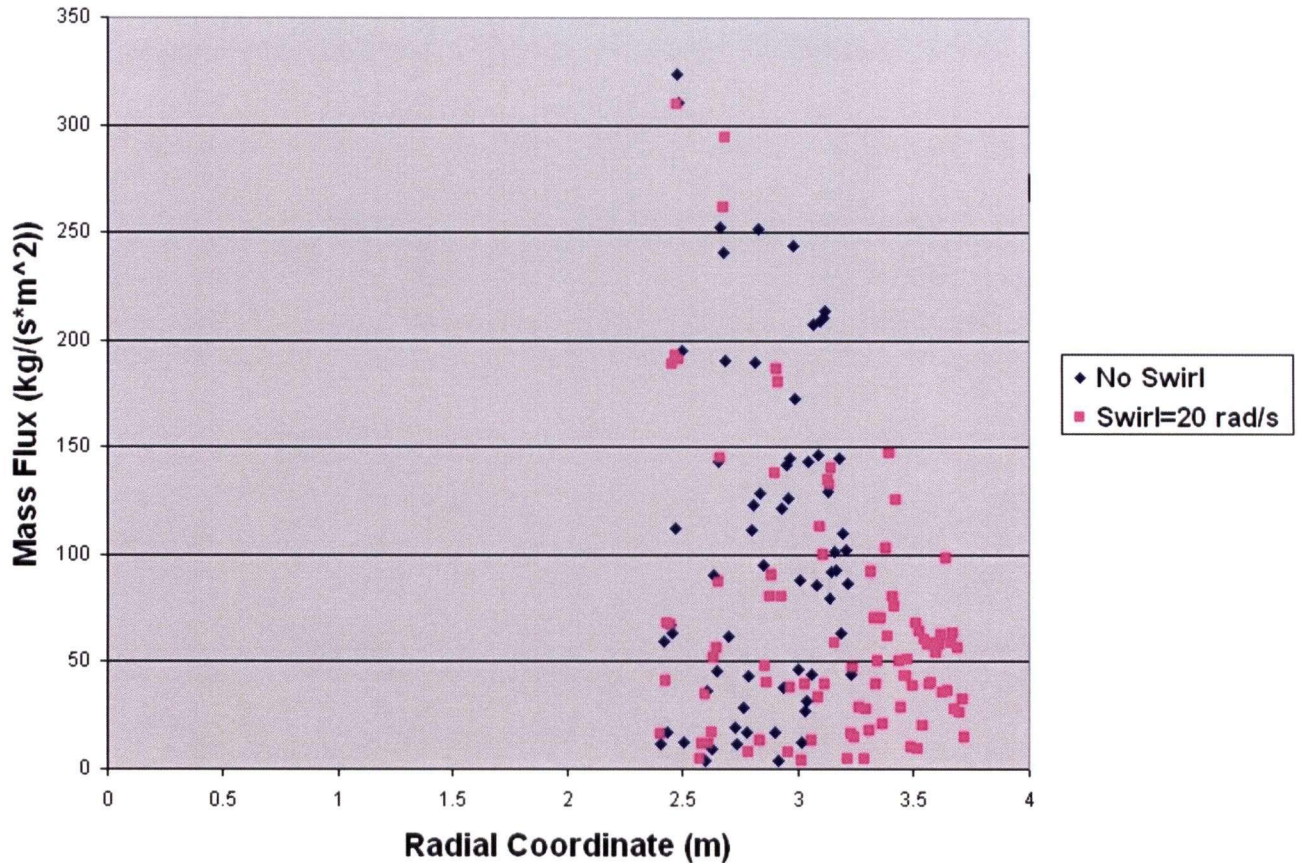
Figure 4.10: 75hp Splash Zone Mass Flux

Once again some spread of the droplets was observed due to drag, source position and velocity, but

the effects due to drag were diminished by air velocities similar to the droplet velocities in the

vicinity of the particle streams. In the previous chapter it was found that a simple ballistics

calculation using the height of the splash plate and the radial velocity at the edge of the plate yielded

a splash zone radius identical to that computed with the discrete phase model. If the same method is

used in this case the splash zone radius is predicted to be 2m. Unlike the results from the

experimental aerator, there still exists a significant axial velocity component at the edge of the

diffusion head. If this velocity component is taken into account a ballistics calculation yields a

splash zone radius of 3m. This phenomena is illustrated in Figures 4.9 and 4.11, where it is shown

that the in both the discrete phase calculation and in a photograph of a 75hp aerator in operation, the height of the droplets exceeds that of the diffusion head.

Figure 4.11: 75 Horsepower Aerators in Operation

4.4 Summary

The methods used in Chapters 3 for analyzing aerator flow and sprays were successfully applied to a full sized aerator model. It was found that the flow velocities at the edge of the diffusion head of the aerator are very similar to the average velocity in the draft tube. Results were found to be quite intuitive as the applied swirl velocities increased the kinetic energy of the flow leaving the aerator. It was also found that 20-30% of the applied swirl velocity magnitude remained at the aerator exit, however once the tangential velocity is transferred to the lagoon by the spray it will likely dissipate to negligible levels at any significant depth or distance from the aerator. The average radial velocity leaving the aerator is higher when swirl velocities are accounted for. This results in an increased splash zone radius. The splash zone radius computed with the discrete phase model is once again comparable to that computed from a ballistics calculation; however the axial velocity component at the edge of the diffusion head must be accounted for. The applied swirl velocity magnitudes were chosen as high estimates representing the maximum swirl velocity magnitudes which may be present in an aerator.

5   Validation of Residence Time Distribution Modeling

5.1 Problem Description

As is the original goal of this thesis, it is desired to reproduce the behaviour of aerated lagoons via computational means. The experimental lagoon setup of Jenkinson involved the same model aerator studied in the previous chapters, placed in the center of a flow through basin as shown in Figure 5.1. Tracer dye was added to the lagoon in the mixing region shown and stirred. Near the outlet region, samples were removed with a test tube and analyzed for dye concentration. The results were then used to plot a residence time distribution for the shown configuration. It is therefore required to apply the results of the multiphase and discrete phase simulations to a flow through lagoon simulation. Data from the discrete phase calculation can be used to impose a boundary condition on a single phase lagoon which is representative of the splash zone induced by a real aerator. This condition can then be applied to a single phase lagoon domain and the residence time distribution can be calculated. In order to validate a proposed model, comparisons can be made between the computed results and those obtained by Jenkinson.
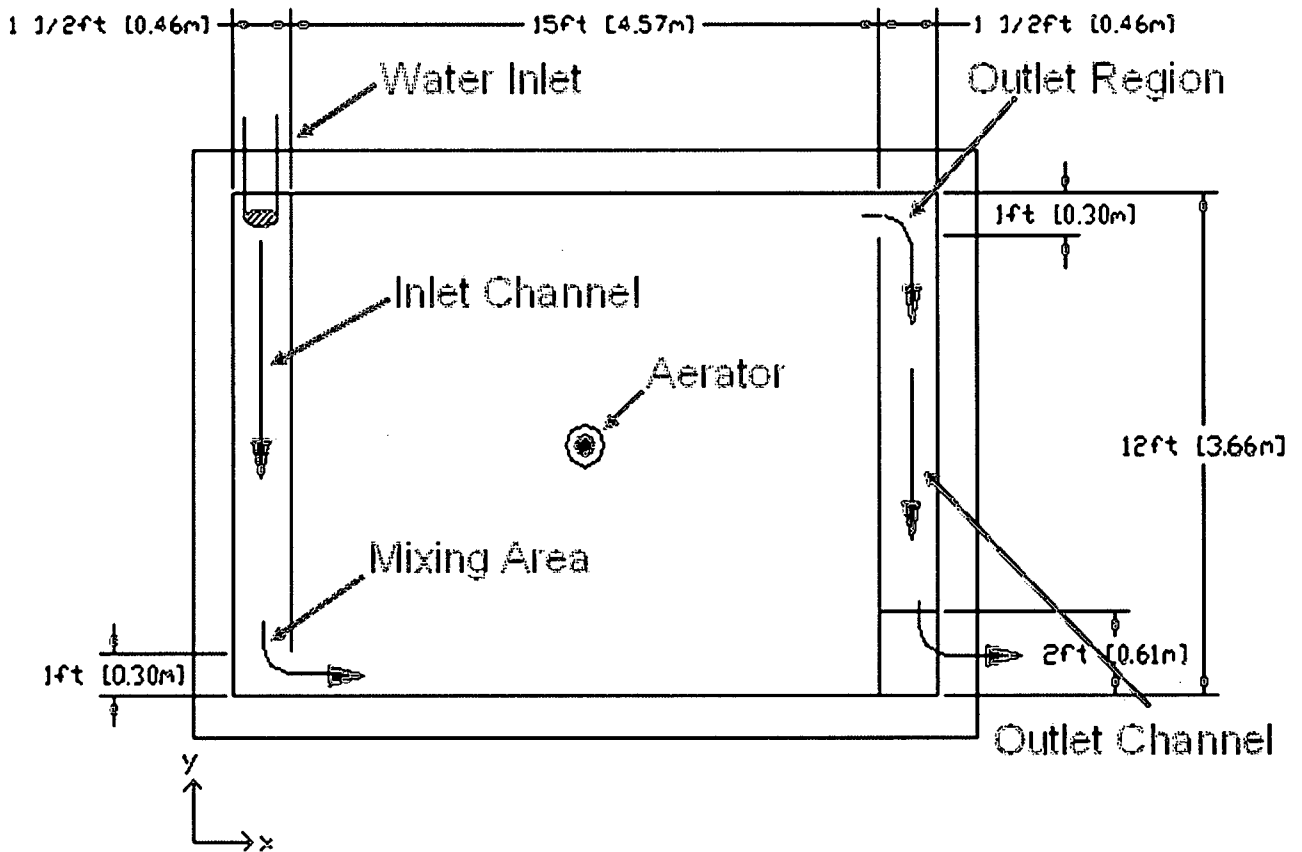
Figure 5.1: Plan View of Flow-Through Lagoon

5.2 Computational Grid

The domain was defined with features identical to those of the experimental apparatus with the exception of the outlet channel. Since the tracer concentration samples were taken at the entrance to the outlet channel, this part was removed, and replaced with the outlet of the domain. With this configuration, tracer sampling was done by computing the mass weighted average of tracer leaving the domain. All dimensions shown in Figure 5.1 were carried over to the computational grid including the depth of 0.42m. Some issues arose when assigning grid spacings to the domain due to the vast differences in length scales being resolved. For example the square inlet area measures 0.46m by 0.48m. This area was resolved using 20 nodes on each edge, or a grid spacing of 2.43 cm. Most of the domain was solved with this spacing. The inlet of the aerator draft tube is 4 cm in diameter. Since the accuracy of the amount of tracer entering the aerator is highly critical to the

accuracy of the solution, a reasonable number of cells is required on the draft tube boundary. A grid

spacing of 4 mm was used on the draft tube boundary. The difference in grid spacing, combined

with the circular shape of the draught tube required that the domain be separated into two main

zones. The second smaller domain containing the aerator boundary conditions used a finer,

unstructured mesh to resolve the aerator geometry as shown in Figure 5.2.
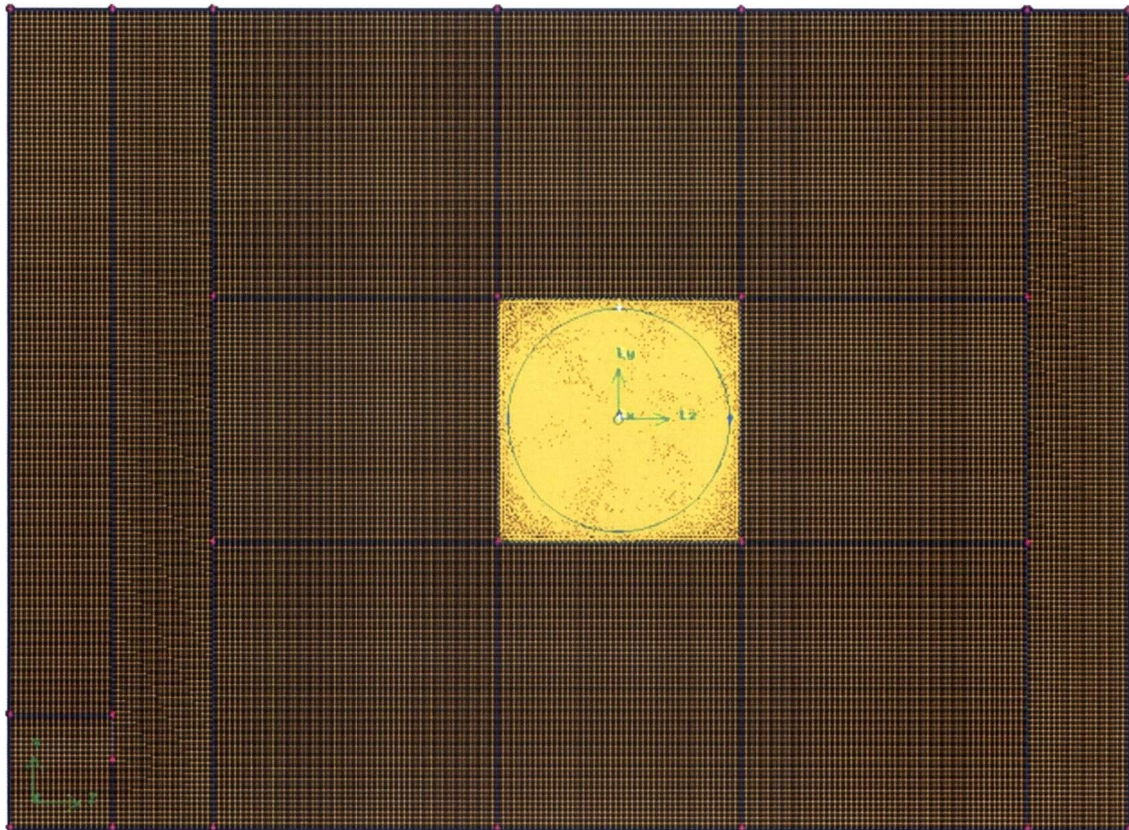
Figure 5.2: Computational Grid

5.3 Boundary Conditions

Several solutions were computed using the described grid, with all boundary conditions not

pertaining to the aerator splash zone left unchanged. Those conditions are described in Table 5.1,

and shown in Figure 5.3. The side walls and floor or the basin are set as zero mass flux walls with

shear computed as described in Section 3.2.2. Wave action was neglected by modeling the lagoon

surface as a free slip wall without any shear.

Boundary	Imposed Conditions	
Water Inlet	mass flux	$\dot{m} = 4kg/s$
	turbulence intensity	10%
Basin Outlet	Imposed Normal Velocity	Vn=-3.18 cm/s
Basin Surface	Zero Mass Flux	Vn=0m/s
	Zero Shear	$\tau_{xy} = 0Pa$
		$\tau_{xz} = 0Pa$
Draft Tube Inlet	Imposed Normal Velocity	Vn=-2.47m/s

Table 5.1: Basin Boundary Conditions
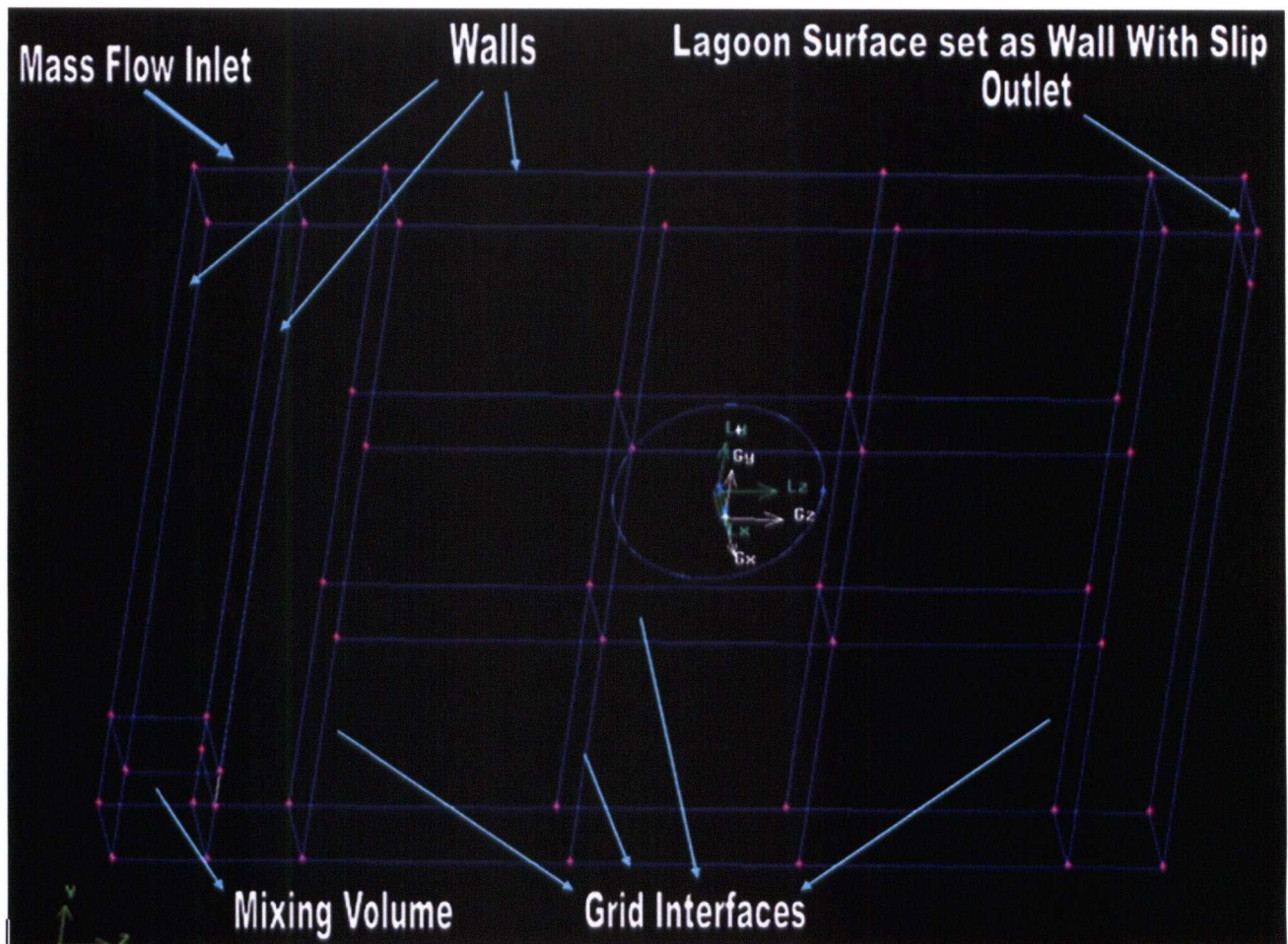
Figure 5.3: Lagoon Domain and Boundary Conditions

As shown in Figure 5.4 the effects of the aerator on the domain are reproduced using two different

boundary conditions. The draft tube is represented by a solid cylinder, protruding downwards from

the surface. The bottom of the cylinder is set as a prescribed velocity outlet.   As described in

Chapter 3, the results from the discrete phase simulation do not fully encapsulate the processes

taking place in the experiment. Jet breakup is assumed rather than simulated, and the interactions

between the spray and the free surface are neglected. In reality, these interactions are very complex,

as droplets may exhibit some bouncing behaviour, or may induce new splash as they strike the

lagoon surface. This zone is both difficult to observe and difficult to calculate as waves, secondary

splash and bubbles form around the periphery of the zone. This being the case it was decided to test

various assumptions about the splash zone, and compare the effect of each change on the computed

residence time distribution.
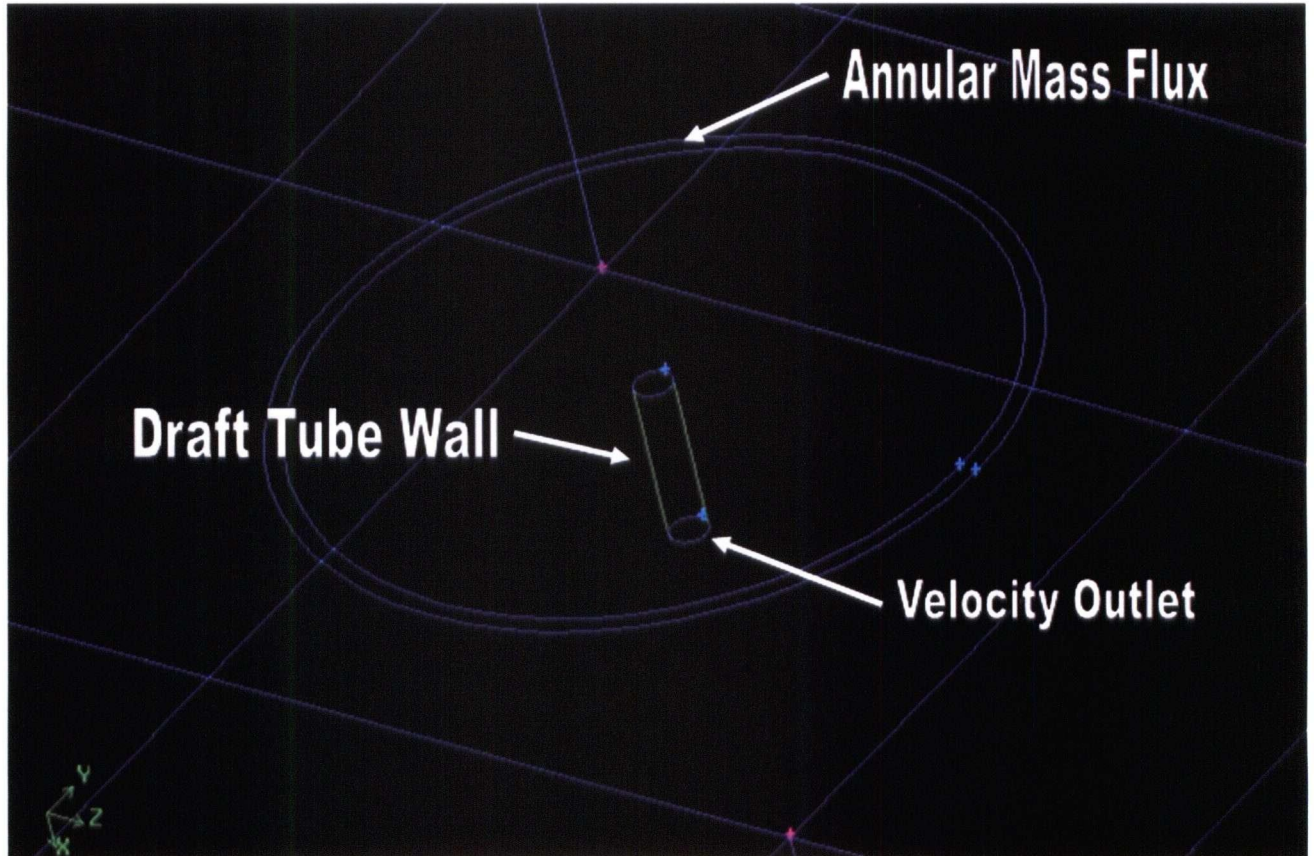
Figure 5.4: Aerator Boundaries

Different placements, thicknesses and multiple, concentric annular zones were used as

summarized in Table 5.2. As the process of droplets impinging the basin surface is expected to

induce highly turbulent flows a turbulence intensity of 30% was applied to the splash zone boundary

for all cases.

Case	Notes	Splash Zone Dimensions	Velocities
Case 1	Thin ring splash zone in middle of computed trajectories	Rout=0.377m Area=2.82*10^-3 m^2	Vnormal=1.15m/s Vradial=1.55m/s
Case 2	Thin ring zone at outer extent of observed splash zone	Rout=0.5m Area=2.82*10^-3 m^2	Vnormal=1.15m/s Vradial=1.55m/s
Case 3	Thicker splash zone from maximum to minimum calculated droplet landing radius	Rout=0.388m Rin=0.368m Area=4.74*10^-3 m^2	Vnormal=0.0655m/s Vradial=2.02m/s (velocities changed to conserve mass and total momentum)
Case 4a	4 Evenly spaced splash zones	Rout1=0.368m Rout2=0.417cm Rout3=0.456cm Rout4=0.5m Total Area=2.82*10^-3 m^2	Vnormal=1.15m/s Vradial=1.55m/s
Case 4b	4 Evenly spaced splash zones, Overall zone thickness decreased by 25%	Rout1=0.368m Rout2=0.403m Rout3=0.438m Rout4=0.474m Total Area=2.82*10^-3 m^2	Vnormal=1.15m/s Vradial=1.55m/s
Case 4c	4 Evenly spaced splash zones, Overall zone thickness increased by 25%	Rout1=0.368m Rout2=0.417m Rout3=0.467m Rout4=0.517m Total Area=2.82*10^-3 m^2	Vnormal=1.15m/s Vradial=1.55m/s

Table 5.2: Case Summary

5.4 Solution Procedure

The fist step in establishing a residence time distribution is solving for the flowfield in the lagoon. The transport equations are solved as described in Section 2.3.1. Turbulence is accounted for using the standard K-epsilon turbulence model as described in Section 2.4. The solution converged without any problems, in approximately 24 hours. The next step was to apply a species transport model to the problem and determine the residence time distribution. Details of the species transport model are described in Section 2.3.2. In order to conserve the amount of tracer in the lagoon and provide realistic results, a user defined function had to be written for Fluent. The function performed the task of calculating the average species mass fraction leaving the domain via the draft tube, and applying that mass fraction to the splash zone boundary, thereby reproducing the effect of tracer passing through the aerator. In the experiment, the tracer was added and manually stirred in the mixing area (shown in Figure 5.1) at the beginning of each trial. In order to reproduce this procedure, a mixing volume (shown in Figure 5.3) was defined in the lagoon domain. Before solving the unsteady species transport equations the mixing volume was initialized with a volume fraction of tracer. A timestep of 0.5 seconds was used. The simulation was marched forward in time for 7200 timesteps (1 hour). This took approximately 72 hours. The grid used contained approximately one million cells. At this level of refinement, there are only 30 faces on the draft tube inlet boundary. It was not desired to reduce the number of cells as this would reduce the accuracy of the calculated tracer concentration entering the draft tube. This value is critical in maintaining mass conservation of the tracer. Furthermore it was not practical to increase the number of cells as the solution was already very slow to converge. For this reason, once tracer conservation was verified, the same grid spacing was used for all cases.

5.5 Results

5.5.1 Investigation of Residence Time Distribution

As described in Section 5.3 several different splash zone boundaries were applied to the basin domain in order to assess the affects on the RTDs produced. The Cases are summarized in Table 5.2 and described in the following section along with the computed results.

Case 1

In this case it was decided to place a single annular boundary at the mid-radius between the longest and shortest droplet trajectories calculated from the discrete phase model (r=37.75cm). In order to conserve both the mass and momentum imparted to the lagoon, this splash zone was represented as a very thin ring as shown in Figure 5.5.
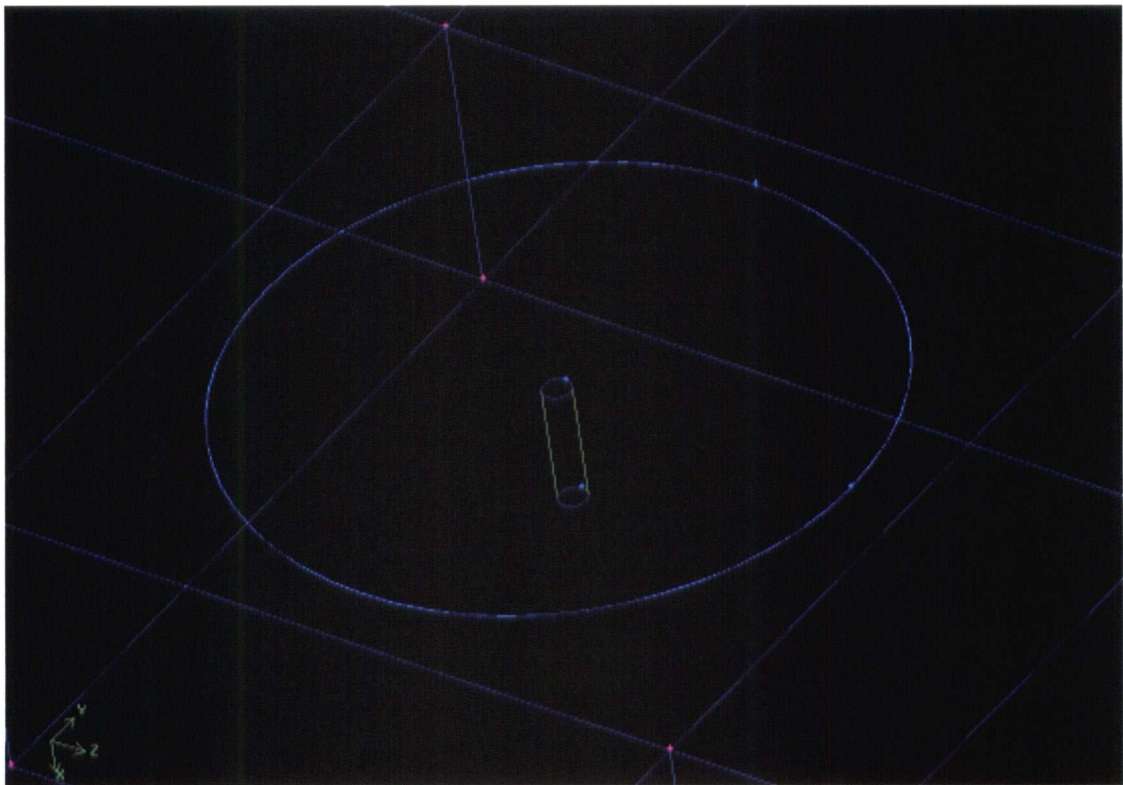

Figure 5.5: Thin Ring Splash Zone Condition

In reality the droplets strike the lagoon as a diffuse spray. By reducing the area to a thin ring we are essentially assuming that all the droplets land at the same distance from the aerator. This allows a boundary of pure water mass flux, with the same average normal and radial velocity components as calculated in Chapter 3. The resulting residence time distribution is shown in Figure 5.6 as compared with the experimental results of Jenkinson [2].
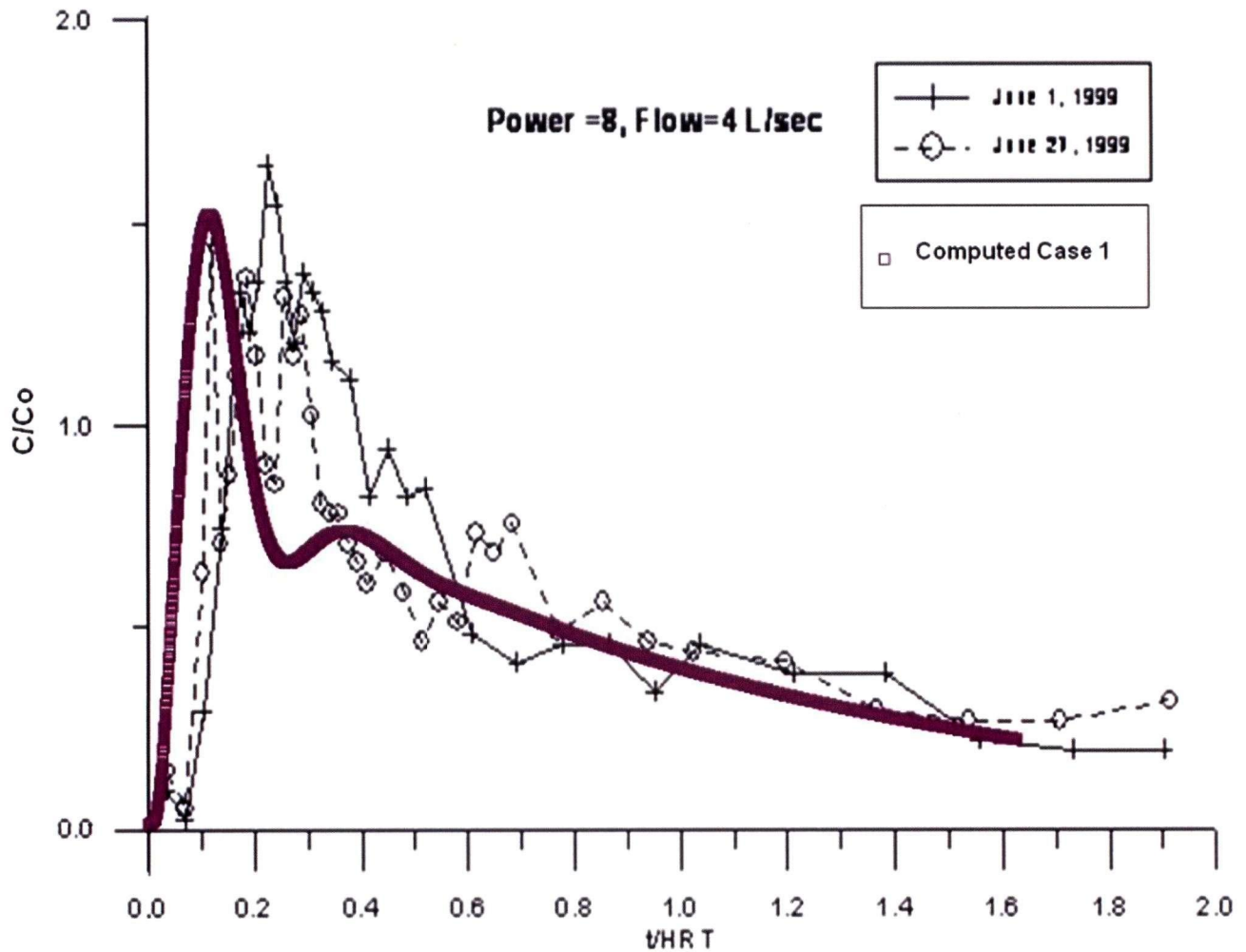
Figure 5.6: Case 1 Residence Time Distribution

The results show the same general trends as found in the experiments. Initially there is a sharp increase followed by a sharp decrease in the amount of tracer leaving the lagoon. This is followed by another, smaller increase and a long slow decay of the outlet concentration. This residence time distribution appears to demonstrate a combination of the distributions described by Danckwerts [3].

The sharp rise and decrease is typical of flow-through reactors whereas long, gradual decay is observed in highly mixed reactors. Figure 5.7 shows time elapsed tracer concentration contours within the lagoon. We see a large bulk of fluid making its way along the bottom wall and up towards the outlet. This corresponds to the time of the first peak in the distribution. All of the tracer which does not escape in the first pass is drawn into the aerator, and is released slowly in a highly mixed fashion. There are some differences between the experimental RTD and the one obtained in Case 1. The initial peak occurs slightly sooner than expected and the curve is much narrower than in the experimental case. This implies that the experimental aerator may impart slightly more mixing to the lagoon than that which is observed in this initial simulation.
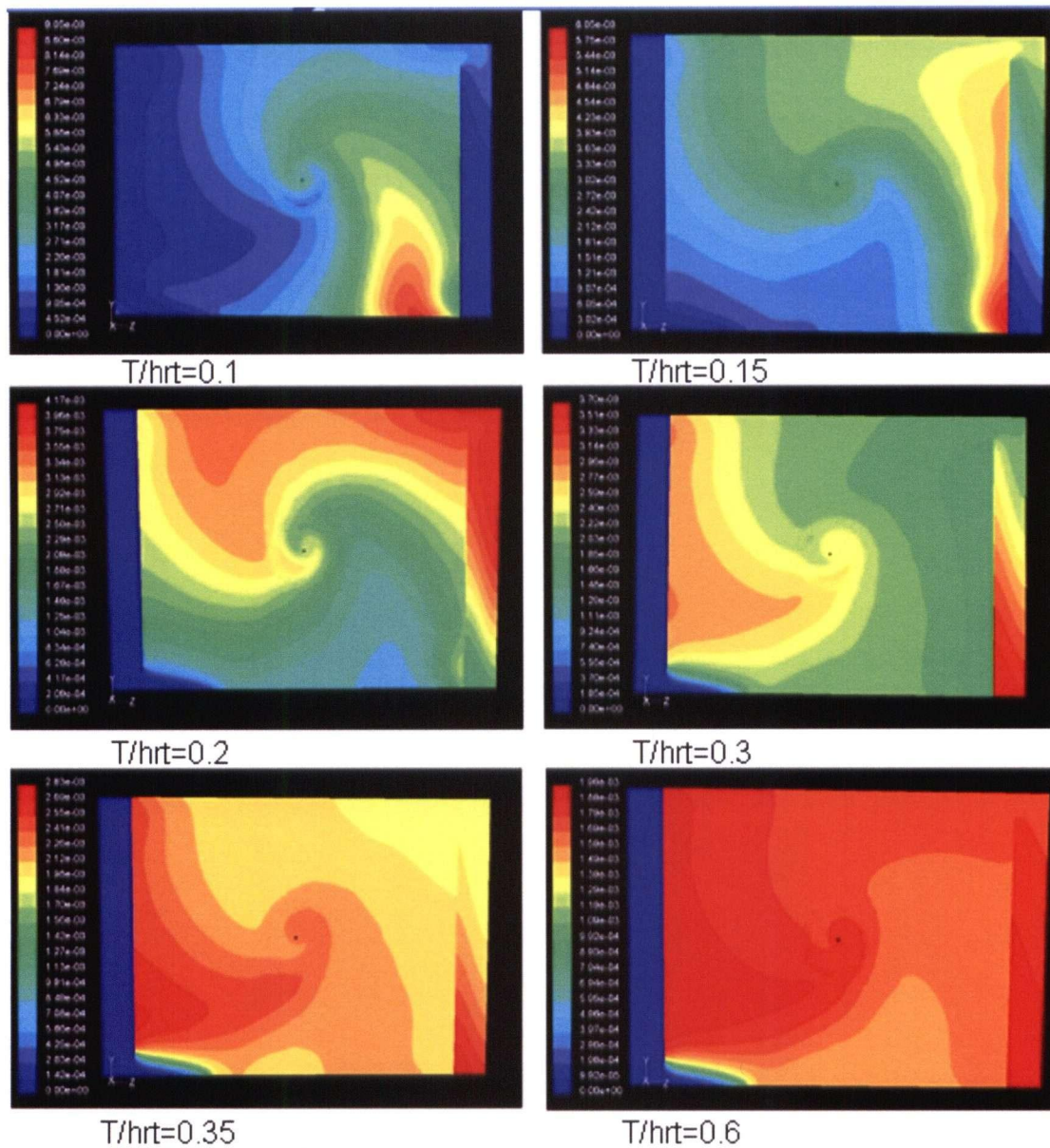
Figure 5.7: Tracer Concentration variation with time

Case 2

Case 2 was set up in very similar fashion to Case 1. Once again, the thin annular splash zone was used, maintaining the same velocity components as before. The only difference in Case 2 is that the radius of the splash zone was set at 50cm. This corresponds to the observed outer extent of the splash zone created by the experimental apparatus. The simulation seemed fairly insensitive to this change, the only difference being a slight shifting of the curve as shown in Figure 5.8.
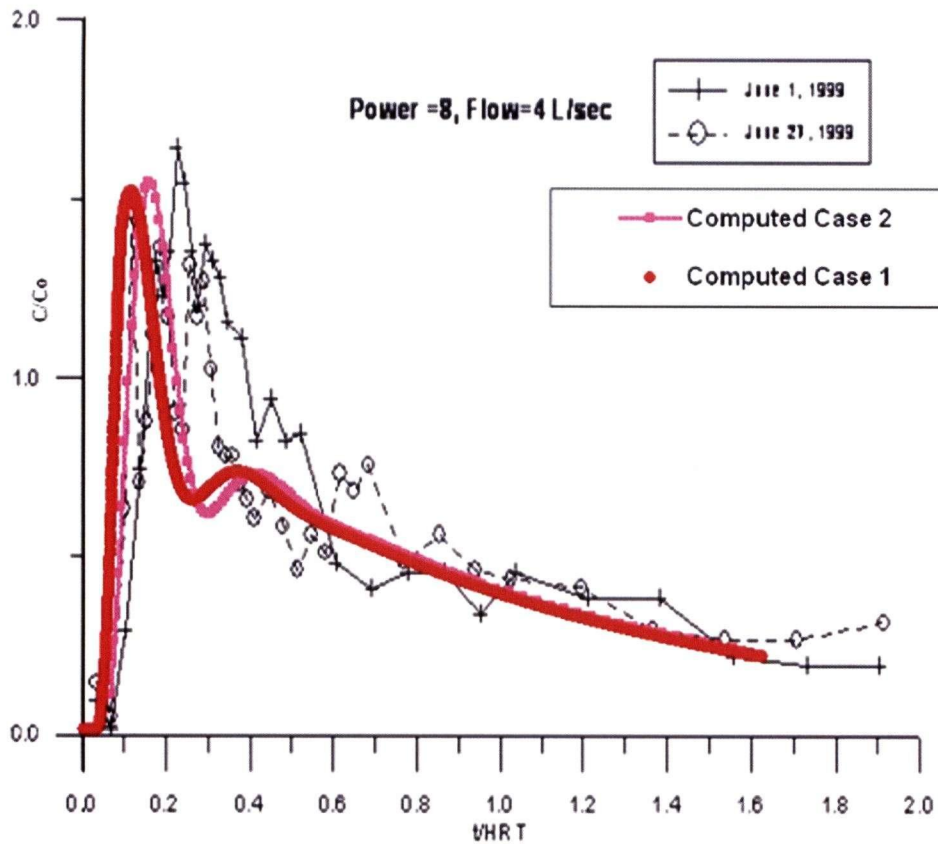
Figure 5.8: Case 1 and 2 Residence Time Distributions

Case 3

This case did not use the assumption of a thin splash zone. A single splash zone was again applied; however the annular region had an inner radius of 36.75cm and an outer radius of 38.75cm (shown in Figure 5.4). These values correspond to the range of droplet distances calculated in discrete phase calculation. The discrete phase calculation involved a diffuse spray whereas only a pure mass flow was applied in these single phase calculations. If the droplet velocity components would be applied to this boundary, the normal component would cause more mass entering the lagoon than that leaving via the draft tube. If the normal velocity component is reduced, then the momentum imparted to the lagoon is underestimated. The normal and radial components of the momentum flux across the splash zone boundary can be calculated as follows:

$$\Phi_{zz} = \rho \upsilon_z \upsilon_z \text{ (Normal component)} \tag{5.1}$$

$$\Phi_{zr} = \rho w_z w_r \quad \text{(Radial component)} \tag{5.2}$$

Therefore,

$$\text{Total Momentum} = Area * \sqrt{\Phi_{zz}^2 + \Phi_{zr}^2} \tag{5.3}$$

Since the normal velocity component must be reduced to maintain the same mass flux of the spray, the radial velocity component must be increased to conserve the total momentum. With the velocities adjusted to satisfy both of these constraints, the code was run again and the results are shown in Figure 5.9. As compared with Case 1, the flow-through mass of tracer is virtually unaffected. This is a fairly logical result as both mass and momentum are added in the same vicinity of the lagoon. The only major difference lies in the start time of the highly mixed part of the distribution. This part begins sooner in Case 3. This is due to the fact that the radial component of the splash zone velocity was increased to maintain the total momentum flux into the lagoon, sending the aerated tracer towards the exit with higher velocity.
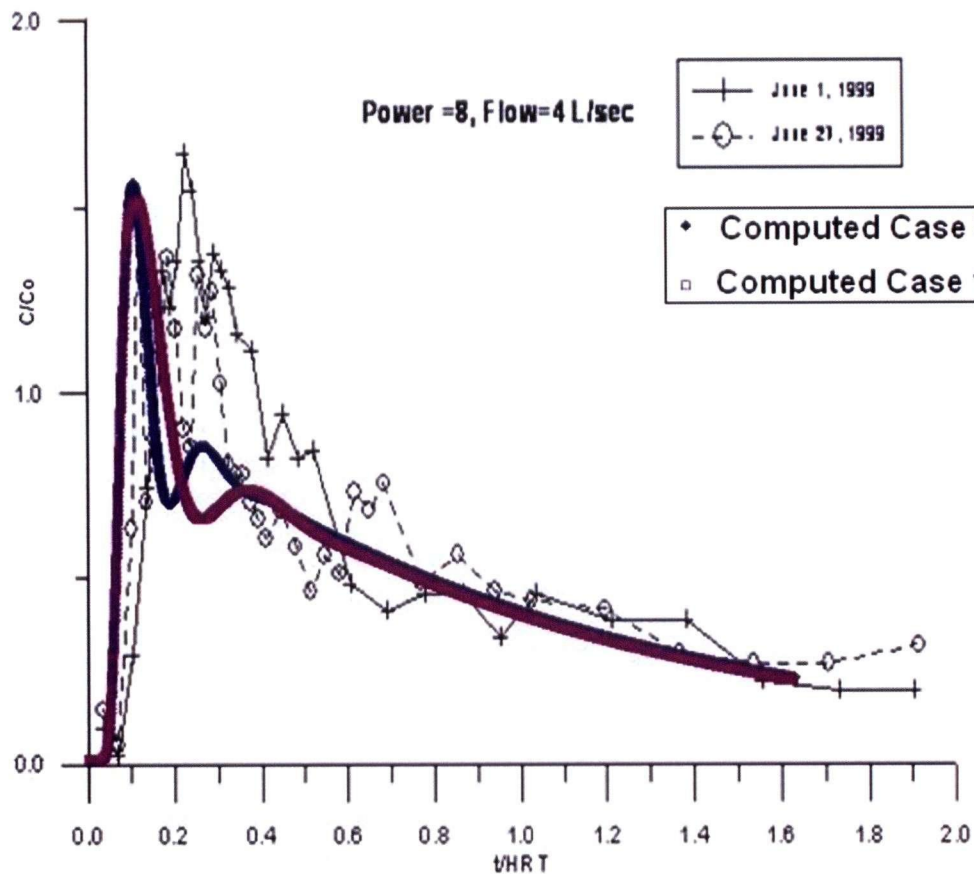
Figure 5.9: Case 1 and Case 3 Residence Time Distribution

Case 4

In Case 4 assumptions were made based on the results of the discrete phase calculation, experimental observations as well physical reasoning. As described previously, the splash zone is a chaotic region where both mass and momentum are imparted to the lagoon via secondary splash and wave actions. Results of the discrete phase calculation showed that the minimum landing radius of the droplets is 36.75cm. It was observed by Jenkinson that the splash zone created by the experimental apparatus extended to no more than 50cm from the aerator centerline. It was therefore decided to impart mass and momentum to the lagoon in a series of four evenly spaced, concentric annular regions with radii ranging from 36.75cm to 50cm as shown in Figure 5.10.
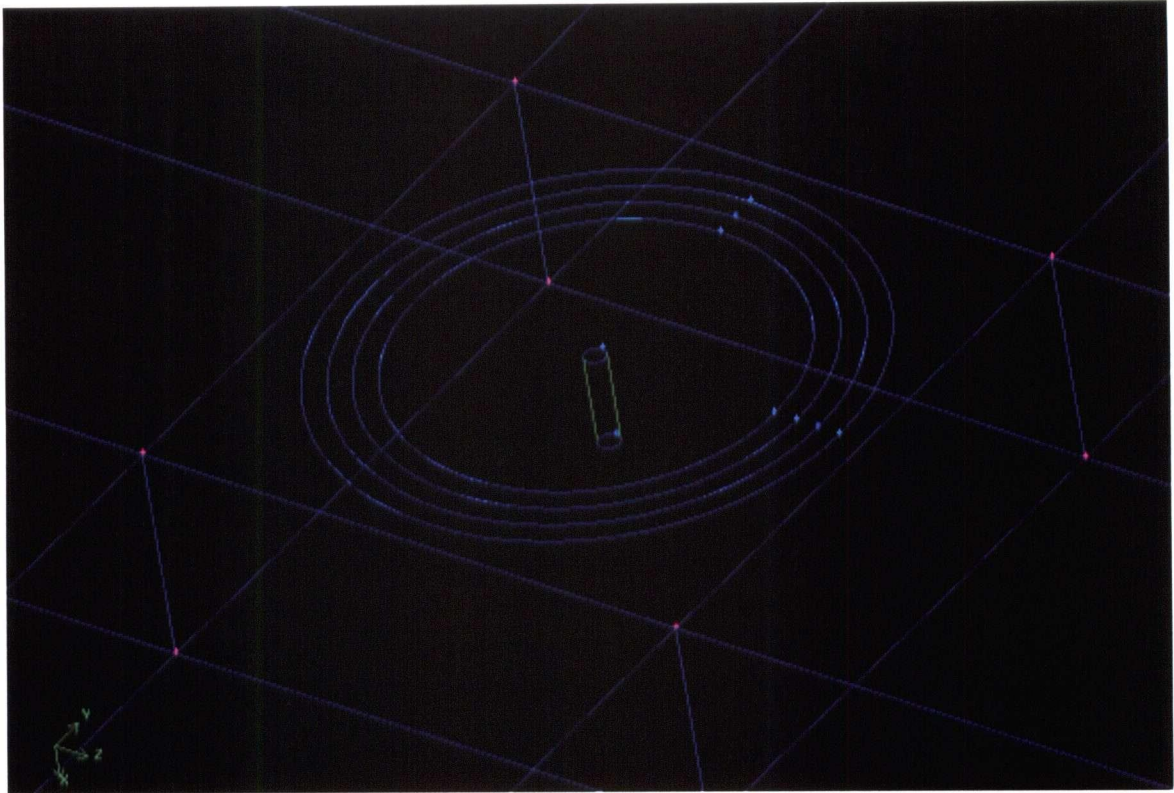
Figure 5.10: Case 4 Concentric Splash Zones

The residence time distribution (shown in Figure 5.11) shows definite improvement as compared with the previous distributions. The peak of the distribution occurs at the right time and it has the same width as the experimental curves. This implies that the concentric splash zones impart the right amount of mixing to the lagoon, as both the flow-through, and the highly-mixed masses of tracer exhibit the same behaviour as in the experimental cases.
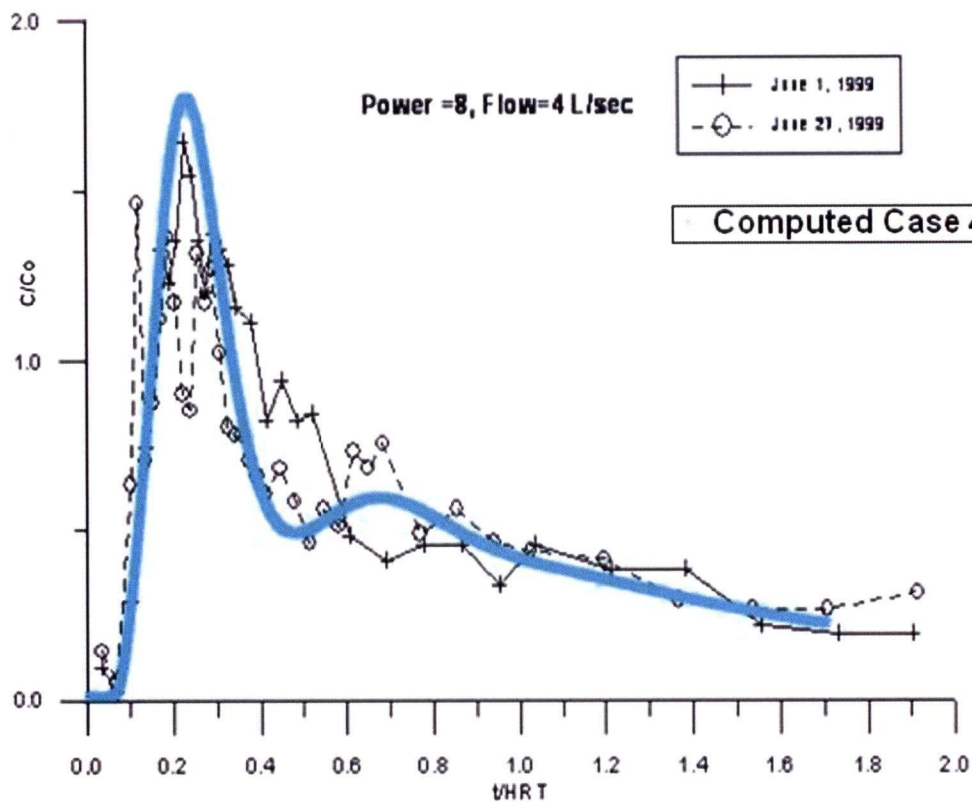
Figure 5.11: Case 4 Residence Time Distribution

In one fairly significant respect all the cases were virtually identical. The t50 value (the time

required for 50% of the added tracer to ext the lagoon) is the same in all of the cases. The integrated

RTD curve has a t50 value of 1120 seconds +/- 15 seconds for all cases. It is also important to

verify that the mass of tracer is conserved as it passes through the lagoon and the aerator. This is

difficult to verify as once the outflow becomes mixed, the tracer concentration at the outlet decays

very slowly over time. Given that the computed residence times took over three days each to

compute, it was not practical to run the simulations until there was no tracer left in the outflow. It

was found that the aerated outlet concentration could be extrapolated well with an exponential decay

function as there were sufficient data points. Using this method the extrapolated function could then

be integrated to obtain a total tracer mass flux out of the lagoon. This was computed for several of

the cases, and the total mass flux was never underestimated by more than 8%.

5.5.2 Sensitivity Analysis

The computed residence time distribution of Case 4 matches the experimental data quite well, however the outer extent of the concentric splash zones has been determined by the observations of Wayne Jenkinson. With wave, bubble and secondary splash phenomena taking place throughout the splash zone, an observed outer extent of any splash zone may be subject to significant interpretation. For this reason it was decided to both increase and decrease the total distance between the innermost and outermost concentric splash zones by 25%. The residence times were then computed again with the same procedure as before. A comparison of the computed residence times is shown in Figure 5.12.
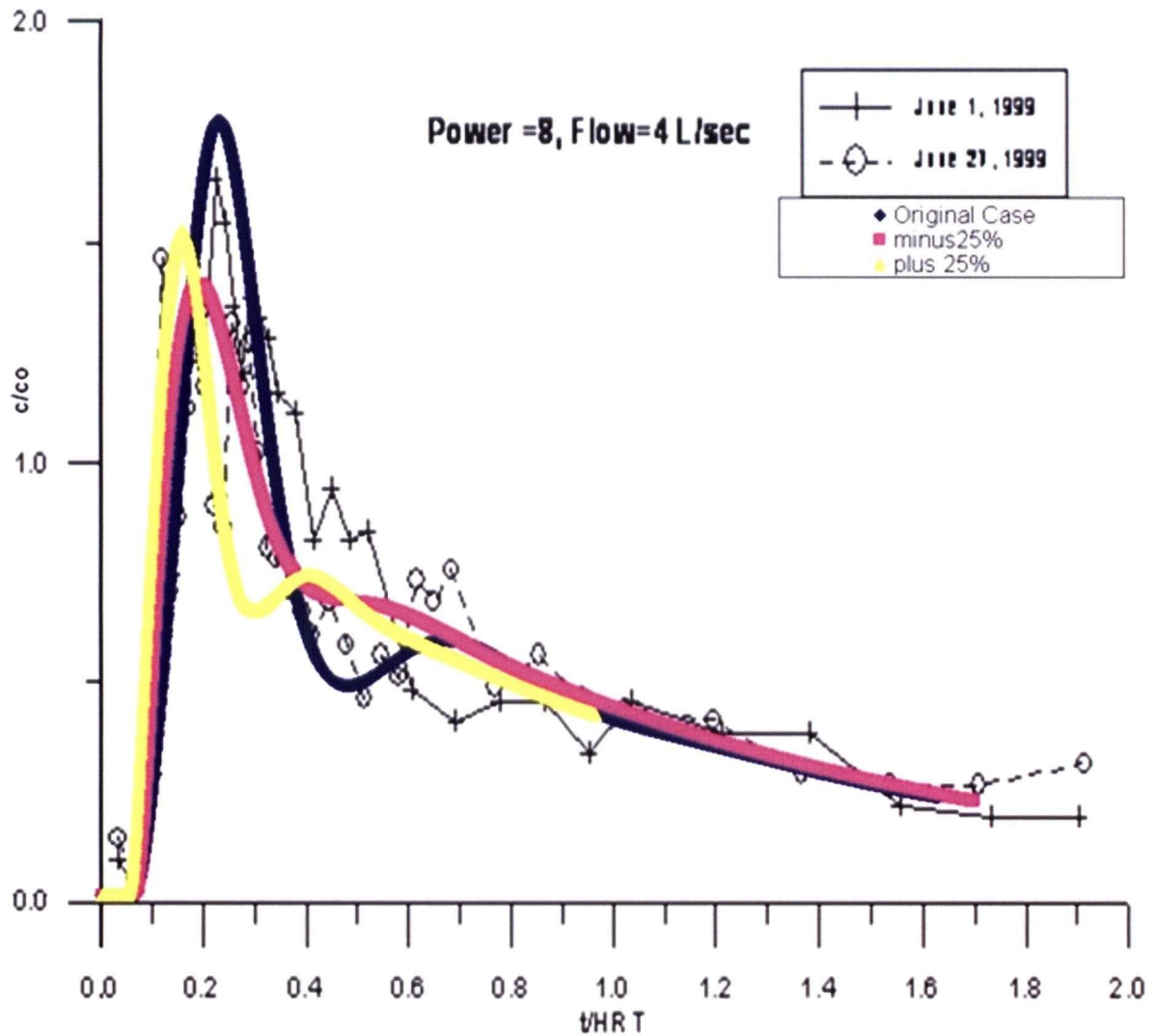
Figure 5.12: Splash Zone Thickness Sensitivity

All three cases produce results very close to the experimental data. Only slight variations in the

flow through component of the curves are observed. The RTDs appear to be fairly insensitive to the

exact placement of the splash zone.

5.5.3 Error Analysis

Although the results of Case 4 intersect both experimental curves quite well, it should be noted

that the experimental curves are not nearly as smooth as the computed ones. Outlet concentrations

seem to oscillate significantly. In the experimental cases, water samples were tested by retrieving a

test tube of lagoon water in the outlet region (Figure 5.1). This process was done manually, and if

the concentration was not uniform this could induce errors in the measurements. It was decided to

try to estimate the probable extent of this particular source of error in order to gain a better

understanding of why these fluctuations are present in the experimental data. The first step was to

modify the grid being used in order to include the area following the lagoon exit in which the

samples were taken during the experiments. A residence time trial could then be run in the exact

same fashion as previously done, however this time the tracer concentrations at all points in the area

following the lagoon exit were recorded at regular time intervals. The rms values of the difference

between the point concentrations in the sampling region and the average lagoon outlet tracer

concentration can then be represented as error bars as shown in Figure 5.13.
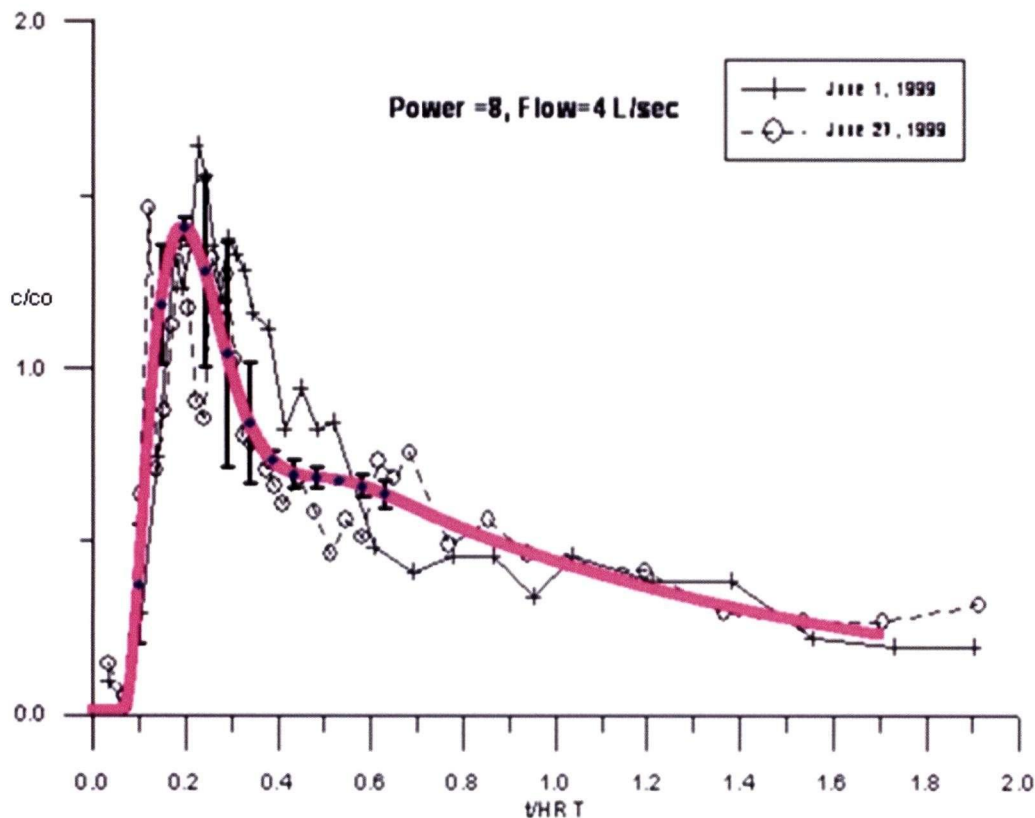
Figure 5.13: Residence Time Computed Error Bars

The analysis performed does explain many of the fluctuations in the experimental data. It is clear

that during the flow-through phase of the residence time that the concentration distribution in the

outlet region is highly non-uniform. This is reflected by the large error bars during the flow through time period, and explains why the largest discrepancies in the experimental data were found during that particular phase of the residence time distribution. Fluctuations do remain in the experimental data following the flow-through period, and these cannot be accounted for by simply looking at non-uniformity of the tracer concentration in the sampling region.

5.6 Summary

The proposed method of modeling the presence of an aerator through the use of annular velocity inlets along the surface has shown very good agreement with the previously collected experimental data. Since a variety of assumptions about how exactly mass and momentum are imparted to the lagoon within the splash zone can be made, we can test any number of combinations of these annular splash regions. Providing that the proper mass and momentum flux are applied in the splash zone, the RTDs produced were fairly insensitive to the exact placement of the splash zone. Only slight changes in the flow through component of the outlet concentrations curves were observed when modifying the splash zone. This is unlikely to be an issue when simulating highly mixed basins with multiple aerators as the highly mixed tracer outlet concentrations were identical in all cases.

6   Aerated Lagoon Studies

6.1 Introduction

Given that a model for reproducing the performance of a laboratory scale aerator and basin has been developed and validated in the preceding chapters, it now becomes possible to vary certain basin parameters and study the effects on the RTDs produced.

It is desired to understand what range of influence an aerator may have on the surrounding water. In order to minimize costs, lagoon designers naturally want to minimize the number of aerators used and the power requirement of those aerators. Also, a flow field with a significant flow through component must be avoided, so a lagoon designer must also understand how to optimally position aerators. In addition to understanding the radius of action of an aerator, it should also be understood how many aerators are required for a given lagoon volume. Table 6.1 shows two lagoon installations and their respective specific aeration rates. This value, measured in hours represents the ratio between the total lagoon volume and the total aerated volumetric flow rate.

Mill	Volume (m^3)	Number of Aerators	Volume / Flow Ratio (hrs)
Grande Prairie, AB	836 000	30	6.9
Boyle, AB	100 000	21	1.2

Table 6.1: Alberta Lagoon Facilities [2]

6.2 Aerator Radius of Action Study

6.2.1 Computational Grid

In order to study the range of influence of the experimental aerator a grid similar to the one used in Chapter 5 was designed. The length and width of the lagoon were lengthened slightly to 5.64 m, and the depth of 0.42 m was kept constant, to give a Volume/Flow ratio of 1.2 hours, identical to the installation in Boyle, Alberta. The aerator splash zone was set using the same configuration of

concentric splash zones used in Case 4b, as this seemed to provide the best fit to the experimental

data.
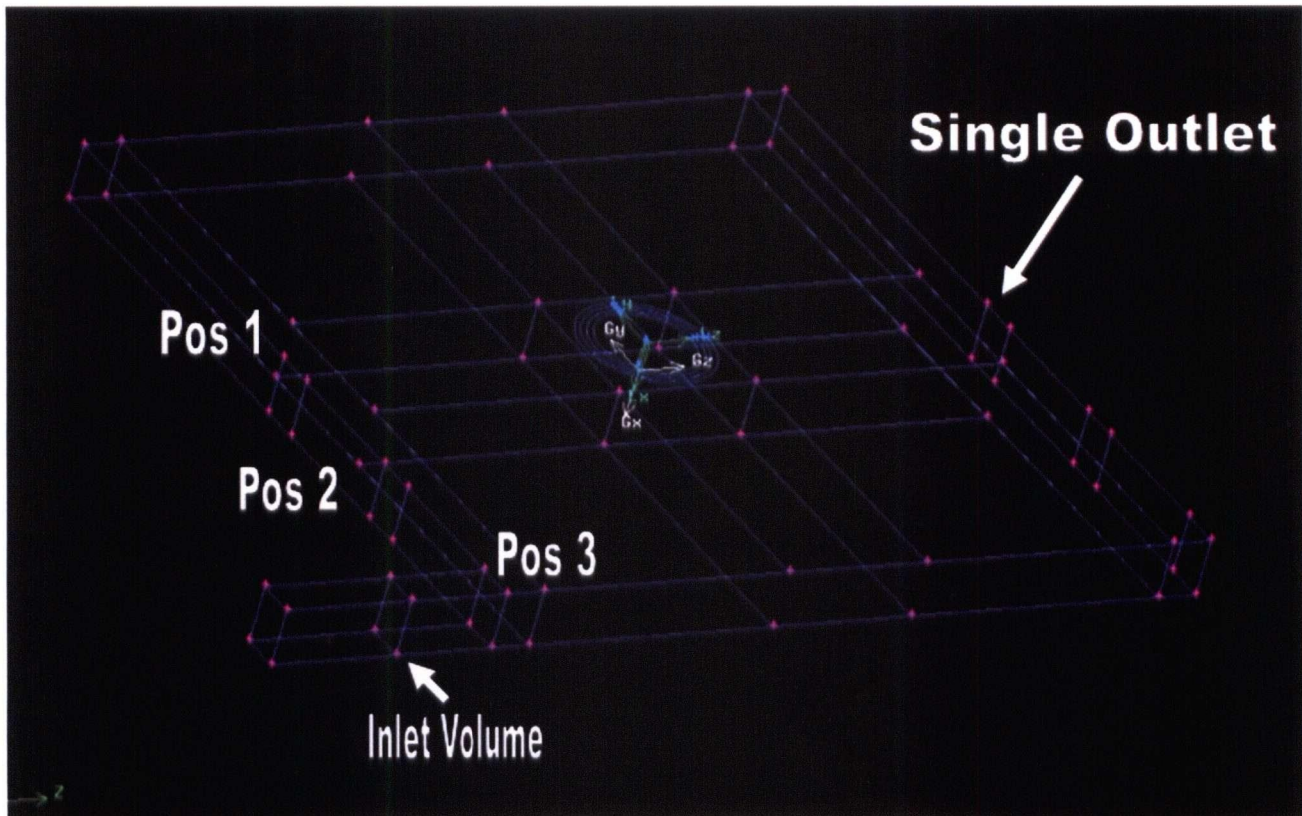
Figure 6.1: Multiple Inlet Lagoon Grid

As shown in Figure 6.1 the grid has three possible inlet positions, and one single outlet. The inlet

volume was moved from positions one through three for each case. Boundary conditions were again

set as described in Table 5.1. It is proposed that by varying the relative position between basin inlet

and the aerator, and measuring the resulting quantity of tracer which bypasses the aerator that some

conclusions can be drawn on how aerators should best be positioned in aerated lagoons.

6.2.2 Solution Procedure

The same procedure developed in the previous chapter was used in all cases. A volume fraction

of tracer of 0.2 was initialized in the inlet volume and the unsteady species transport equations were

solved once the steady state velocity field had converged. For each of the three inlet positions, two

residence time distributions were computed. The first was calculated in the same fashion as the previous trials with the average mass fraction of tracer leaving the domain via the draft tube applied to the splash zone boundary at each iteration. The second set of RTDs was computed with this feature disabled. Therefore none of the tracer entering the draft tube was returned to the lagoon. This provided a set of RTDs of the flow-through, or bypass mass of tracer passing through the lagoon.

6.2.3 Results

Figures 6.2, 6.3 and 6.4 show both RTDs for each of the three inlet positions.
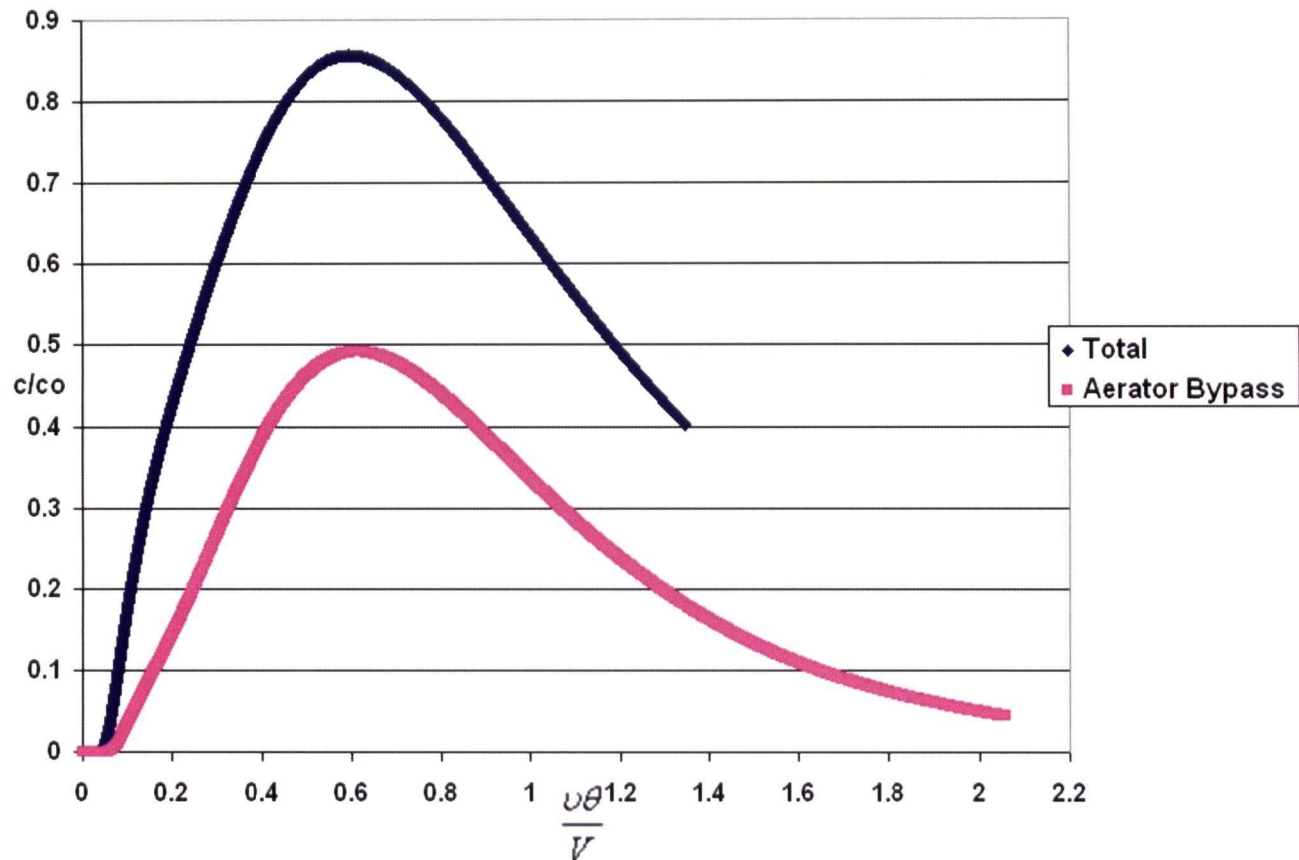
**Figure 6.2: Position 1 Total and Aerator Bypass Outlet Tracer Concentrations**
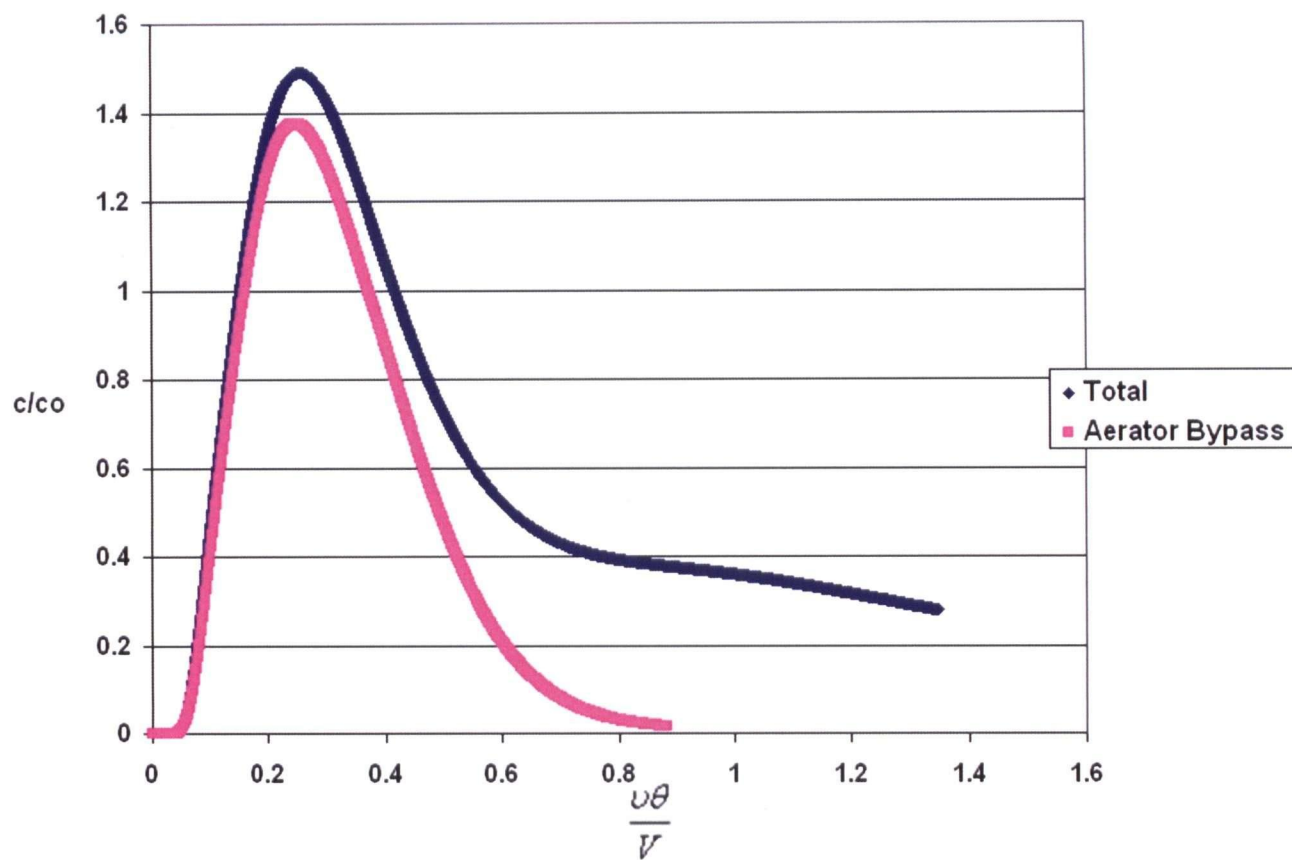
Figure 6.3: Position 2 Total and Aerator Bypass Outlet Tracer Concentrations
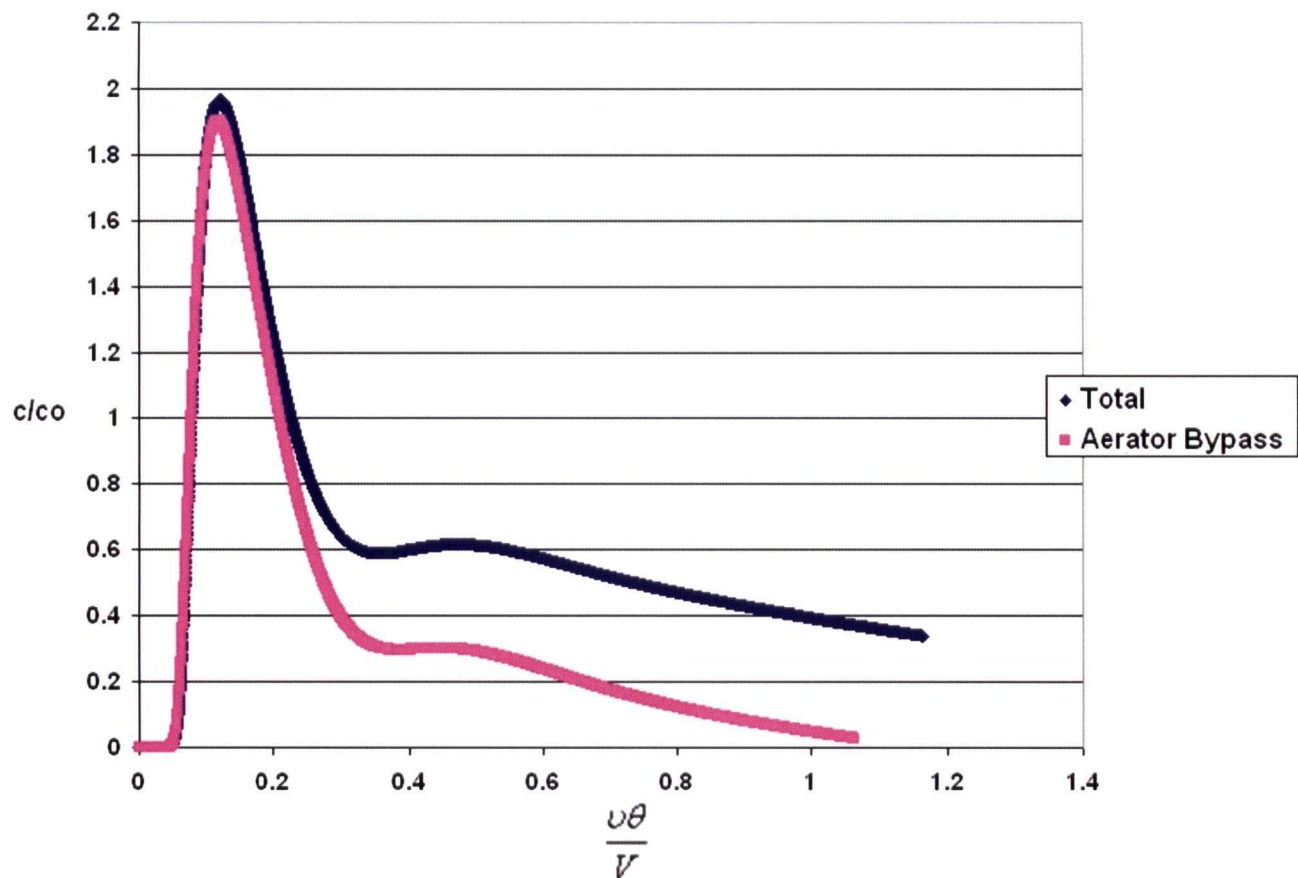
Figure 6.4: Position 3 Total and Aerator Bypass Outlet Tracer Concentrations

By integrating the aerator bypass RTDs and subtracting the result from the total initial tracer in the mixing volume the effect of the aerators on the tracer can be compared for each of the three cases. These results are shown in Table 6.1. Considering that the lateral separation between the inlet and the aerator was set at 0, 5 and 10 splash zone radii for positions 1, 2 and 3 respectively, the change in the aerated mass fraction of tracer is small. It was suspected that most of the flow through mass of tracer described in the previous chapter (the first peak in the RTDs) would enter the aerator if the inlet was aligned with the aerator. Only a small decrease in the bypass of the aerator was observed. Figure 6.5 shows the tracer mass fraction distribution midway through the computed RTD for the position 1 case. Although it was expected that tracer directed at the aerator would enter the aerator, it appears that much of the tracer is actually diverted towards the two corners of the basin by the aerator splash zone.

Position	Aerated Mass Fraction
1	0.58
2	0.54
3	0.52

Table 6.1: Total Aerated Mass Fractions

These results in no way imply that there is no benefit to having either a high density of aerators and/or placing an aerator directly in front of the inlet of a lagoon. If Figure 6.2 is compared to Figure 6.4 it is clear that the RTDs are significantly different. Although a similar mass fraction of the tracer bypasses the aerator in Figure 6.2 the bypass becomes highly mixed within the basin. The typical "flow-through" behaviour described by Danckwerts [3] observed in Figure 6.4 is not present in Figure 6.2. Furthermore, much of the tracer which bypasses the aerator in Figure 6.4 has a residence time approximately 1/6 of that of the peak outlet concentration of Figure 6.2 in which the bypass tracer becomes highly mixed. It is this high level of mixing, which causes an increase in residence time which and will increase the BOD removal of a given aerated lagoon. For lagoons with a high number of aerators, it is unlikely that a direct flow through stream would develop in the velocity field, however in smaller installations where a small number of low powered aerators are used, the results indicate that aerators should always be placed close to, and aligned with the inlet and outlet flows to ensure adequate mixing.
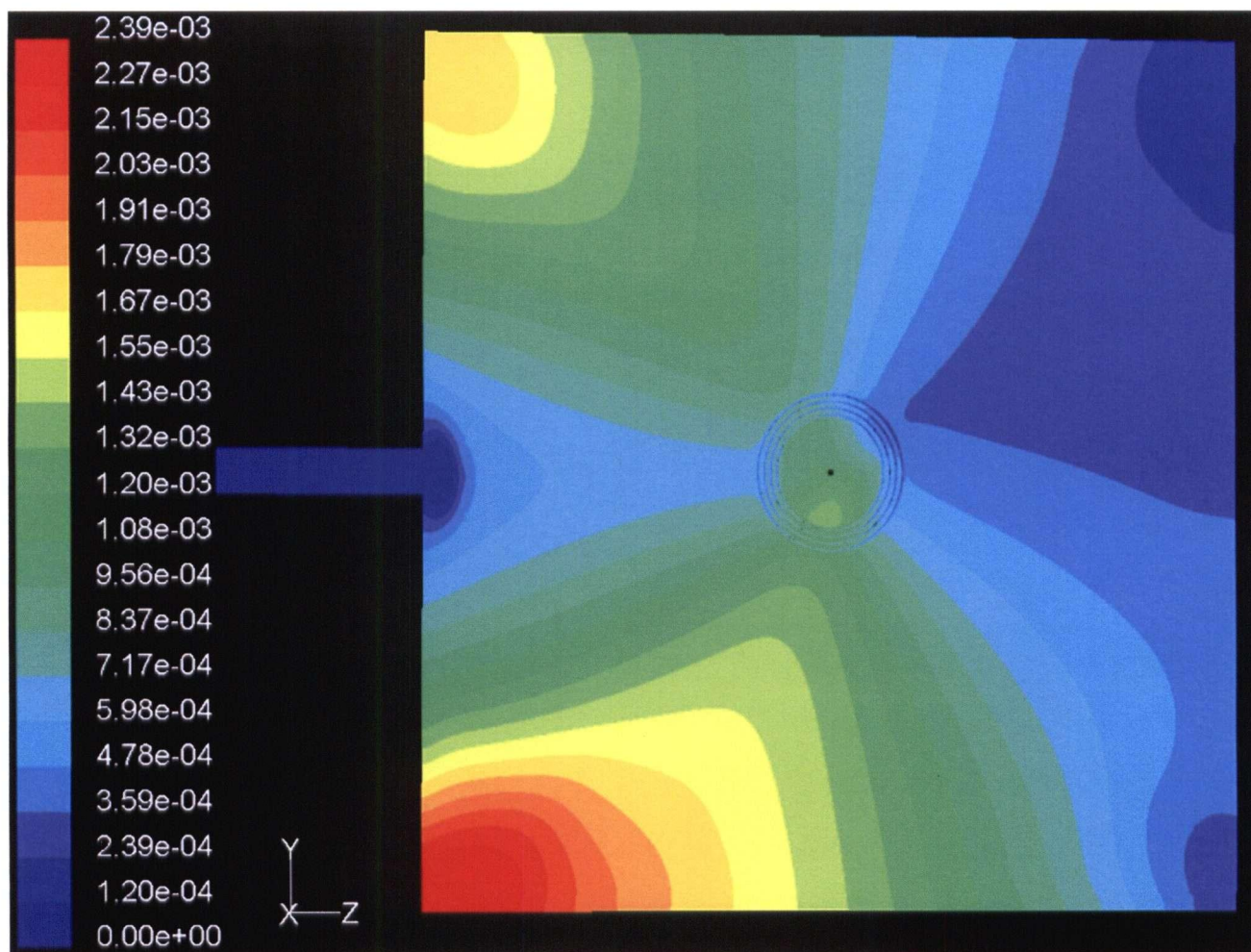
Figure 6.5: Inlet Position 1 Tracer Mass Fraction

6.3 Lagoon Volume Study

6.3.1 Computational Grids

It was also desired to vary the Volume/Flow ratio of the lagoon from that of the Boyle installation

to that of the Grand Prairie installation to observe the effect on the RTD. The volume of the tank

was therefore varied from 13.36 cubic meters to 77 cubic meters, with three separate grids. The

largest of these grids is 13.54 meters long and is shown in Figure 6.6. Edge length aside, all the

girds are identical in terms of depth, inlet/outlet configuration and aeration.
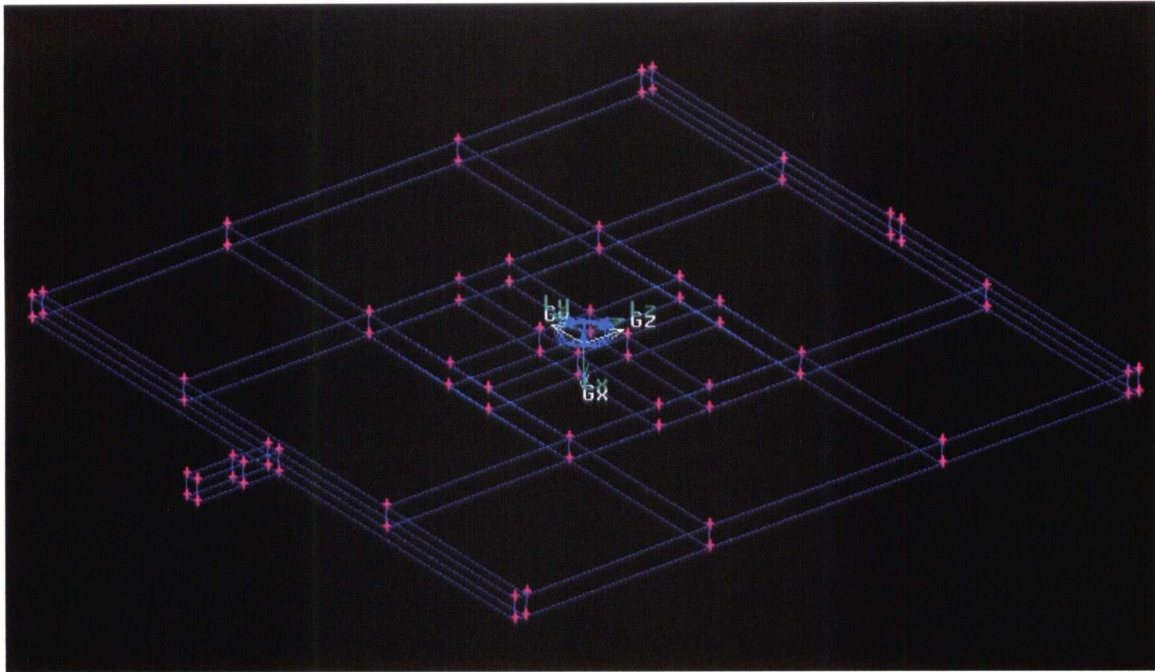
Figure 6.6: Large Tank Grid

6.3.2 Results

The same solution procedure used in Chapter 5 was applied to all cases. RTDs were generated for the three previously described grids which are plotted in Figure 6.7. The peak outlet concentration occurs later with increasing tank volume. Figure 6.8 shows the relationship between the Volume/Flow ratio and the t50 time. A clear linear trend is observed. Analysis of the RTDs produced show clear differences in the effectiveness of the different basins. The RTDs in the 45m^2 77m^2 show a very long gradual decrease in outlet tracer concentration. This characteristic, according to Danckwerts [3] is typical of reactors with large "dead zones" of very slow moving water and represents ineffective use of the available basin volume. The three following recommendations are made in order to decrease this type of behaviour in full scale aerated lagoons:

- The aerated volumetric flowrate or the total aerator power input should be shared between multiple, smaller aerators thereby increasing mixing and decreasing the prevalence of stagnant flows throughout the dead zones.

- The use of baffles is a common solution used to channel the flow through the lagoon volume, maintaining adequate flow velocity and therefore preventing the formation of dead zones. Although not as effective as aerators, the use of baffles requires little additional power.
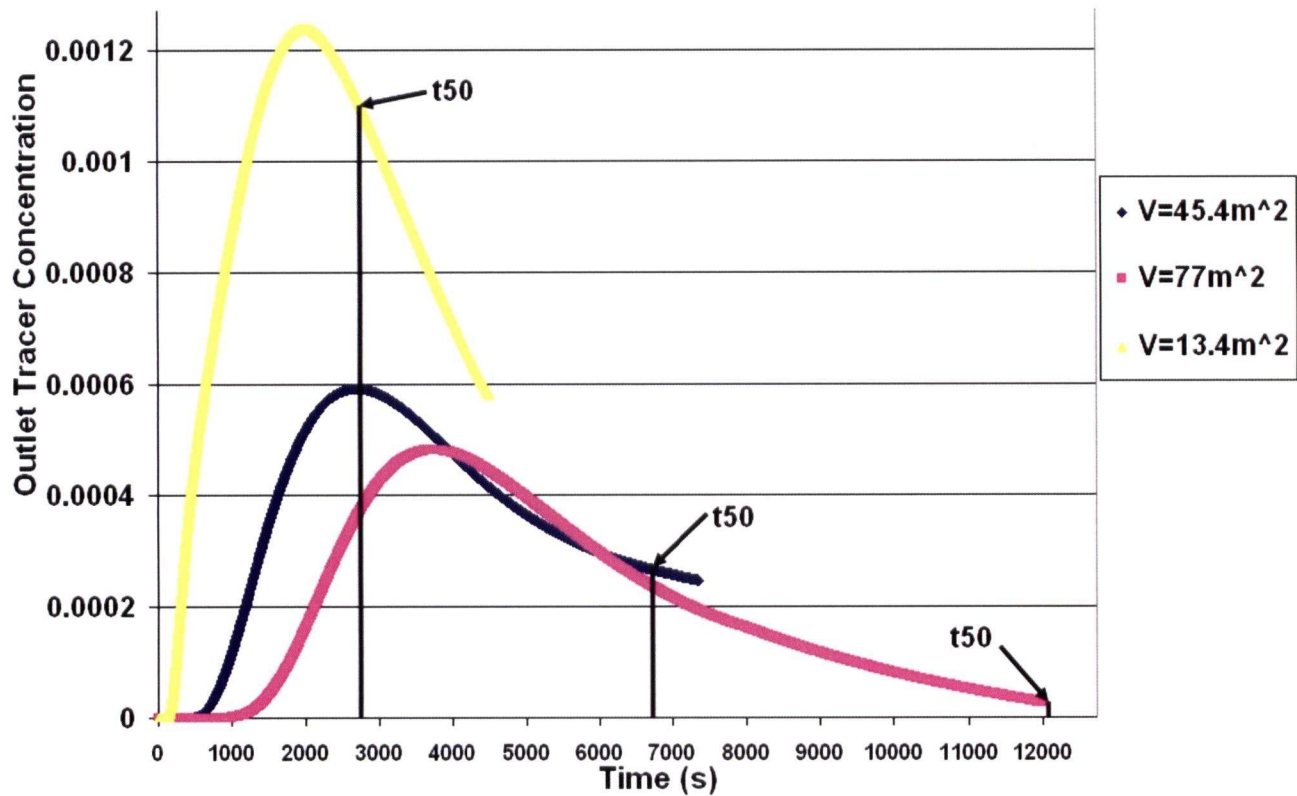

Figure 6.7: Plotted Residence Time Distributions
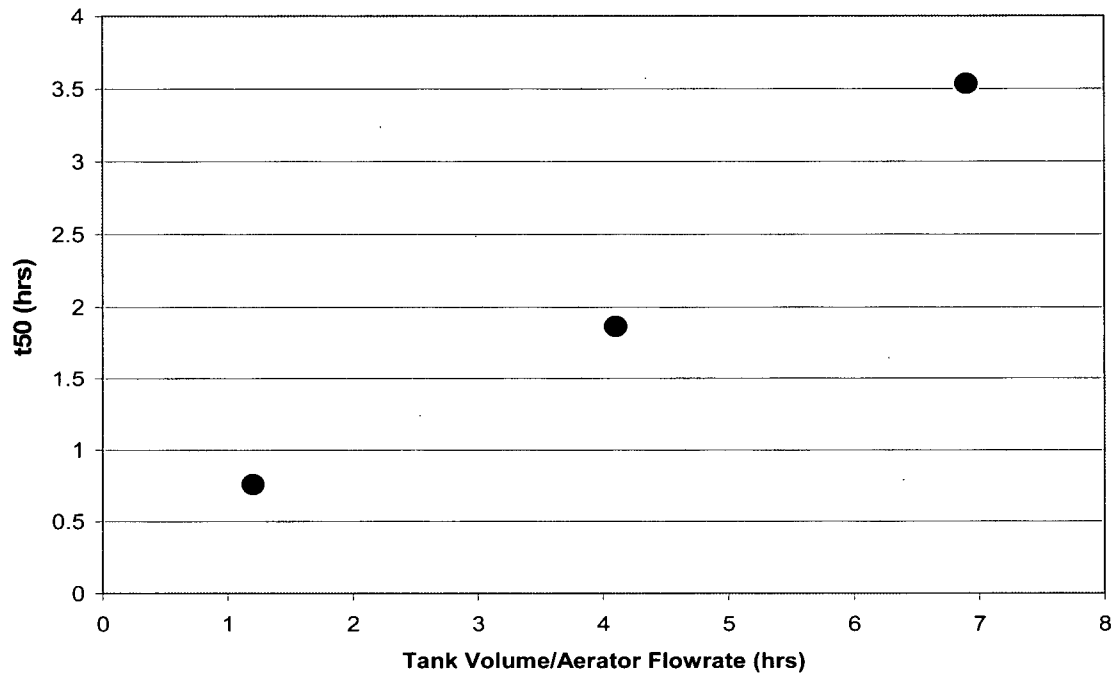
Figure 6.8: Plotted Trend of t50 vs. Tank Volume/Aerator Flow

7   Conclusions and Recommendations

7.1 Conclusions

It was the objective of this thesis to examine the potential of modeling the interactions of mechanical surface aerators with aerated lagoons using various CFD models. Previously collected experimental data was used to validate the methods and fine tune the model. The project was successful in that the residence RTD produced by the experimental apparatus was reproduced with sufficient accuracy.

A method of analyzing the flow through the internal aerator geometry using the Volume of Fluid model was used in conjunction with a Lagrangian particle tracking technique to predict the splash zone of an experimental aerator. The results were then applied to a flow-through basin simulation. Very good agreement was observed between the computed RTD and the experimental data regardless of the exact placement of the splash zone.

It was found that the computed flow through the experimental aerator apparatus varied significantly from the flow through a 75hp aerator. The flow losses through a 75hp aerator are very small resulting in a velocity at the tip of the diffusion head very close to that through the draft tube. Ballistics calculations yielded identical splash zone radii to those computed with the Lagrangian particle tracking method. As the RTD was fairly insensitive to a variety of splash zone placements and thicknesses, it can be concluded that a sound estimate of the splash zone radius, using a combination of the VOF methods applied in this thesis along with a ballistics calculation is sufficient in providing a splash zone boundary used in single phase lagoon calculations. The effect of swirl velocities in aerators was computed. It was found that even when the magnitude of the applied swirl is of the same magnitude as the axial velocity in the aerator that the splash zone radius is only enlarged by 15%. RTD's were found to be fairly insensitive to changes of splash zone radius of up to 25%, therefore the effects of swirl can be disregarded when analyzing aerated lagoons.

RTDs were also computed for domains representative of the experimental basin, but of varying tank volume. It was found that, for dimensionally similar lagoons that the t50 time varies in a linear fashion relative to tank volume. It was also observed that an increase in tank volume relative to the aerated flowrate can lead to a large mass of slow moving water which leads to poor lagoon performance. The use of baffles or multiple aerators can be used to eliminate this effect.

For a given tank volume the position of the inlet was varied relative to the position of the aerator. It was found that the level of mixing in the basin increased significantly when the aerator was aligned with the inlet and the outlet of the basin

7.2 Recommendations for Future Work

The following list outlines some of the recommendations for further study:

1. The methods used to compute the RTDs in this thesis were very computationally expensive. It required approximately 12 days to compute the RTD for the 77 m^2 basin on a 2 GHz Pentium computer. This could become a serious obstacle if large lagoons with multiple aerators are to be analyzed. Although a faster computer will always minimize this problem the following two options could be investigated in the future:

- A less computationally expensive numerical method should be developed.

- A different definition of lagoon performance should be determined which allows for the analysis of a lagoon with less computational expense.

2. A "complete" model of aerated lagoons should eventually be developed which accounts for the oxygen added to the lagoon by each aerator as well as the decay of BOD concentration as the effluent passed through the lagoon,

Appendix A: Fluent User Defined Function

The user defined function written which allows Fluent to impose the tracer concentration leaving via the draft tube at the splash zone boundary.

```
/****************************************************************
 udfdev.c
 UDF for specifying a steady-state velocity profile boundary condition
 ****************************************************************/

#include "udf.h"  /* must be at the beginning of every UDF you write */

DEFINE_PROFILE(mass_frac, t, i)
{
int suck_id=18;            /*  suck id      */
Domain *d=Get_Domain(1);
Thread *suck_t= Lookup_Thread(d,suck_id);
face_t f;
real sum=0;
real mflux=3.1;   /* declare mass flux already solved, constant*/
real frac=0;      /* declare species mass fraction*/

/*these variables are declared for the spray boundary*/
/*these are not needed-thread *t will carry the thread pointer to
* spray boundary when you will hook this to the spray boundary */
/****************************************************/
/*these lines don't compile  if they are after the loop*
int spray_id=5;

Thread *spray_t= Lookup_Thread(d,spray_id);
face_t f2;
/****************************************************/
begin_f_loop(f, suck_t) /* loops over faces in the suck thread */
{

sum+=F_FLUX(f,suck_t)*F_YI(f,suck_t,0);

}
end_f_loop(f, suck_t);

frac=sum/mflux;       /*calculates average species mass fraction at suck*/

begin_f_loop(f,t)
{
```

```
F_PROFILE(f, t, i) = frac; /*applies the species mass fraction to spray*/
}
end_f_loop(f,t)


}
```

Appendix B: Residual Calculation Method

After discretization, the conservation equation for a general variable ϕ at a cell P can be written as

$$a_p \phi_p = \sum_{nb} a_{nb} \phi_{nb} + b \tag{B.1}$$

Here a_p is the center coefficient, a_{nb} are the influence coefficients for the neighboring cells, and b is the contribution of the constant part of the source term S_c in

$$S = S_c + S_p \phi \tag{B.2}$$

and of the boundary conditions. In Equation B.2,

$$a_p = \sum_{nb} a_{nb} - S_p \tag{B.3}$$

The residual R^ϕ computed by FLUENT's segregated solver is the imbalance in Equation B.1 summed over all the computational cells P. This unscaled residual may be written as:

$$R^\phi = \sum_{cellsP} \left| \sum_{nb} a_{nb} \phi_{nb} + b - a_p \phi_p \right| \tag{B.4}$$

The scaled' residual is defined as

$$R^\phi = \frac{\sum_{cellsP} \left| \sum_{nb} a_{nb} \phi_{nb} + b - a_p \phi_p \right|}{\sum_{cellsP} \left| a_p \phi_p \right|} \tag{B.5}$$

References

1. David H.F. Liu, Bela G. Lipták Environmental Engineers' Handbook, Second Edition, CRC Press; 2nd edition (August 29, 1997)

2. Jenkinson, R.W., Analysis of Laboratory Scale Aerated Basin Using Computational Techniques, UBC, MASc Thesis, 155pp

3. Danckwerts, P.V., Continuous Flow Systems. Distribution of Residence Times, *Chem. Eng. Sci.*, **2** (1) pp.1-13

4. Nameche, Th; Vasel, J. L; (1998) Hydrodynamic Studies and Modelization for Aerated Lagoons and Waste Stabilization Ponds, Wat. Research. 12 (10) pp.3039-3045

5. Wood, M.G., Greenfield, Howes T., Johns and Keller, J., Computational Fluid Dynamic Modeling of Wastewater Ponds to Improve Design, Wat. Sci. Tech. Vol.31 No. 12 pp 111-118, 1995.

6. Ta, C.T., Brignal W.J., Application of Computational Fluid Dynamics Technique To Storage Reservoir Studies, Wat. Sci. Tech. Vol. 37, No. 2, pp. 219-226,1998

7. Salter, H.E., Ta, C.T., Ouki, S.K., Williams, S.C., Three-dimensional computational fluid dynamic modeling of a facultative lagoon, Water Science and Technology Vol 42 Nos 10-11 pp 335-342

8. Parmigiani, H.S., Revel, A. and Huynh B.P., Residual Swirl in Axial-Flow Pump, 14th Australasian Fluid Mechanics Conference, Adelaide, Australia 10-14 December 2001

9. Lefebvre, H. ; (1989), Atomization and Sprays, Hemisphere Publishing Corporation

10. S. A. Morsi and A. J. Alexander, An Investigation of Particle Trajectories in Two-Phase Flow Systems, *J. Fluid Mech.*, 55(2):193-208, September 26 1972.

11. Modeling of Aerated Lagoons; Presentation; Salcudean,

Gartshore, Pougatch, Stropky, Yuan, Nowak, Dong, Toma.

April 28, 2004

12. Fluent 6.0 Documentation; Fluent Inc, 2001